A THERMODYNAMICS BASED ANALYSIS OF EXERGY DESTRUCTION IN VAPOR COMPRESSION CYCLE SYSTEMS

BY

MEGAN KANIA

THESIS

Submitted in partial fulfillment of the requirements
for the degree of Master of Science in Mechanical Engineering
in the Graduate College of the
University of Illinois at Urbana-Champaign, 2013

Urbana, Illinois

Adviser:

Professor Andrew Alleyne

Abstract

In the last few decades, vapor-compression cycle systems (VCSs) have undergone many advances in actuation, allowing for variable aperture valves, variable speed compressors, and variable speed heat exchanger fans. Numerous efforts have been undertaken to quantify the energy efficiency of these components through the use of exergy analysis. Despite many studies varying across different types of refrigerants, different physical components, and different cooling capacities, there has been no effort made to analyze the exergy destruction caused by combinations of the variable actuators.

In order to obtain information regarding the variable actuators, a physics based model of a VCS at the University of Illinois at Urbana-Champaign (UIUC) was created. Additionally, an offline, static exergy destruction minimization technique was developed, which provides predictions of the thermodynamic operating points within the VCS. Using linear quadratic integrator (LQI) controllers, the variable actuator combinations were tested at the predicted operating points for three different cooling capacities to determine the relative exergy destruction in each configuration.

The combined variable valve aperture, evaporator fan speed, and condenser fan speed produced the most exergetically favorable configuration, with a 12.8% savings in exergy destruction over the baseline case. Implementation of variable actuators was found to be most beneficial at higher cooling capacities. Actuator combinations with only one variable component showed little benefit over the baseline conditions. The combinations of both heat exchanger fans as variable and the compressor and condenser fan as variable showed significantly worse exergy destruction over the baseline value.

To Jessica

Acknowledgements

I am grateful for the help and support that the members of the Alleyne Research Group have given me in my time here at the University of Illinois, both in the office and in my personal life. Graduate school would be very difficult without other people with whom to discuss ideas and very boring without a set of close friends. I am particularly grateful to Professor Andrew Alleyne, for the time and effort that he put forth in making sure I had a meaningful experience in his research group.

I am also indebted to my teachers, from graduate school back to preschool. They helped push me to better myself, even when I didn't think I would be able to. While I may not have agreed with or liked all of them, they all provided valuable lessons beyond the classroom.

I would be remiss if I didn't mention my family, without whose love and support I would not be the person that I am today. To my father, who spent his nights helping me memorize multiplication tables, which allowed me to become an engineer. To my mother, who gave me the freedom to spread my wings and push my boundaries. And to my sister, with whom I have shared many laughs, many tears, and who is far more precious to me than mere words could possibly describe.

Table of Contents

List of Tables

List of Figures

Nomenclature

a	Valve aperture	$[\%]$
A_{CR}	Cross-sectional area	$[m^2]$
C	Cooling capacity	$[kW]$
C_d	Coefficient of discharge	$[-]$
cp_{wall}	Wall specific heat	$\left[\frac{kJ}{kg\ K}\right]$
E	Energy	$[kJ]$
e	Error	$[-]$
F_a	Fraction of heat exchanger covered in fans	$[-]$
g	Gravitational constant	$\left[\frac{m}{s^2}\right]$
H	Enthalpy	$[kJ]$
h	Specific enthalpy	$\left[\frac{kJ}{kg}\right]$
J	Cost function	$[-]$
k	Conductivity	$\left[\frac{kW}{m\ K}\right]$
K	Heating correlation between offline and ATTMO models	$[-]$
K_γ	Gain in the mean void fraction	$\left[\frac{1}{s}\right]$
L	Length	$[m]$
m	Mass	$[kg]$
m_{wall}	Mass of heat exchanger wall	$[kg]$

$\dot{m}$	Mass flow rate	$\left[\frac{kg}{s}\right]$
P	Pressure	$[kPa]$
Q	Heat transfer	$[kJ]$
$\dot{Q}$	Heat transfer rate	$[kW]$
S	Entropy	$\left[\frac{kJ}{K}\right]$
s	Specific entropy	$\left[\frac{kJ}{kg\ K}\right]$
t	Time	$[s]$
$tkns$	Thickness	$[m]$
T	Temperature	$[K]$
T_r	Wall temperature in moving boundary model	$[K]$
T_{wall}	Wall temperature	$[K]$
U	Internal energy	$[J]$
UA	Heat transfer coefficient	$\left[\frac{kW}{K}\right]$
$\tilde{u}$	Actuator deviation	$[-]$
u^*	Final actuator values	$[-]$
$\hat{u}^*$	Feed forward actuator values	$[-]$
V	Volume	$[m^3]$
v	Velocity	$\left[\frac{m}{s}\right]$
v^*	Optimized vector	$[-]$
var	Entropy affecting variables with time derivatives not dependent on another parameter	$[-]$
W	Work	$[kJ]$
$\dot{W}$	Work rate	$[kW]$
X	Exergy	$[kJ]$
$\dot{X}$	Exergy rate	$[kW]$
$\bar{x}$	Mean quality	$[-]$
y	System output	$[-]$

y^*	Control variables	$[-]$
z	Height	$[m]$
z	Integral of the error	$[-]$
α	Heat transfer correlation	$\left[\frac{kW}{m^2\ K}\right]$
$\bar{\gamma}$	Mean void fraction	$[-]$
$\bar{\gamma}_{tot}$	Equilibrium mean void fraction for complete condensation from saturated vapor to saturated liquid	$[-]$
δ	Deviation between offline and ATTMO models	$[-]$
ΔP	Pressure difference	$[kPa]$
ζ_j	Fraction of heat exchanger length covered by zone j	$[-]$
η	Efficiency	$[-]$
Λ	Transformation matrix	$[-]$
ρ	Density	$\left[\frac{kg}{m^3}\right]$
τ_{shell}	Compressor shell time constant	$[s]$
ψ	Specific flow exergy	$\left[\frac{kJ}{kg}\right]$
ω	Speed (compressor, heat exchanger fans)	$[rpm]$, [%]

Subscripts

a	Air
adb	Adiabatic
ai	Inlet of the air
ao	Outlet of the air
ave	Average
c	Condenser
$chem$	Chemical
$comp$	Compressor
$cond$	Condenser
cs	Closed system
cv	Control volume
des	Desired
$dest$	Destroyed
e	Evaporator
$evap$	Evaporator
f	Saturated liquid
$flow$	Fluid dynamic flow
g	Saturated vapor
gen	Generated
H	High side of the refrigeration cycle
$heat$	Heat transfer

i (1,2,3,4)	Location in refrigeration cycle 1 = intro to compressor, 2 = intro to condenser, 3 = intro to valve, 4 = intro to evaporator
in	Into the component
iso	Isentropic
j (1,2 & 1,2,3)	Subscript for zone number In the evaporator, 1 = two-phase, 2 = superheated In the condenser, 1 = superheat, 2 = two-phase, 3 = subcooled
$j_1 j_2$	Between two zones in the heat exchangers (e.g. 23)
k	Compressor
L	Low side of the refrigeration cycle
out	Out of the component
P	At specific pressure
r	Refrigerant
ref	Refrigerant
rev	Reversible
ri	Inlet of the refrigerant
ro	Outlet of the refrigerant
sat	Saturation condition
sc	Subcooled
sec	Secondary side
sh	Superheat
$shell$	Compressor shell
$static$	No heat transfer from compressor shell
$surr$	Surroundings
v	Valve
VCS	Complete system
vol	Volumetric
w	Wall

$work$	Moving boundary work
X	Exergy
0	Indicates the dead space reference for exergy

Abbreviations

AC/DC	Alternating Current to Direct Current
AFRL	Air Force Research Laboratory
ATTMO	AFRL Transient Thermal Modeling and Optimization
C	Condenser
COP	Coefficient of Performance
E	Evaporator
HVAC	Heating, Ventilation, and Air Conditioning
K	Compressor
LQG	Linear Quadratic Gaussian
LQI	Linear Quadratic Integrator
LQR	Linear Quadratic Regulator
MIMO	Multi-Input, Multi-Output
PCKA	PC Krause and Associates
P-h	Pressure - Enthalpy
SISO	Single-Input, Single-Output
T-s	Temperature - Entropy
UIUC	University of Illinois at Urbana-Champaign
V	Valve
VCS	Vapor-Compression Cycle System

Chapter 1
Introduction

This thesis aims to explore the use of exergy destruction minimization as a performance objective for vapor-compression cycle systems (VCSs). Specifically, how the increased capability for actuator control has resulted in more efficient systems. From this, it is the motivation of the author to be able to recommend a level of flexibility in a subset of the available actuators for wide scale commercial implementation. An introduction to the VCS is given in Section 1.1, with specific emphasis placed on the optimization and control of the system. The history of actuator advancement is given in Section 1.2, and the specific area of research is highlighted in Section 1.3.

1.1 Vapor-compression cycle systems (VCSs)

VCSs are prevalent in modern society. A survey of US households conducted in 2009 showed 87.1% of the 130,000 households responded that they have either central or wall unit air conditioners and 97.4% had refrigerators [1]. Additionally, 213 million cars and light trucks were on the road in 2000, all with air conditioners [2]. The influence of VCSs continues to grow when commercial office buildings, industrial shipping, and specific refrigeration applications (e.g. produce storage, chemical synthesis, tempering of metals, etc. [3]) are taken into account. Given the widespread use of VCSs, even marginal increases in efficiency have a large effect across so many units, especially if the proposed changes are relatively simple to implement.

1.1.1 Modeling efforts

Motivated by the extensive use and flexibility of the VCS, there have been many efforts to model and optimize the performance of these systems. In 2002, Bendapudi and Braun released a review of modeling methods for VCSs [4]. Modeling efforts have also been specifically conducted with the end goal of developing a model suitable for controller design [5].

1.1.2 Linear quadratic regulation control

Many individuals have analyzed the use of linear quadratic regulators (LQR) and linear quadratic Gaussian (LQG) controllers on VCSs to achieve good performance [6][7][8][9]. All of this work uses multi-input, multi-output (MIMO) control of either two or three system actuators. In [6], all four actuators are variable, but only three are used on the controller while the fourth is used in disturbance rejection testing.

1.1.3 Exergy as an efficiency technique

The use of exergy as an efficiency technique has existed for many years. In 1982, Moran outlined the concept for energy availability in a system [10]. Additionally, he motivated the desire to develop more efficient systems and introduced avenues for applying exergy to a variety of different systems, including cryogenics, fuel chemical systems, and solar applications.

Exergy analysis of VCSs is expanding as an efficiency technique. In 2011, Ahamed, Saidur, and Masjuki conducted an extensive review of exergy in VCS analysis [11]. Kotas highlighted how exergy has been used to conduct design changes at both the system and component levels [12]. The compressor has been shown to destroy the most exergy in the four component VCS by an order of magnitude over the other components [11][12]. An in-depth analysis of the compressor exergy destruction can be found in [13].

1.2 Advances in VCS actuation

A VCS needs to have four basic components to operate: a compressor, condenser, expansion device, and evaporator. It is possible to construct a system such that none of these components are variable. The expansion device can be an orifice tube, the compressor can run at

a constant speed, and the heat exchangers can have a constant flow rate of the secondary side medium. This results in a system with no flexibility in operation.

As the heating, ventilation, and air conditioning (HVAC) industry advanced, it became obvious that these systems needed to be more flexible. First, thermostatic expansion valves replaced the fixed orifice tubes. Thermostatic expansion valves maintain a set amount of superheat at the evaporator exit, but must be tuned offline due to a preload spring [14]. Advancing to electronic expansion valves has allowed the same system performance through an online controller instead of a manual coupling [15]. Variable speed compressors can be used to alter the mass flow rate in the system, and permit the VCS to perform away from the original design point, thus allowing to system to handle more flexible loading conditions [16][17]. Between 1980 and 1990, advances in motor control and physical hardware facilitated flexibility in the heat exchanger fan speed. This resulted in 30-40% more efficient refrigeration units and 26% more efficient air conditioners [18]. As VCS systems have matured, there has been a significant movement to more efficient and more flexible systems.

Movement toward variable actuator systems does come at a price [19]. Obviously, components which allow for variable performance will have a higher initial cost associated with the purchase. Moreover, full actuation of a VCS system may be useful in the design stages or at a research level, but it may be unnecessary and impractical for most commercial applications. Manufactures need a method for determining the level of flexibly in actuators that are the most critical to an efficient system performance. To be able to have a method for determining this performance will allow designers to install a smaller collection of variable actuators without sacrificing in-operation system performance.

1.3 Specific research contribution

As is evidenced by the literature survey, while there has been work done to use exergy destruction as an efficiency metric for VCSs, analysis of exergy destruction at the component level has only observed the actuators in isolation and not expanded to multiple combinations of variable actuators. This thesis aims to provide information on the relative exergy destruction savings that can be obtained by using a combination of the available variable actuators. To complete this goal, a specific offline exergy destruction minimization technique will be

developed, which will provide suggested thermodynamic operating points in order to minimize exergy destruction. The recommended points will then be applied to a complete system model and the exergy destruction will be extracted at three distinct cooling capacities for all subsets of actuator combinations. Propositions regarding which combination of actuators should be pursued in a commercial setting will be provided.

Chapter 2
Component Modeling

In this chapter, a vapor-compression cycle system (VCS) is broken down into its constituent components. Equations are used to define the behavior of the individual components, both physics-based and empirically derived. Additionally, the Air Force Research Laboratory (AFRL) transient thermal modeling and optimization (ATTMO) environment is used to construct the complete system model and allow for user interfacing.

2.1 Introduction to VCSs

VCSs are used to move heat from one physical location to another through a fluid refrigerant. Relatively few components are needed to create a basic VCS: a compressor, condenser, evaporator, and expansion device, as shown in Figure 2.1. VCSs are known for their adaptability in scale (from residential air conditioners to commercial refrigeration facilities [20]) as well as their ability to incorporate supplementary components (receivers, etc.) and additional refrigerant flow paths (multi-evaporator, multi-compressor, etc.). For the work done in this thesis, the VCS will be the simple, four component system shown in Figure 2.1 using R134a as the active refrigerant.

2.1.1 Thermodynamic system modeling

For the VCS laid out in Figure 2.1, the thermodynamic variables of interest are denoted on a pressure-enthalpy (P-h) diagram in Figure 2.2. Due to the nature of the fluid medium used in the VCS, the thermodynamic properties of the refrigerant at different stages within the cycle can be completely specified by the location of a vertex on the P-h diagram [21]. Additionally, the

numbers marked at the vertices in Figure 2.2 correspond to the transition between components in Figure 2.1.

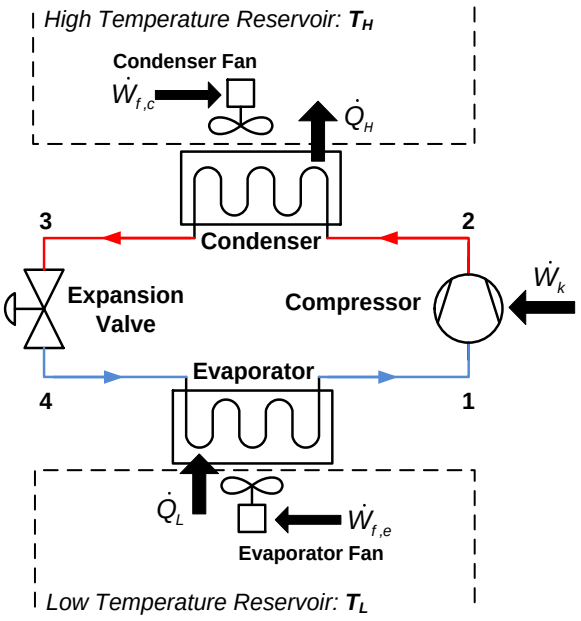

Figure 2.1: VCS with environmental and loading interfaces

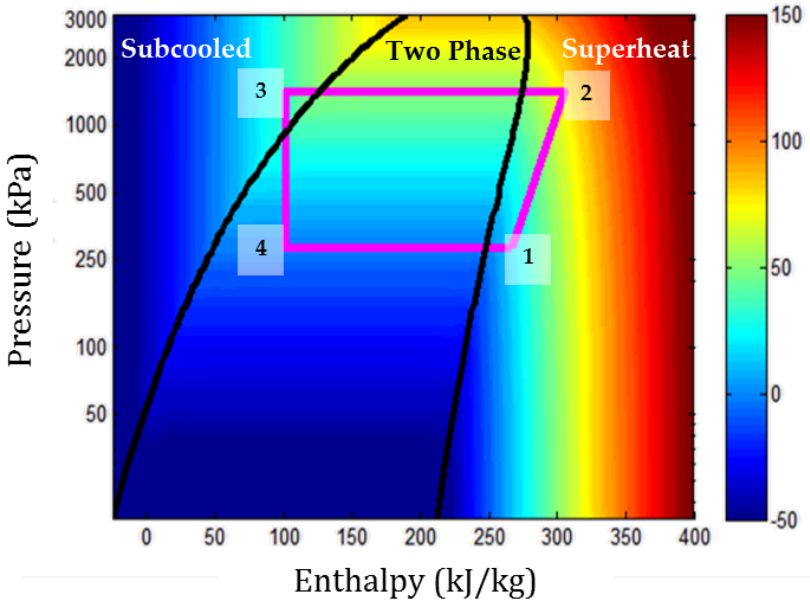

Figure 2.2: VCS represented on a pressure-enthalpy diagram

The refrigerant travels in a repeatable pattern in a VCS. Superheated (gaseous) refrigerant enters the compressor at point 1. The refrigerant is compressed to a higher pressure and

temperature, but remains gaseous at point 2. The condenser extracts energy in the form of heat from the highly energetic refrigerant by interfacing it with a secondary side medium. Due to this energy loss, the refrigerant exits the condenser at point 3 as a subcooled liquid. The liquid is then passed to an expansion device (e.g. an expansion valve) which drops the pressure of the refrigerant, creating a two-phase mixture of gas and liquid at point 4. The evaporator takes in the low pressure refrigerant and increases its energy through interaction with a different secondary side medium than the condenser. In the evaporator, the refrigerant gains sufficient energy to be entirely gaseous, and the process begins again at point 1.

Due to several assumptions made to approximate the physical VCS as an idealized model, specific constraints are placed on the refrigerant in VCS models, which dictate its thermodynamic properties. Here we assume:

1) Isentropic compression ($s_1 = s_2$)
2) Isobaric condensation ($P_2 = P_3$)
3) Isenthalpic expansion ($h_3 = h_4$)
4) Isobaric evaporation ($P_4 = P_1$)
5) Evaporation to a superheated state ($T_1 > T_{sat,P_1}$)
6) Condensation to a subcooled state ($T_3 < T_{sat,P_2}$)

While these constraints denote fairly accurate modeling assumptions, small discrepancies still exist, as modeling error can never be completely eliminated.

2.1.2 Efficiency metrics [22]

A variety of efficiency metrics exist to determine the optimal operation of the VCS. The coefficient of performance (COP) is a measure of the cooling capacity achieved by the system divided by the amount of work required to operate the system. Referencing the thermodynamic states in Figure 2.1 and Figure 2.2, the equation becomes

$$COP = \frac{cooling\ capacity}{supplied\ power} = \frac{\dot{Q}_L}{\dot{W}_{VCS}} = \frac{\dot{m}(h_1 - h_4)}{\dot{m}(h_2 - h_1)} \tag{2.1}$$

The maximum possible COP of a system is given by the Carnot COP [23]. Figure 2.3 shows the net work of the system compared to the cooling capacity of the system achieved on a

temperature-entropy (T-s) diagram. T_H and T_L refer to the high and low temperature reservoirs which interface with the VCS through the heat exchangers.

$$COP_{Carnot} = \frac{cooling\ capacity}{net\ work} = \frac{T_1(s_1 - s_4)}{(T_2 - T_1)(s_1 - s_4)} = \frac{T_1}{T_2 - T_1} \tag{2.2}$$

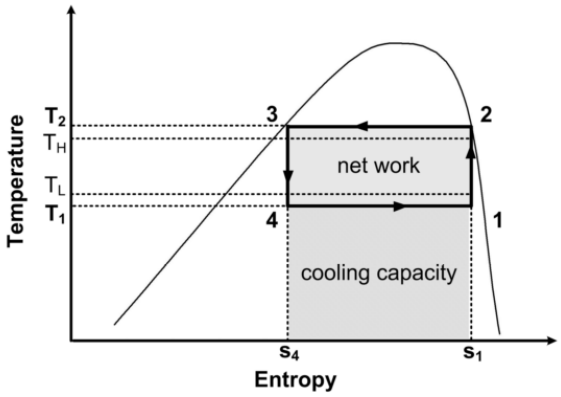

Figure 2.3: Work required versus cooling capacity achieved by a VCS for a Carnot refrigeration cycle

In order to maintain a temperature gradient and promote heat transfer

$$T_2 > T_H \tag{2.3}$$

$$T_1 < T_L \tag{2.4}$$

thereby bounding the realizable COP and Carnot COP as

$$COP \leq COP_{Carnot} = \frac{T_1}{T_2 - T_1} < \frac{T_L}{T_H - T_L} \tag{2.5}$$

The principle of exergy, discussed in depth in Chapter 3, can be incorporated to produce another type of efficiency known as a 'second law efficiency' [21]. Rather than just focusing on the thermal efficiency (as in the case of the COP), exergy couples the thermal efficiency to the amount of energy supplied to the system. Through this coupling, the performance of a VCS is compared to the ideal VCS operating at the same conditions. Thus, the second law efficiency is always bounded by 0 and 1, see Equation 2.6, making it a more intuitive efficiency metric than COP. A conversion between exergetic efficiency and COP is given in Equation 2.7.

$$0 \leq \eta_X = 1 - \frac{exergy\ destroyed}{exergy\ supplied} \leq 1 \tag{2.6}$$

$$\eta_X = \frac{COP}{COP_{Carnot}} \tag{2.7}$$

2.2 Physical equations governing component behavior

Due to the prevalence of vapor-compression cycle systems in numerous aspects of engineering [3], there is a natural desire to model these systems in order to determine system behavior and develop control schemes. In general, both first principles and empirical models can be used to capture the proper behavior of a VCS. Here we provide our modeling approach to represent the various system components.

2.2.1 Static components

Pressure and thermal dynamics drive the two major time scales in a VCS. The pressure dynamics are primarily driven by the mass flow rate in the system. The slower thermal dynamics are dominate in the system, allowing the pressure to be seen as a constant at any given time. Therefore, the components that calculate mass flow rate (valve and compressor) are modeled as static components whereas the components that calculate the thermal dynamics (evaporator and condenser) are modeled as dynamic components.

2.2.1.1 Valve

Mass flow rate dynamics through the valve are governed by a single equation, Equation 2.8. The discharge coefficient of the valve is determined using empirical data through a process known as mapping. More detailed information regarding the valve map is given in Appendix A.

$$\dot{m} = C_d\sqrt{\rho\Delta P} \tag{2.8}$$

2.2.1.2 Compressor

The compressor is also responsible for calculating a mass flow rate in the system. Similar to the valve, the compressor uses maps (see Appendix A) generated through empirical data to arrive at an accurate mass flow rate for the system [24]. Three maps are used to create three efficiencies in the compressor: volumetric, adiabatic, and isentropic. The volumetric efficiency captures the ability for the compressor to convert the full stroke length into a movement of refrigerant. The adiabatic efficiency addresses the assumption that no heat transfer is taking place

between the compressor and the environment. The isentropic efficiency relates back to the modeling assumption in Section 2.1.1, which assumes that the compressor is completely isentropic. This efficiency is needed in the exergy destruction minimization technique and appears in Section 4.1.3.

The compressor mass flow rate is given in Equation 2.9. During operation, the compressor shell will heat up due to friction, causing a first order dynamic in the enthalpy of the refrigerant. The enthalpy is also sensitive to changes in the adiabatic efficiency. Both of these phenomena are captured in Equations 2.10 and 2.11.

$$\dot{m} = \omega V \rho \eta_{vol} \tag{2.9}$$

$$h_{static} = h_{in} + \frac{h_{out,iso} - h_{in}}{\eta_{adb}} \tag{2.10}$$

$$\dot{h}_{out} = \frac{h_{static} - h_{out}}{\tau_{shell}} \tag{2.11}$$

From the refrigerant side, the dynamics of the compressor shell can be captured by measuring the temperature of the compressor shell over time and calculating an appropriate time constant to describe the shell dynamics. This method is restrictive in the fact that the temperature of the compressor shell may be affected by many parameters, including the current condition of the ambient environment, and the exact result obtained for the time constant may not be accurate with a slightly different ambient environment. Equation 2.12 outlines a more rigorous approach to determine the temperature of the compressor shell. Through this method, it is possible to capture changes in the ambient environment, such as temperature or humidity, which affect the dynamics of the compressor shell. Further analysis of this phenomenon is provided in Section 3.3.1.

$$\dot{T}_{shell} = \frac{\dot{Q}_{ref} + \dot{Q}_{surr}}{Cp_{shell} m_{shell}} \tag{2.12}$$

2.2.2 Dynamic components

Thermal dynamics within the VCS are manifested in the heat exchangers. Due to the phase change of the refrigerant within the heat exchangers, modeling of these components can be accomplished by using a lumped parameter analysis [5][25][26][27][28][29]. Similar to a finite

element analysis, which assumes refrigerant parameters are not significantly changing over a discrete length, the lumped parameter analysis assumes parameters are not significantly changing within a given refrigerant phase. Because the location of the interface between two refrigerant zones is not fixed, the heat exchanges allow the length of a given refrigerant zone to change in a 'moving boundary' model. Therefore, the evaporator can be thought of as a two zone finite element, moving boundary model and the condenser can be thought of as a three zone finite element, moving boundary model. A graphical representation of this phenomenon is shown for the evaporator in Figure 2.4 and the condenser in Figure 2.5. The numbers corresponding to the zone type serve as indices in the component equations.

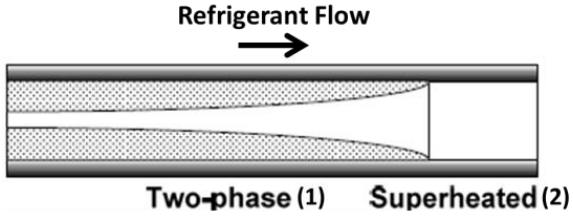

Figure 2.4: Refrigerant modes within the evaporator

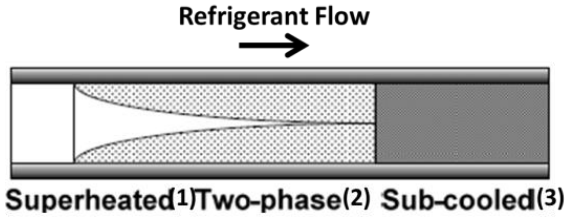

Figure 2.5: Refrigerant modes within the condenser

In operation, it is possible for a particular refrigerant zone to disappear, especially during startup, shut down, and other large transient conditions, e.g. step change in specified load. Because of the coupled nature of the physical equations describing the evaporator, Section 2.2.2.1, and the condenser, Section 2.2.2.2, a disappearance of a zone would result in a trivial equation which produces no useful information. For example, if the superheat zone of the condenser disappeared, an energy balance over the non-existent zone would yield no information as the zone technically has no energy if it does not exist. In order to preserve a smooth model of the VCS, a different set of coupled differential equations are used to describe the heat exchangers during the loss of one or more refrigerant zones. While it is not within the scope of this thesis,

individuals seeking more detailed information regarding the disappearance of these zones within the heat exchangers and the subsequent modeling changes are directed to [30].

2.2.2.1 Evaporator

The evaporator is the component where the external space is coupled with the VCS. Excess heat from the ambient environment enters the evaporator and increases the energy of the refrigerant within the heat exchanger. The majority of the heat transfer occurs in the two phase region and VCSs are generally designed to run with a small superheated region to promote this efficient heat transfer. It is necessary to have some superheat, as the compressor can be damaged by liquid refrigerant at the inlet.

The evaporator uses five coupled differential equations to calculate the state vector $[\zeta_1 \quad P \quad h_2 \quad \bar{\gamma} \quad \dot{m}_{12}]^T$. The evaporator model is able to provide insight that would be challenging to obtain from a physical system, specifically, the normalized zone length for the two phase region (and by subtraction, for the superheated region as well).

The equations shown below follow from the conservation of mass (Equation 2.13) and conservation of energy (Equation 2.14) in the two phase region as well as the superheated region (Equations 2.15 and 2.16). Equation 2.17 represents the mean void fraction in the two phase zone. Void fraction [31] refers to the volume amount of gaseous refrigerant compared to the total possible volume, resulting in a measurement of emptiness.

$$\frac{d\zeta_1}{dt} - \frac{\zeta_2}{\rho_2}\frac{\partial \rho_2}{\partial P}\frac{dP}{dt} - \frac{\zeta_2}{\rho_2}\frac{\partial \rho_2}{\partial h_2}\frac{dh_2}{dt} + \frac{\dot{m}_{12}}{\rho_2 V} = \frac{\dot{m}_{out}}{\rho_2 V} \tag{2.13}$$

$$-\frac{1}{\rho_2}\frac{dP}{dt} + \frac{dh_2}{dt} - \frac{h_g - h_2}{\rho_2 V \zeta_2}\dot{m}_{12} = \frac{\dot{Q}_2 - \dot{m}_{out}(h_2 - h_g)}{\rho_2 V \zeta_2} \tag{2.14}$$

$$\frac{d\zeta_1}{dt} + \frac{\zeta_1}{\rho_1}\frac{\partial \rho_1}{\partial P}\frac{dP}{dt} + \frac{\zeta_1}{\rho_1}\frac{\partial \rho_1}{\partial \bar{\gamma}}\frac{d\bar{\gamma}}{dt} + \frac{\dot{m}_{12}}{\rho_1 V} = \frac{\dot{m}_{in}}{\rho_1 V} \tag{2.15}$$

$$\left[\frac{\partial h_1}{\partial P} - \frac{1}{\rho_1}\right]\frac{dP}{dt} + \frac{\partial h_1}{\partial \bar{\gamma}}\frac{d\bar{\gamma}}{dt} + \frac{h_g - h_1}{\rho_1 V \zeta_1}\dot{m}_{12} = \frac{\dot{Q}_1 + \dot{m}_{in}(h_{in} - h_1)}{\rho_1 V \zeta_1} \tag{2.16}$$

$$\frac{\partial \bar{\gamma}_{tot}}{\partial P}\frac{dP}{dt} - \frac{d\bar{\gamma}}{dt} = K_\gamma(\bar{\gamma} - \bar{\gamma}_{tot}) \tag{2.17}$$

In addition to calculating refrigerant parameters, the evaporator model also calculates the wall temperatures in each zone. The parameter T_{r1} allows the wall temperatures to vary as the

length of each zone varies within the evaporator, taking on the value of the zone that is *decreasing* in length. E.g. if the length of the two-phase region is increasing, $T_{r1} = T_{wall2}$ and if the length of the superheat region is increasing, $T_{r1} = T_{wall1}$. The wall temperatures play a critical role in modeling the heat transfer from the secondary fluid to the refrigerant in the evaporator.

$$\dot{T}_{wall1} = \frac{1}{\zeta_1}\left[(T_{r1} - T_{wall1})\dot{\zeta}_1 - \frac{\dot{Q}_{ref1} + \dot{Q}_{sec1}}{Cp_{wall} m_{wall}}\right] \tag{2.18}$$

$$\dot{T}_{wall2} = \frac{1}{\zeta_2}\left[(T_{wall2} - T_{r1})\dot{\zeta}_1 - \frac{\dot{Q}_{ref2} + \dot{Q}_{sec2}}{Cp_{wall} m_{wall}}\right] \tag{2.19}$$

2.2.2.2 Condenser

Similar to the evaporator, the condenser serves to move heat from the VCS to the ambient environment, decreasing the energy of the refrigerant as it passes through the condenser. The refrigerant enters the condenser as a superheated vapor, due to the operating restrictions of the compressor, and is condensed through the two phase region and into the subcooled liquid region. While the complete condensation into a subcooled liquid is not strictly necessary to prevent damage to other components, it is a good indication that most of the easiest energy to access from the refrigerant has been extracted, as two phase heat transfer is the most efficient form of heat transfer. An overly large subcooled region indicates that the condenser is oversized for the system [32].

The condenser calculates a vector of eight variables, due to the coupled nature between the differential equations that govern the component: $[\zeta_1 \quad \zeta_2 \quad P \quad h_3 \quad \dot{m}_{12} \quad \dot{m}_{23} \quad h_1 \quad \bar{\gamma}]^T$. As before, the two normalized zone lengths are calculated, which allows the user access to the third zone length and thus a way to validate the sizing of the condenser.

The differential equations used to obtain these variables are as follows. The conservation of mass and energy in the subcooled zone are given by Equations 2.20 and 2.21, Equations 2.22 and 2.23 for the superheated zone, and Equations 2.25 and 2.26 for the two phase zone. Equation 2.24 determines the average enthalpy in the superheated zone. Equation 2.27 gives the mean void fraction in the two phase zone.

$$\frac{d\zeta_1}{dt} + \frac{d\zeta_2}{dt} - \frac{\zeta_3}{\rho_3}\frac{dh_3}{dt} + \frac{\dot{m}_{23}}{\rho_3 V} = \frac{\dot{m}_{out}}{\rho_3 V} \tag{2.20}$$

$$\frac{dh_3}{dt} - \frac{h_f - h_3}{\rho_3 V \zeta_3}\dot{m}_{23} - \frac{1}{\rho_3}\frac{dP}{dt} = \frac{\dot{Q}_3}{\rho_3 V \zeta_3} \tag{2.21}$$

$$\frac{d\zeta_1}{dt} + \frac{\zeta_1}{\rho_1}\frac{\partial \rho_1}{\partial P}\frac{dP}{dt} + \frac{\dot{m}_{12}}{\rho_1 V} = \frac{\dot{m}_{in}}{\rho_1 V} \tag{2.22}$$

$$\frac{dh_1}{dt} - \frac{1}{\rho_1}\frac{dP}{dt} + \frac{h_g - h_1}{\rho_1 V \zeta_1}\dot{m}_{12} = \frac{\dot{Q}_1 + \dot{m}_{in}(h_{in} - h_1)}{\rho_1 \zeta_1} \tag{2.23}$$

$$\frac{dh_1}{dt} = \frac{1}{2}\left(\frac{dh_{in}}{dt} + \frac{dh_g}{dt}\right) = \frac{1}{2}\frac{dh_{in}}{dt} + \frac{1}{2}\frac{\partial h_g}{\partial P}\frac{dP}{dt} \tag{2.24}$$

$$\frac{d\zeta_2}{dt} + \frac{\zeta_2}{\rho_2}\frac{\partial \rho_2}{\partial P}\frac{dP}{dt} + \frac{\dot{m}_{23}}{\rho_2 V} - \frac{\dot{m}_{12}}{\rho_2 V} + \frac{\zeta_2}{\rho_2}\frac{\partial \rho_2}{\partial \bar{\gamma}}\frac{d\bar{\gamma}}{dt} = 0 \tag{2.25}$$

$$\left[\frac{\partial h_2}{\partial P} - \frac{1}{\rho_2}\right]\frac{dP}{dt} + \frac{h_f - h_2}{\rho_2 V \zeta_2}\dot{m}_{23} - \frac{h_g - h_2}{\rho_2 V \zeta_2}\dot{m}_{12} + \frac{\partial h_2}{\partial \bar{\gamma}}\frac{d\bar{\gamma}}{dt} = \frac{\dot{Q}_2}{\rho_2 V \zeta_2} \tag{2.26}$$

$$\frac{\partial \bar{\gamma}_{tot}}{\partial P}\frac{dP}{dt} - \frac{d\bar{\gamma}}{dt} = K_\gamma(\bar{\gamma} - \bar{\gamma}_{tot}) \tag{2.27}$$

As with the evaporator, the condenser calculates the wall temperature of the three regions. Due to the changing lengths of the zones, T_{r1} and T_{r2} are used to define the temperature at the interaction boundary of the superheat and two phase regions and the two phase and subcooled regions, respectively. They take on the value of the zone that is *decreasing* in length.

$$\dot{T}_{wall1} = \frac{1}{\zeta_1}\left[(T_{r1} - T_{wall1})\dot{\zeta}_1 - \frac{\dot{Q}_{ref1} + \dot{Q}_{sec1}}{Cp_{wall} m_{wall}}\right] \tag{2.28}$$

$$\dot{T}_{wall2} = \frac{1}{\zeta_2}\left[(\dot{\zeta}_1 + \dot{\zeta}_2)T_{r2} - \dot{\zeta}_1 T_{r1} - \dot{\zeta}_2 T_{wall2} - \frac{\dot{Q}_{ref2} + \dot{Q}_{sec2}}{Cp_{wall} m_{wall}}\right] \tag{2.29}$$

$$\dot{T}_{wall3} = \frac{1}{\zeta_3}\left[(\dot{\zeta}_1 + \dot{\zeta}_2)(T_{wall3} - T_{r2}) - \frac{\dot{Q}_{ref3} + \dot{Q}_{sec3}}{Cp_{wall} m_{wall}}\right] \tag{2.30}$$

2.2.2.3 Fan maps

As with the valve and compressor models, the heat exchanger models use empirical data to ensure proper modeling of a physical VCS. Fan speed is correlated with the mass flow rate of air over the heat exchanger. Additional information and specific equations are available in Appendix A.

2.3 Modeling environment

The ARFL (Air Force Research Laboratory) transient thermal modeling and optimization (ATTMO) toolbox was developed through a joint effort between the University of Illinois at Urbana-Champaign (UIUC), PC Krause and Associates (PCKA), and the Air Force Research Laboratory at Wright-Patterson Air Force Base.

2.3.1 Created from the THERMOSYS toolbox

The ATTMO toolbox is primarily based on the THERMOSYS toolbox developed at UIUC. The THERMOSYS toolbox has been validated on a variety of experimental systems [30][33][34], as well as used in the development of advanced control strategies [30][35][36]. Through PCKA, the THERMOSYS toolbox, which runs a combination of Simulink models and MATLAB files, was converted into an entirely Simulink environment. Additionally, the ATTMO toolbox was validated, both against the THERMOSYS toolbox and the particular test hardware at the University of Illinois used in this work [37]. The system is shown in Figure 2.6.

Figure 2.6: VCS at the University of Illinois

2.3.2 Benefits of the modeling environment

The ATTMO modeling environment offers a variety of unique benefits. Foremost, the environment is entirely modular. This allows for a simple 'drag and drop' capability on the part of the user. Figure 2.7 shows some of the components available in the toolbox. Figure 2.8 provides a sample VCS in the ATTMO environment.

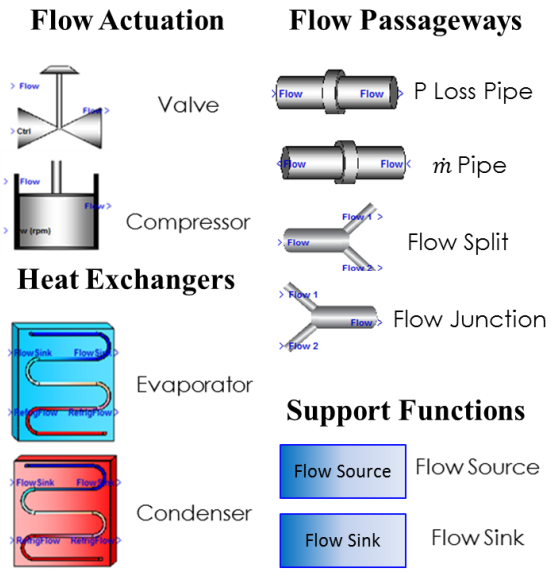

Figure 2.7: Available components supported by the ATTMO toolbox

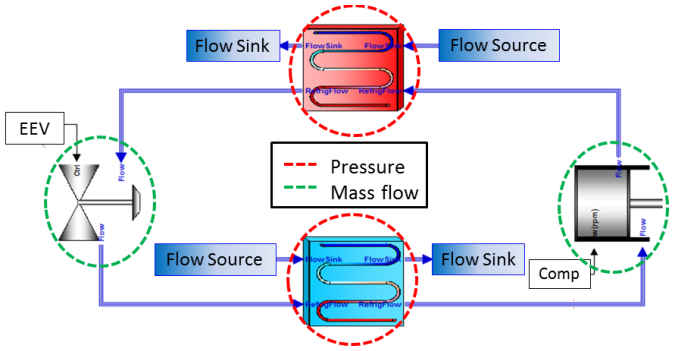

Figure 2.8: Sample model of a VCS in the ATTMO environment

Pressure and mass flow rate are calculated in an alternating pattern, partially to ensure that any point between components has access to both pieces of information. The necessity of alternating the pressure and mass flow rate calculating components is motivated by a bond graph analysis of the VCS [38]. In bond graph analysis, the efforts exerted on the system (pressure) and

the flow in the system (mass flow rate) can be analyzed at a component location through the use of 0 and 1 junctions. A 0 junction corresponds to sum of the flows equal to zero with a constant effort, similar to Kirchhoff's current law, and a 1 junction corresponds to the efforts summing to zero with a constant flow, similar to Kirchhoff's voltage law. To preserve the causality of the system, the same type of junction cannot be adjacent to each other. In the VCS model, if two components with the same junction type are placed next to each other, the causality of the system will be broken and the model cannot be evaluated.

Flow source and sink blocks are used to model the secondary side of the heat exchangers, which allow the user to enter thermodynamic information without additional loops and external dynamics. Additionally, a buss structure is used to wire the components, allowing for multiple signals to be transferred in a given line. The environment is capable of running with both fixed and variable step solvers, which allow for a faster than real time execution of the models. Depending on the solver used and the complexity of the system model, models have executed as fast as 400 times real time [37].

Chapter 3

Exergy

In this chapter, exergy is introduced and analyzed as a tool to quantize the efficiency of a given system. Additionally, the efficiency of the four component vapor-compression cycle system (VCS) is studied, both at the total system level and at the component level.

3.1 Introduction to exergy

When using an efficiency metric to characterize a system, it is possible to fall into a trap where the efficiency metric takes into account too little information to paint a complete picture of the operation of the system. This is the case when one uses a purely 'first law efficiency' [10][21], such as coefficient of performance (COP). This type of efficiency refers to the first law of thermodynamics, which says that the difference between the energy from a system and the energy supplied to the system must be the change in internal energy of the system. First law efficiencies do not address the maximum amount of work that could have been extracted from the system, only the quantitative value of that work. When the second law of thermodynamics is included in the analysis, it is possible to determine how close to optimal a system is performing. This efficiency is fittingly named a 'second law efficiency' [10][21], more commonly known as an exergetic efficiency.

3.1.1 Benefit of exergy

Exergy is a thermodynamic quantity which combines the first and second laws of thermodynamics. The first law is used to determine how efficiently a system is performing from a thermal perspective and the second law compares the system to an ideal system with no

irreversibilities. Exergy can be used as an efficiency metric when the relative amount of exergy destroyed during a specific process is compared to the exergy supplied to the system.

To understand the benefit of incorporating the second law, Figure 3.1 shows two systems performing with the same thermal efficiency e.g. same COP [21]. Under the first law of thermodynamics, the two systems are performing equally as well. However, if system B has a larger temperature difference between the high temperature and low temperature sinks, then more energy is available to system B than to system A. This is apparent by looking at the efficiency if the two engines were operating completely reversibly, Equations 3.1 and 3.2. Therefore, for system B to have the same thermal efficiency as system A, system B must be squandering the excess energy from the larger thermal gradient. Using Equation 3.3 to calculate the exergy efficiency of the two systems, system A is 60% efficient and system B is 43% efficient.

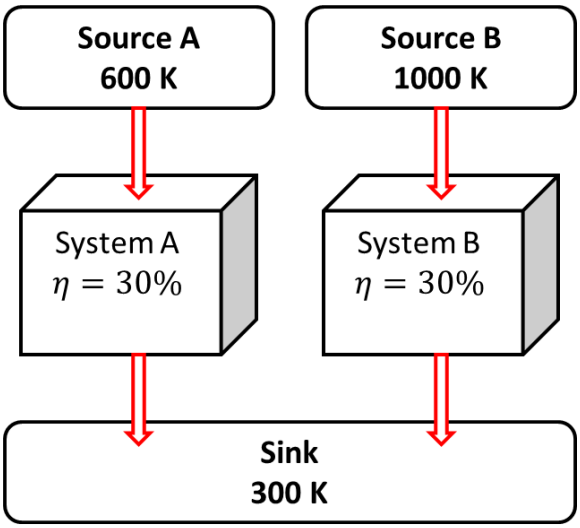

Figure 3.1: Exergy comparison of two systems

$$\eta_{rev,A} = \left(1 - \frac{T_L}{T_H}\right) = \left(1 - \frac{300}{600}\right) = 50\% \tag{3.1}$$

$$\eta_{rev,B} = \left(1 - \frac{T_L}{T_H}\right) = \left(1 - \frac{300}{1000}\right) = 70\% \tag{3.2}$$

$$\eta_{exergy} = \frac{\eta_{thermal}}{\eta_{reversible}} \tag{3.3}$$

3.1.2 Sources of exergy

Exergy, or availability, can be thought of as the work potential in a system [10]. Consistent with the definition of all potentials, there exists a "dead state" for exergy, which is the point where the system is in thermodynamic equilibrium with its surroundings. In Figure 3.2, the dead state is indicated by the orange cloud. The dead state is an infinite reservoir, such as the ambient environment, with which the system interacts. At this dead state, there is no ability for the system to do work. When denoting exergy of a system, the dead state is identified by the *0* subscripts on variables.

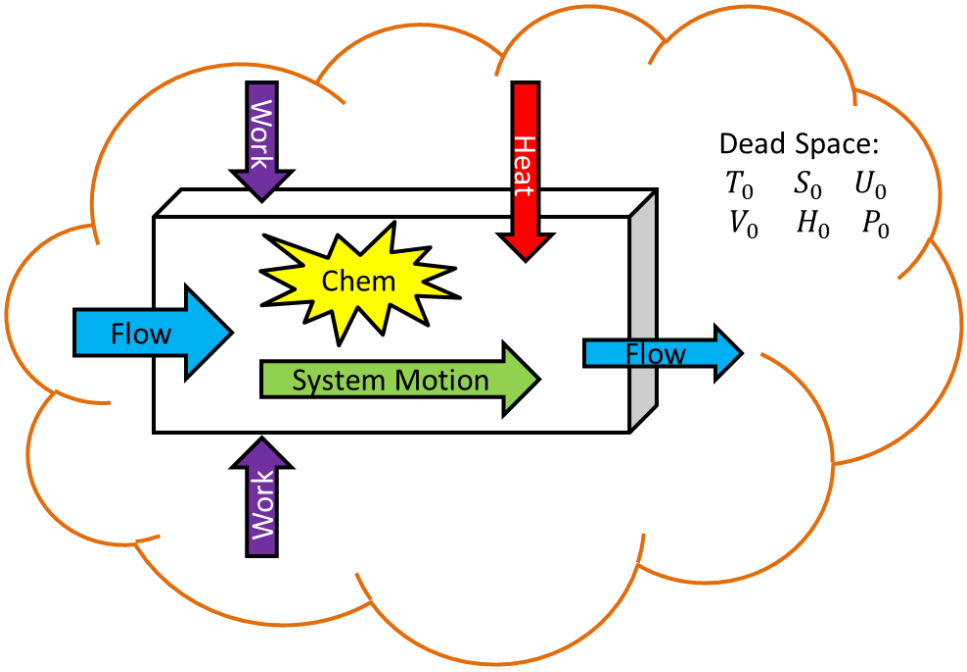

Figure 3.2: Exergy sources for a sample system

An all-inclusive definition for exergy efficiency is given in Equation 3.4, with the subsequent equations providing more detailed definitions of exergy. Exergy can be catalogued by the closed system exergy (Equation 3.5), through mass flow across component boundaries (Equation 3.6), through heat (Equation 3.7), and through work (Equation 3.8) [21].

$$\eta_X = 1 - \frac{exergy\ destroyed}{exergy\ supplied} \tag{3.4}$$

$$X_{cs} = (U - U_0) + P_0(V - V_0) - T_0(S - S_0) + m\frac{v^2}{2} + mgz \tag{3.5}$$

$$X_{flow} = (H - H_0) - T_0(S - S_0) + m\frac{v^2}{2} + mgz \tag{3.6}$$

$$X_{heat} = \left(1 - \frac{T_0}{T}\right) Q \tag{3.7}$$

$$X_{work} = W \quad or \quad X_{work} = W - W_{surr} \tag{3.8}$$

Using Figure 3.2 as an example, the closed system energy is shown through the green motion of the system, resulting in exergy due to kinetic energy. The blue mass flow into the system is larger than the exit mass flow, resulting in an increased system exergy (if the thermodynamic properties of the fluid have not changed). Heat is injected into the system via the red arrow and work is done on the system through the purple, compressive arrows. For completeness, exergy due to chemical changes within the system is denoted by the yellow explosion.

The exergy transferred by work must incorporate the work done by the surroundings, Equation 3.8, as a system may be able to take advantage of this work (or be required to actively oppose it) resulting in a decrease (or increase) of the change in exergy from the dead state. It should also be noted that exergy may be included in the system due to chemical changes, X_{chem}. However, such terms are beyond the scope of this document and unnecessary to the analysis of VCSs. Simplifying assumptions and physical behavior would cause many of these terms to drop out of the equations. Even with those simplifications, cataloging the various sources of exergy is no small task.

3.1.3 Constraints on exergy

Exergy stems from a combination of the first and second laws of thermodynamics. Therefore, constraints placed upon those laws will also affect exergy. The first law of thermodynamics holds that energy cannot be created or destroyed, it can only change form. The second law states that entropy must increase for a real system, or at minimum, remain constant for a perfectly reversible system. The Gouy-Stodola theorem [39] shows that

$$X_{dest} = T_0 S_{gen} \geq 0 \tag{3.9}$$

Equation 3.9 indicates that there must be some quantitative amount of energy potential which is destroyed during system operation, due to irreversibilities. As with entropy, the exergy

destruction of a system is bounded below by zero. Zero exergy destruction corresponds with a perfectly reversible system.

3.2 Exergy auditing in a VCS [22]

The following derivation of exergy for each specific component of the VCS is heavily based on the work performed in [22]. Jain performed a dynamic exergy analysis for each of the four major components within the VCS, as well as exploring a novel method of addressing the entropy derivatives created in the dynamic analysis. The work from [22] is presented below for continuity and clarity.

There are many choices of control volumes within a VCS. Figure 3.3 demonstrates one particular choice. In this selection of the control volumes, only the refrigerant side is considered, thus ignoring any thermal capacitance of the component walls. Both the valve and compressor have a single control volume whereas the evaporator and condenser have a unique control volume for each phase of refrigerant. Recall from Section 2.2.2 that many thermodynamic properties can be considered constant within a given refrigerant zone.

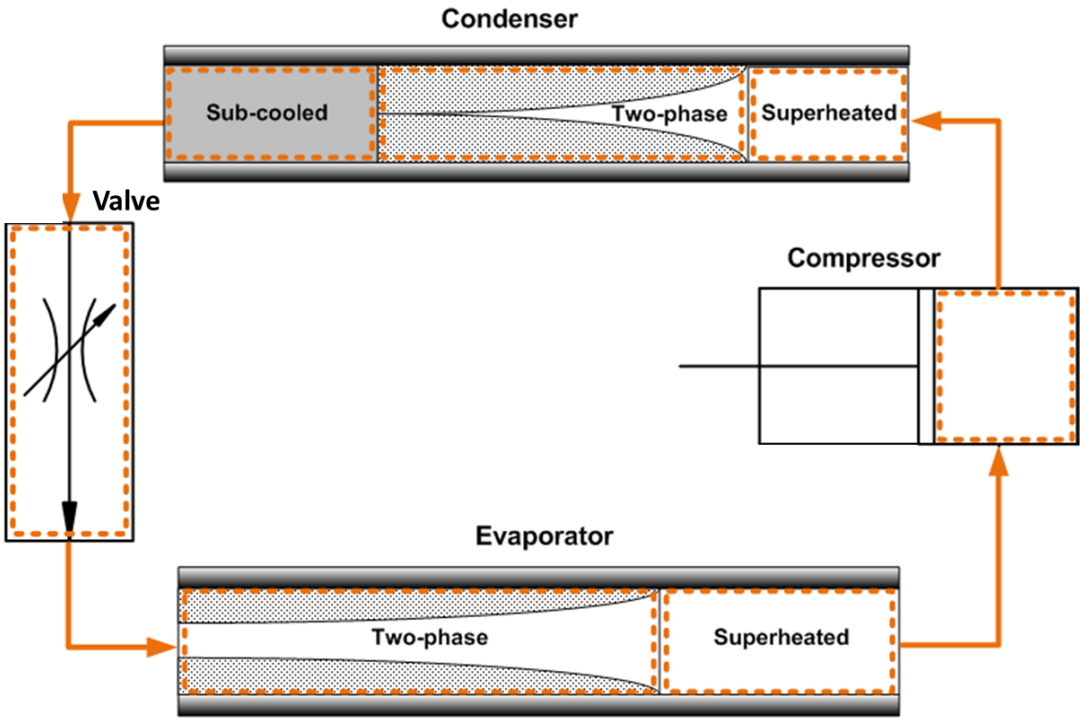

Figure 3.3: Control volume assignments in a VCS

From a combination of the first and second laws acting on a given control volume, it is possible to define the rate equation of exergy destruction as

$$\frac{dX_{cv}}{dt} = \frac{dE_{cv}}{dt} - T_0 \frac{dS_{cv}}{dt} \tag{3.10}$$

where

$$\frac{dE_{cv}}{dt} = \dot{Q} - \dot{W} + \sum_{in} \dot{m}_{in} \left(h_{in} + \frac{v_{in}^2}{2} + g z_{in} \right) - \sum_{out} \dot{m}_{out} \left(h_{out} + \frac{v_{out}^2}{2} + g z_{out} \right) \tag{3.11}$$

$$\frac{dS_{cv}}{dt} = \sum_j \frac{\dot{Q}_j}{T_j} + \sum_{in} \dot{m}_{in} s_{in} - \sum_{out} \dot{m}_{out} s_{out} + \dot{S}_{gen} \tag{3.12}$$

The j indexing terms in Equation 3.12 apply for every location where the instantaneous temperature is given by T_j. If the control volumes are chosen as shown in Figure 3.3, $j = 1,2,3$ for the condenser and $j = 1,2$ for the evaporator, where the numbers correspond to a given refrigerant phase. The rate form of Equation 3.9 is used to supply $\dot{S}_{gen}$ in Equation 3.12.

Combining Equations 3.11 and 3.12 into Equation 3.10 gives the total rate of exergy destruction in a control volume.

$$\frac{dX_{cv}}{dt} = \sum_j \left(1 - \frac{T_0}{T_j} \right) \dot{Q}_j - \left(\dot{W}_{cv} - P_0 \frac{dV_{cv}}{dt} \right) + \left(\sum_{in} \dot{m}_{in} \psi_{in} - \sum_{out} \dot{m}_{out} \psi_{out} \right) - \dot{X}_{dest} \tag{3.13}$$

where ψ refers to the specific flow exergy, defined as

$$\psi = (h - h_0) - T_0 (s - s_0) + \frac{v^2}{2} + g z + \psi_{chem} \tag{3.14}$$

The *0* subscript refers to the dead state, or reference environment, at which point, there is no work potential (exergy) of the system.

Exergy obeys superposition [21], which means that the exergy of the complete system can be expressed as a linear sum of the individual components, shown explicitly in Equation 3.15.

$$\dot{X}_{dest,VCS} = \dot{X}_{dest,v} + \dot{X}_{dest,k} + \dot{X}_{dest,e} + \dot{X}_{dest,c} \tag{3.15}$$

The subscripts denote the valve, compressor, evaporator, and condenser, respectively. For the analysis that follows, the dead state is the ambient environment for all components.

3.2.1 Valve

As introduced in Section 2.2.1, the valve is a static component in the VCS. Due to the physical operation of the valve, a fluid entering has the same enthalpy as a fluid leaving. The control volume for the valve is chosen to be the refrigerant contained within the valve at any given time, Figure 3.4.

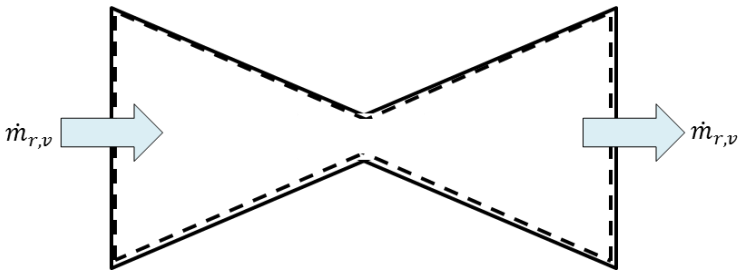

Figure 3.4: Control volume for the valve

Beginning from Equations 3.13 and 3.14, and taking steady state operation (so that $\frac{dX_{cv}}{dt}$ is zero) and isenthalpic expansion, as well as assuming a static component with no kinetic or potential energy changes and no exergy transfer except by mass flow rate (i.e. no heat transfer or boundary work), the resulting expression for the rate of exergy destruction is

$$\dot{X}_{dest,v} = -T_H \dot{m}_{v,r}\left(s_{v,ri} - s_{v,ro}\right) \tag{3.16}$$

The dead state temperature has been replaced by the high side sink temperature, as this is the ambient environment with which the system is interacting.

3.2.2 Compressor

Similar to the valve, the compressor is assumed to be a static component during system operation. While it is common to apply an isentropic assumption to the fluid entering a leaving the compressor, the exergy analysis will be more accurate by assuming non-isentropic compression of the refrigerant within the compressor. The compressor control volume is drawn as shown in Figure 3.5, which contains the refrigerant being compressed and does not include the compressor piston or shell.

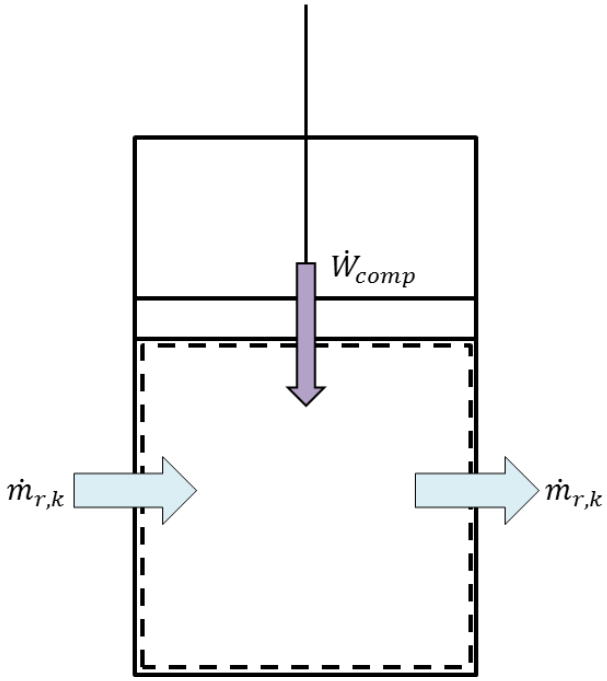

Figure 3.5: Control volume for the compressor

By assuming the compressor is adiabatic, with no potential and kinetic energy contributions, the steady state rate of exergy destruction for a refrigerant in the compressor is given as

$$\dot{X}_{dest,k} = -\left(-\dot{W}_{comp}\right) + \dot{m}_{k,r}\left[\left(h_{k,ri} - h_{k,ro}\right) - T_H\left(s_{k,ri} - s_{k,ro}\right)\right] \tag{3.17}$$

The double negative proceeding the work term is to denote that this is work done *on* the system in order to achieve the desired results. The expression for the rate of work is

$$\dot{W}_{comp} = \dot{m}_{k,r}\left(h_{k,ro} - h_{k,ri}\right) \tag{3.18}$$

which produces a simplified equation for the exergy destruction

$$\dot{X}_{dest,k} = -T_H\dot{m}_{k,r}\left(s_{k,ri} - s_{k,ro}\right) \tag{3.19}$$

3.2.3 Evaporator

As discussed in Section 2.2.2, the evaporator can be modeled using a lumped parameter approach, which assumes specific parameters to be uniform in each phase of the refrigerant [5][25][26][27][28][29]. The wall temperature of the evaporator pipe is one such constant

parameter. As shown in Equation 3.13, the heat transfer can be summed at each location with a unique temperature. Therefore, the exergy analysis of the evaporator lends itself to performing an exergy balance in each refrigerant zone and combining the two zones together to express the complete evaporator exergy balance, as shown in Figure 3.6. For this analysis, the control volume only encompasses the refrigerant, thus neglecting any influence from the thermal capacitance of the wall except where the heat transfer is concerned.

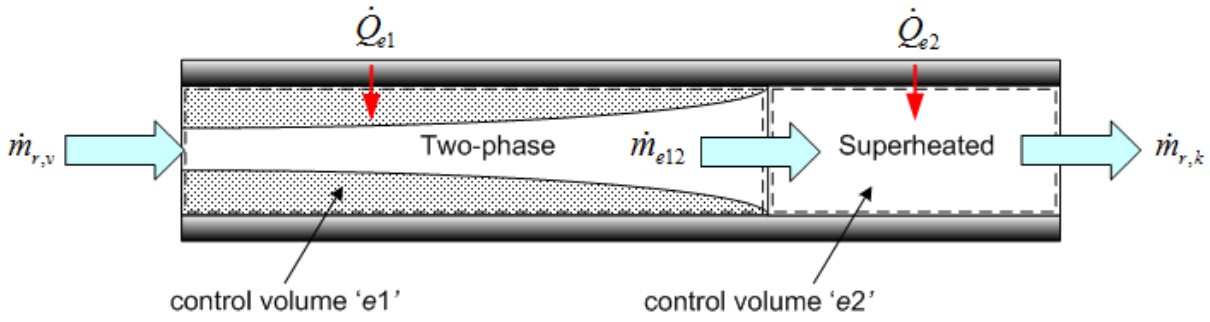

Figure 3.6: Control volume for the evaporator

With the evaporator, there is no exergy transfer by kinetic or potential energy but work is done on the two refrigerant zones through the relative volume changes of the zones. However, due to the large time scales of thermal dynamics, the evaporator must be modeled as a dynamic component. [11] provides a simplified analysis in which the thermal dynamics are ignored. Therefore, the exergy analysis becomes

$$\frac{dX_{e1}}{dt} = \left(1 - \frac{T_H}{T_{e1,w}}\right)\dot{Q}_{e1} + P_0\frac{dV_{e1}}{dt} + \left[\dot{m}_{v,r}\left(h_{e,ri} - T_H s_{e,ri}\right)\right. \tag{3.20}$$

$$\left. - \dot{m}_{e12}\left(h_{e,g} - T_H s_{e,g}\right)\right] - \dot{X}_{dest,e1}$$

$$\frac{dX_{e2}}{dt} = \left(1 - \frac{T_H}{T_{e2,w}}\right)\dot{Q}_{e2} + P_0\frac{dV_{e2}}{dt} + \left[\dot{m}_{e12}\left(h_{e,g} - T_H s_{e,g}\right)\right. \tag{3.21}$$

$$\left. - \dot{m}_{k,r}\left(h_{e,ro} - T_H s_{e,ro}\right)\right] - \dot{X}_{dest,e2}$$

where the two phase refrigerant region is denoted by the $e1$ and the superheated region is denoted by $e2$. The internal mass flow rate between the two regions is given by $\dot{m}_{e12}$ and the inlet and outlet flow rates are specified by the valve and compressor, respectively. Additionally,

due to the division between the two phase and gaseous regions occurring at the saturation line, the g subscript denotes the saturation parameters at the vapor line.

Applying superposition of exergy within the evaporator

$$\dot{X}_{dest,e} = \dot{X}_{dest,e1} + \dot{X}_{dest,e2} \tag{3.22}$$

allows the total exergy destruction within the evaporator to be expressed as

$$\dot{X}_{dest,e} = \left(1 - \frac{T_H}{T_{e1,w}}\right)\dot{Q}_{e1} + \left(1 - \frac{T_H}{T_{e2,w}}\right)\dot{Q}_{e2} + P_0\left(\frac{dV_{e1}}{dt} + \frac{dV_{e2}}{dt}\right) \tag{3.23}$$

$$+ \left[\dot{m}_{v,r}\left(h_{e,ri} - T_H s_{e,ri}\right) - \dot{m}_{k,r}\left(h_{e,ro} - T_H s_{e,ro}\right)\right] - \left(\frac{dX_{e1}}{dt} + \frac{dX_{e2}}{dt}\right)$$

There is assumed to be no heat transfer from one refrigerant zone to the other, such that all of the heat transfer occurs radially. Therefore,

$$\dot{Q}_e = \dot{Q}_{e1} + \dot{Q}_{e2} = (UA)_{e1}\left(T_{e1,w} - T_{e1,r}\right) + (UA)_{e2}(T_{e2,w} - T_{e2,r}) \tag{3.24}$$

This result is difficult to apply, since the exergy derivatives for the control volumes are not easy to evaluate. It is possible to obtain an equation for the exergy destruction from a different approach. Beginning with Equation 3.12 and evaluating at each of the zones

$$\frac{dS_{e1}}{dt} = \frac{\dot{Q}_{e1}}{T_{e1,w}} + \left(\dot{m}_{v,r}s_{e,ri} - \dot{m}_{e12}s_{e,g}\right) + \dot{S}_{e1,gen} \tag{3.25}$$

$$\frac{dS_{e2}}{dt} = \frac{\dot{Q}_{e2}}{T_{e2,w}} + \left(\dot{m}_{e12}s_{e,g} - \dot{m}_{k,r}s_{e,ro}\right) + \dot{S}_{e2,gen} \tag{3.26}$$

Using the superposition of the entropy equation [21] and the Gouy-Stodola theorem [39]

$$\dot{X}_{dest,e} = T_H\dot{S}_{e,gen} = -T_H\left(\frac{\dot{Q}_{e1}}{T_{e1,w}} + \frac{\dot{Q}_{e2}}{T_{e2,w}}\right) - T_H\left(\dot{m}_{v,r}s_{e,ri} - \dot{m}_{k,r}s_{e,ro}\right) + T_H\left(\frac{dS_{e1}}{dt} + \frac{dS_{e2}}{dt}\right) \tag{3.27}$$

The entropy derivatives will be addressed in Section 3.2.5.

3.2.4 Condenser

As with the evaporator, the condenser can be broken up into three distinct regions, based on the phase of the refrigerant in each region. Due to the wall temperature being considered constant within each region, the exergy control volume approach may be applied at each distinct

region and combined through superposition. Again, the control volume only encompasses the refrigerant and does not consider the heat exchanger walls.

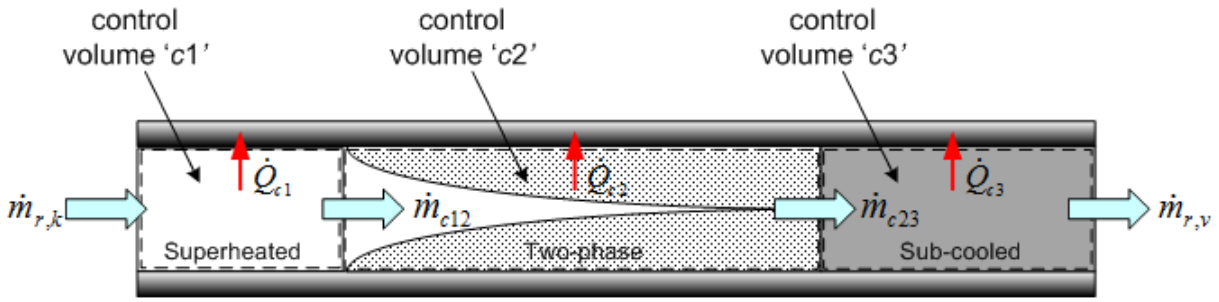

Figure 3.7: Control volume for the condenser

No exergy transfer occurs from kinetic, or potential energy but work is done on the three refrigerant zones through the relative volume changes of the zones. Due to the large time constant of thermal dynamics, the exergy derivative for each of the control volumes becomes

$$\frac{dX_{c1}}{dt} = \left(1 - \frac{T_H}{T_{c1,w}}\right)\dot{Q}_{c1} + P_0\frac{dV_{c1}}{dt} + [\dot{m}_{k,r}(h_{c,ri} - T_H s_{c,ri}) - \dot{m}_{c12}(h_{c,g} - T_H s_{c,g})] - \dot{X}_{dest,c1} \tag{3.28}$$

$$\frac{dX_{c2}}{dt} = \left(1 - \frac{T_H}{T_{c2,w}}\right)\dot{Q}_{c2} + P_0\frac{dV_{c2}}{dt} + [\dot{m}_{c12}(h_{c,g} - T_H s_{c,g}) - \dot{m}_{c23}(h_{c,f} - T_H s_{c,f})] - \dot{X}_{dest,c2} \tag{3.29}$$

$$\frac{dX_{c3}}{dt} = \left(1 - \frac{T_H}{T_{c3,w}}\right)\dot{Q}_{c3} + P_0\frac{dV_{c3}}{dt} + \dot{m}_{c23}(h_{c,f} - T_H s_{c,f}) - \dot{m}_{v,r}(h_{c,ro} - T_H s_{c,ro})] - \dot{X}_{dest,c3} \tag{3.30}$$

where the superheated refrigerant region is denoted by $c1$, the two phase region denoted by $c2$, and the subcooled region denoted by $c3$. The two internal mass flow rates are given by $\dot{m}_{c12}$ and $\dot{m}_{c23}$, with the inlet and outlet mass flow rates specified by the compressor and valve, respectively. Since the boundaries between the refrigerant zones are taken to be the saturation line, the g subscript refers to the gaseous saturation line and the f subscript refers to the liquid saturation line. [11] provides a simplified analysis in which the thermal dynamics are ignored.

Applying superposition of exergy within the condenser

$$\dot{X}_{dest,c} = \dot{X}_{dest,c1} + \dot{X}_{dest,c2} + \dot{X}_{dest,c3} \tag{3.31}$$

allows the total exergy destruction within the condenser to be expressed as

$$\dot{X}_{dest,c} = \left(1 - \frac{T_H}{T_{c1,w}}\right)\dot{Q}_{c1} + \left(1 - \frac{T_H}{T_{c2,w}}\right)\dot{Q}_{c2} + \left(1 - \frac{T_H}{T_{c3,w}}\right)\dot{Q}_{c3} + P_0\left(\frac{dV_{e1}}{dt} + \frac{dV_{e2}}{dt}\right) \tag{3.32}$$

$$\left[\dot{m}_{k,r}\left(h_{c,ri} - T_H s_{c,ri}\right) - \dot{m}_{v,r}\left(h_{c,ro} - T_H s_{c,ro}\right)\right] - \left(\frac{dX_{c1}}{dt} + \frac{dX_{c2}}{dt} + \frac{dX_{c3}}{dt}\right)$$

There is assumed to be no heat transfer from one refrigerant zone to the other, such that all of the heat transfer occurs radially. Therefore,

$$\dot{Q}_c = \dot{Q}_{c1} + \dot{Q}_{c2} + \dot{Q}_{c3} \tag{3.33}$$

$$= (UA)_{c1}\left(T_{c1,w} - T_{c1,r}\right) + (UA)_{c2}(T_{c2,w} - T_{c2,r}) + (UA)_{c3}(T_{c3,w} - T_{c3,r})$$

Again, the problem arises that the exergy derivatives in Equation 3.32 make the result difficult to apply. Therefore, repeating the same procedure in the evaporator and using the entropy derivative allows a more manageable solution to the exergy destruction within the condenser.

$$\frac{dS_{c1}}{dt} = \frac{\dot{Q}_{c1}}{T_{c1,w}} + \left(\dot{m}_{k,r}s_{c,ri} - \dot{m}_{c12}s_{c,g}\right) + \dot{S}_{c1,gen} \tag{3.34}$$

$$\frac{dS_{c2}}{dt} = \frac{\dot{Q}_{c2}}{T_{c2,w}} + \left(\dot{m}_{c12}s_{c,g} - \dot{m}_{c23}s_{c,f}\right) + \dot{S}_{c2,gen} \tag{3.35}$$

$$\frac{dS_{c3}}{dt} = \frac{\dot{Q}_{c3}}{T_{c3,w}} + \left(\dot{m}_{c23}s_{e,f} - \dot{m}_{v,r}s_{c,ro}\right) + \dot{S}_{c3,gen} \tag{3.36}$$

Using the superposition of the entropy equation [21] and the Gouy-Stodola theorem [39]

$$\dot{X}_{dest,c} = T_H\dot{S}_{c,gen} = -T_H\left(\frac{\dot{Q}_{c1}}{T_{c1,w}} + \frac{\dot{Q}_{c2}}{T_{c2,w}} + \frac{\dot{Q}_{c3}}{T_{c3,w}}\right) \tag{3.37}$$

$$-T_H\left(\dot{m}_{k,r}s_{c,ri} - \dot{m}_{v,r}s_{c,ro}\right) + T_H\left(\frac{dS_{c1}}{dt} + \frac{dS_{c2}}{dt} + \frac{dS_{c3}}{dt}\right)$$

The entropy derivatives will be addressed in Section 3.2.5.

3.2.5 Entropy terms

Doty, Camberos, and Yerkes proposed a method for evaluating an entropy derivative in unsteady operation [40]. The entropy derivative is broken up by chain rule into the part that is dependent on mass and the part that is not

$$\frac{dS_{cv}}{dt} = \frac{d}{dt}\{m_{cv} \cdot s_{cv}(var1, var2)\} = \frac{dm_{cv}}{dt}\{s_{cv}(var1, var2)\} + \frac{ds_{cv}}{dt}\{m_{cv}\} \tag{3.38}$$

$$\frac{ds_{cv}}{dt} = \frac{\partial s_{cv}}{\partial var1}\Big|_{var2}\left(\frac{dvar1}{dt}\right) + \frac{\partial s_{cv}}{\partial var2}\Big|_{var1}\left(\frac{dvar2}{dt}\right) \tag{3.39}$$

$$\frac{dS_{cv}}{dt} = s_{cv}\frac{dm_{cv}}{dt} + m_{cv}\left\{\frac{\partial s_{cv}}{\partial var1}\Big|_{var2}\left(\frac{dvar1}{dt}\right) + \frac{\partial s_{cv}}{\partial var2}\Big|_{var1}\left(\frac{dvar2}{dt}\right)\right\} \tag{3.40}$$

where *var1* and *var2* refer to two variables which affect the entropy but produce time derivatives which are not dependent on another parameter. Equation 3.40 highlights the versatility of the lumped parameter approach. By dividing the heat exchanger into regions where one parameter may be favorable to use over another, $\frac{dS_{cv}}{dt}$ can be evaluated optimally for a region, and then combined across all phases in the heat exchanger to produce a complete analysis. To express this result, consider the derivation for $\frac{dS_{cv}}{dt}$ in the evaporator two phase region, given below.

In the two phase region, the entropy derivative is described using the refrigerant mean void fraction, $\bar{\gamma}$, and the pressure. The mean void fraction is related to the mean quality by

$$\bar{x} = \bar{\gamma}\frac{\rho_g}{\rho} \tag{3.41}$$

Using Equation 3.40, mean void fraction, and pressure

$$\frac{dS_{e1}}{dt} = s_{e1}\frac{dm_{e1}}{dt} + m_{e1}\left\{\frac{\partial s_{e1}}{\partial \bar{\gamma}_e}\Big|_{P}\left(\frac{d\bar{\gamma}_e}{dt}\right) + \frac{\partial s_{e1}}{\partial P_e}\Big|_{\bar{\gamma}}\left(\frac{dP_e}{dt}\right)\right\} \tag{3.42}$$

$$\frac{dm_{e1}}{dt} = \left(\dot{m}_{v,r} - \dot{m}_{e12}\right) + \rho_{e,g}A_{e,CR}L_{e,R}\frac{d\zeta_{e1}}{dt} \tag{3.43}$$

$$s_{e1} = \bar{x}_e s_{e,g} + (1 - \bar{x}_e)s_{e,l} \tag{3.44}$$

The mass contained in the two phase region can be expressed as

$$m_{e1} = \rho_{e1}\zeta_{e1}L_{e,R}A_{e,CR} \tag{3.45}$$

Applying Equation 3.41 to Equation 3.44 yields

$$s_{e1} = \frac{\bar{\gamma}_e \rho_{e.g} s_{e,g} + (1-\bar{\gamma}) \rho_{e,f} s_{e,f}}{\bar{\gamma}_e \rho_{e.g} + (1-\bar{\gamma}) \rho_{e,f}} \tag{3.46}$$

This equation can now be used to evaluate $\left.\frac{\partial s_{e1}}{\partial \bar{\gamma}_e}\right|_P$ and $\left.\frac{\partial s_{e1}}{\partial P_e}\right|_{\bar{\gamma}}$

$$\left.\frac{\partial s_{e1}}{\partial \bar{\gamma}_e}\right|_P = \frac{(\bar{\gamma}_e \rho_{e.g} + (1-\bar{\gamma}) \rho_{e,f})(\rho_{e.g} s_{e,g} - \rho_{e,f} s_{e,f}) - (\bar{\gamma}_e \rho_{e.g} s_{e,g} + (1-\bar{\gamma}) \rho_{e,f} s_{e,f})(\rho_{e.g} - \rho_{e,f})}{(\bar{\gamma}_e \rho_{e.g} + (1-\bar{\gamma}) \rho_{e,f})^2} \tag{3.47}$$

$$\left.\frac{\partial s_{e1}}{\partial P_e}\right|_{\bar{\gamma}} = \frac{\beta_1 - \beta_2}{\beta_3} \tag{3.48}$$

where

$$\beta_1 = (\bar{\gamma}_e \rho_{e.g} + (1-\bar{\gamma}) \rho_{e,f})(\bar{\gamma}_e \rho_{e.g} \frac{ds_{e,g}}{dP_e} + \bar{\gamma}_e s_{e,g} \frac{d\rho_{e,g}}{dP_e} + (1-\bar{\gamma}) \rho_{e,f} \frac{ds_{e,f}}{dP_e} + (1-\bar{\gamma}) s_{e,f} \frac{d\rho_{e,}}{dP_e}) \tag{3.49}$$

$$\beta_2 = (\bar{\gamma}_e \rho_{e.g} s_{e,g} + (1-\bar{\gamma}) \rho_{e,f} s_{e,f}) \left(\bar{\gamma}_e \frac{d\rho_{e,g}}{dP_e} + (1-\bar{\gamma}) \frac{d\rho_{e,f}}{dP_e}\right) \tag{3.50}$$

$$\beta_3 = (\bar{\gamma}_e \rho_{e.g} + (1-\bar{\gamma}) \rho_{e,f})^2 \tag{3.51}$$

Evaluating Equation 3.40 for the evaporator superheat region, using enthalpy and pressure, yields

$$\frac{dS_{e2}}{dt} = s_{e2} \frac{dm_{e2}}{dt} + \rho_{e2} \zeta_{e2} L_{e,R} A_{e,CR} \left\{\left.\frac{\partial s_{e2}}{\partial h_{e2}}\right|_P \left(\frac{dh_{e2}}{dt}\right) + \left.\frac{\partial s_{e2}}{\partial P_e}\right|_h \left(\frac{dP_e}{dt}\right)\right\} \tag{3.52}$$

$$\frac{dm_{e2}}{dt} = (\dot{m}_{e12} - \dot{m}_{k,r}) + \rho_{e,g} A_{e,CR} L_{e,R} \frac{d\zeta_{e1}}{dt} \tag{3.53}$$

The condenser can be evaluated in the same way. For the superheated region, using enthalpy and pressure,

$$\frac{dS_{c1}}{dt} = s_{c1} \frac{dm_{c1}}{dt} + \rho_{c1} \zeta_{c1} L_{c,R} A_{c,CR} \left\{\left.\frac{\partial s_{c1}}{\partial h_{c1}}\right|_P \left(\frac{dh_{c1}}{dt}\right) + \left.\frac{\partial s_{c1}}{\partial P_c}\right|_h \left(\frac{dP_c}{dt}\right)\right\} \tag{3.54}$$

$$\frac{dm_{c1}}{dt} = (\dot{m}_{k,r} - \dot{m}_{c12}) + \rho_{c,g} A_{c,CR} L_{c,R} \frac{d\zeta_{c1}}{dt} \tag{3.55}$$

For the two phase region, using mean void fraction and pressure

$$\frac{dS_{c2}}{dt} = s_{c2}\frac{dm_{c2}}{dt} + \rho_{c2}\zeta_{c2}L_{c,R}A_{c,CR}\left\{\frac{\partial s_{c2}}{\partial \bar{\gamma}_c}\Big|_P\left(\frac{d\bar{\gamma}_c}{dt}\right) + \frac{\partial s_{c2}}{\partial P_c}\Big|_{\bar{\gamma}}\left(\frac{dP_c}{dt}\right)\right\} \quad (3.56)$$

$$\frac{dm_{c2}}{dt} = (\dot{m}_{c12} - \dot{m}_{c23}) + \rho_{c,f}A_{c,CR}L_{c,R}\left(\frac{d\zeta_{c1}}{dt} + \frac{d\zeta_{c2}}{dt}\right) - \rho_{c,g}A_{c,CR}L_{c,R}\frac{d\zeta_{c1}}{dt} \quad (3.57)$$

For the subcooled region, using enthalpy and pressure

$$\frac{dS_{c3}}{dt} = s_{c3}\frac{dm_{c3}}{dt} + \rho_{c3}\zeta_{c3}L_{c,R}A_{c,CR}\left\{\frac{\partial s_{c3}}{\partial h_{c3}}\Big|_P\left(\frac{dh_{c3}}{dt}\right) + \frac{\partial s_{c3}}{\partial P_c}\Big|_h\left(\frac{dP_c}{dt}\right)\right\} \quad (3.58)$$

$$\frac{dm_{c3}}{dt} = \left(\dot{m}_{c23} - \dot{m}_{v,r}\right) + \rho_{c,f}A_{,CR}L_{c,R}\left(\frac{d\zeta_{c1}}{dt} + \frac{d\zeta_{c2}}{dt}\right) \quad (3.59)$$

While complicated, the entropy derivatives for the evaporator and condenser offer a means of calculating the exergy destruction within the two heat exchangers without resorting to taking an exergy derivative. With these terms, there is a clear, transient calculation for exergy destruction in every component of the VCS.

3.3 Expansion of control volume analysis

The control volumes used for the VCS analysis thus far have been restricted to the refrigerant side of the system. It is possible to expand the control volumes of interest further than the refrigerant to obtain a better understanding of the component interaction with its near surroundings. Two examples are given below: the compressor interaction with its metal shell and the inclusion of the fan work used to move the secondary side fluid in the heat exchangers.

3.3.1 Compressor shell interaction

Due to friction and other internal losses, a compressor in operation will generate some heat. This heat is distributed across the compressor shell. As previously discussed in Section 2.2.1.2, the heating of the compressor shell is transferred to the refrigerant by using a first order filter and the instantaneous temperature of the compressor shell can be determined through an energy balance. The compressor will also be venting the excess heat to the ambient environment, as shown in Figure 3.8. An exergy balance can be performed on the compressor shell to determine the relative efficiency of conduction.

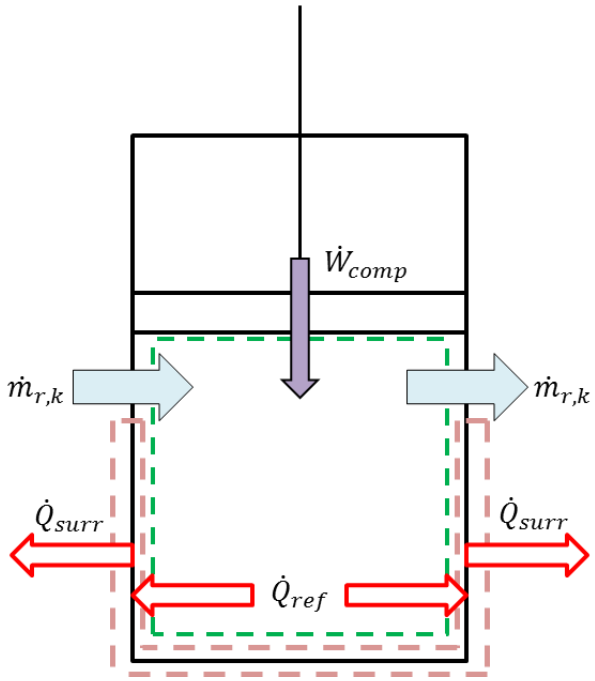

Figure 3.8: Compressor with expanded control volume

In Figure 3.8, the green control volume represents the refrigerant, for which the exergy analysis can be found in Section 3.2.2. The pink control volume represents the compressor shell. Since there is no work, mass flow, kinetic energy, or potential energy changes in the shell, the exergy balance becomes

$$\frac{dX_{cv}}{dt} = \left(1 - \frac{T_H}{T_{shell}}\right)\left(\dot{Q}_{ref} - \dot{Q}_{surr}\right) - \dot{X}_{dest} \tag{3.60}$$

3.3.2 Heat exchanger interaction with fan work

In Section 3.2, the control volume for the components of the VCS was specifically drawn such that only the refrigerant side was included in the analysis. However, there can be a substantial contribution to exergy destruction through the evaporator and condenser fans. To illustrate this point, Figure 3.9 incorporates an additional control volume around the air side of the condenser. For a physical heat exchanger, this control volume would extend from the frontal area at the heat exchanger inlet to the exhaust. For the condenser interfacing with the ambient environment, the air supplied comes from the dead state. For the evaporator, the supplied air would come from the cooled space.

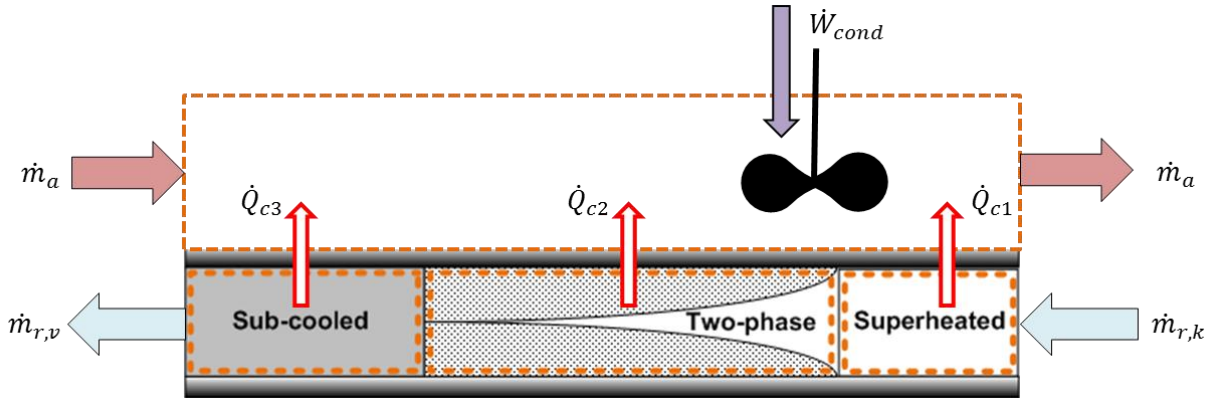

Figure 3.9: Secondary side control volume for the condenser

The following exergy analysis is performed at steady state conditions. It is assumed that there are no lingering thermal dynamics in either of the two fluids or the heat exchanger wall. By assuming no longitudinal conduction in the wall, the heat flow is restricted to be entirely radial and the wall may be neglected without consequence.

The exergy destruction for the three condenser zones are given in Equations 3.61 through 3.63 and for the external control volume in Equation 3.64. When the four control volumes are summed, the final rate of exergy destruction is given in Equation 3.65.

$$\dot{X}_{dest,c1} = -\left(1 - \frac{T_H}{T_{c1,w}}\right)\dot{Q}_{c1} + \left[\dot{m}_{k,r}\left(h_{c,ri} - T_H s_{c,ri}\right) - \dot{m}_{c12}\left(h_{c,g} - T_H s_{c,g}\right)\right] \tag{3.61}$$

$$\dot{X}_{dest,c2} = -\left(1 - \frac{T_H}{T_{c2,w}}\right)\dot{Q}_{c2} + \left[\dot{m}_{c12}\left(h_{c,g} - T_H s_{c,g}\right) - \dot{m}_{c23}\left(h_{c,f} - T_H s_{c,f}\right)\right] \tag{3.62}$$

$$\dot{X}_{dest,c3} = -\left(1 - \frac{T_H}{T_{c3,w}}\right)\dot{Q}_{c3} + \left[\dot{m}_{c23}\left(h_{c,f} - T_H s_{c,f}\right) - \dot{m}_{v,r}\left(h_{c,ro} - T_H s_{c,ro}\right)\right] \tag{3.63}$$

$$\dot{X}_{dest,air} = \left[\left(1 - \frac{T_H}{T_{c1,w}}\right)\dot{Q}_{c1} + \left(1 - \frac{T_H}{T_{c2,w}}\right)\dot{Q}_{c2} + \left(1 - \frac{T_H}{T_{c3,w}}\right)\dot{Q}_{c3}\right] - \left(-\dot{W}_{cond,fan}\right) \tag{3.64}$$
$$+ \dot{m}_{ai}\left(h_{ai} - T_H s_{ai}\right) - \dot{m}_{ao}\left(h_{ao} - T_H s_{ao}\right)$$

$$\dot{X}_{dest,cond} = -\left(-\dot{W}_{cond,fan}\right) + \dot{m}_{ai}\left(h_{ai} - T_H s_{ai}\right) - \dot{m}_{ao}\left(h_{ao} - T_H s_{ao}\right) \tag{3.65}$$
$$+\dot{m}_{k,r}\left(h_{c,ri} - T_H s_{c,ri}\right) - \dot{m}_{v,r}\left(h_{c,ro} - T_H s_{c,ro}\right)$$

The exchange of heat between the internal and external control volumes is entirely motivated by the exergetic properties of the two refrigerant flows and the additional work term. The heat is more of a byproduct of the two flows rather than a driving factor.

Repeating the above analysis for the evaporator results in

$$\dot{X}_{dest,evap} = -\left(-\dot{W}_{evap,fan}\right) + \dot{m}_{ai}(h_{ai} - T_H s_{ai}) - \dot{m}_{ao}(h_{ao} - T_H s_{ao}) \quad (3.66)$$
$$+\dot{m}_{v,r}\left(h_{c,ri} - T_H s_{c,ri}\right) - \dot{m}_{k,r}\left(h_{c,ro} - T_H s_{c,ro}\right)$$

For the VCS at the University of Illinois, it was found that fan power consumption scales as a square of the mass flow rate, see Figure 3.10 and Figure 3.11. When analyzing a VCS to determine locations of inefficiency, it is erroneous to not address the power consumed by the components of the system. The power measurement used to generate the polynomial fits was taken downstream of the AC/DC converter, immediately before entering the fan. While there will be an additional inefficiency caused by the conversion of the electrical power into pneumatic power, it was neglected in this analysis. The limitations of this analysis restrict the system to steady state operation before Equations 3.65 and 3.66 can be accurately applied, as is evidenced by the exclusion of the entropy derivatives in the expression for the total exergy destruction rate.

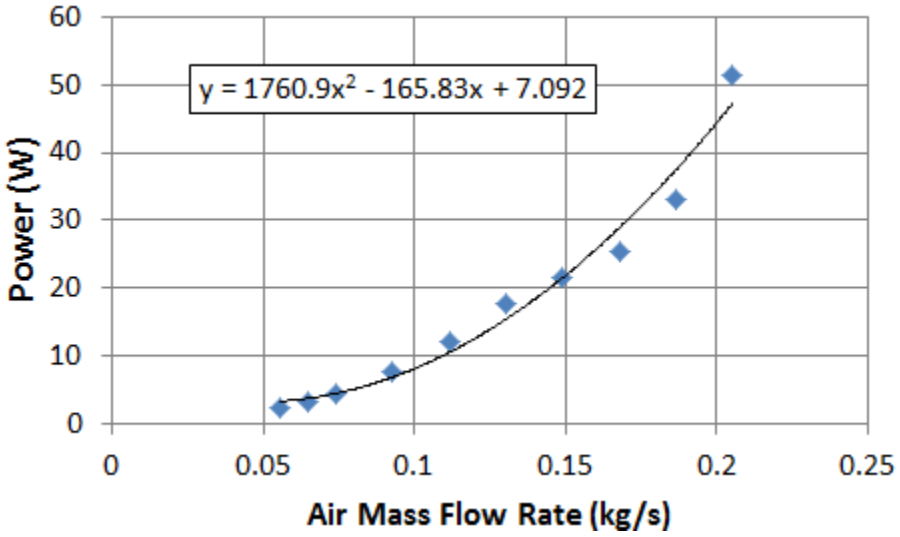

Figure 3.10: Polynomial fit to evaporator fan data

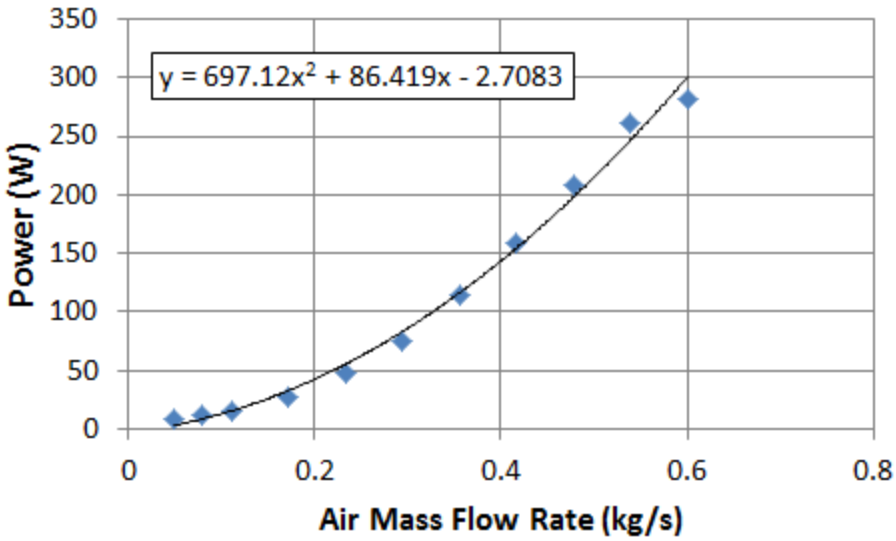

Figure 3.11: Polynomial fit to condenser fan data

In the following chapter, the exergy destruction outlined here will be coupled to an offline, static optimization framework. This framework serves to minimize the total exergy destruction by providing optimal thermodynamic conditions and predictions for actuator input values. Using these recommendations, the exergy destruction for each component can be calculated with the equations presented here and inefficiencies in the system can be addressed.

Chapter 4
Exergy Destruction Minimization Technique

Due to the level of complexity required to solve the exergy equations for a given component and the coupled nature of a system wide exergy optimization, running a system at the exergetic minimum is a two part problem. A non-linear, static system model is used offline to determine the optimal operating points of the system. These optimal points are then passed to the complete system model as set points for a linear quadratic regulator (LQR) controller. In this chapter, the governing equations for the offline optimization model are presented. The use of an LQR controller is justified and the design process of the controller is discussed.

4.1 Multivariable offline optimization

The level of complexity required to fully characterize the exergy destruction within a complete vapor-compression cycle system (VCS) makes a real time, online implementation of a controller to minimize exergy destruction very challenging. The problem is also highly coupled, as comparing one operating point to another may result in better exergy efficiency for one component while giving worse efficiency for another. Both of these characteristics motivate the use of an offline, multivariable minimization solver.

4.1.1 Equivalency of minimization

For a physical system, it is common to optimize the power consumption (or generation), as this quantity is generally related to the monetary cost of operating the system. According to the Gouy-Stodola theorem [39], it is possible to define the exergy destruction rate as

$$\dot{X}_{dest} = \dot{W} - \dot{W}_{rev} \tag{4.1}$$

where $\dot{W}_{rev}$ refers to the work required to operate the system without any irreversibilities. The cost function associated with this system would be

$$J = \dot{X}_{dest} = \dot{W} - \dot{W}_{rev} \tag{4.2}$$

For a specific cooling capacity in a VCS, the reversible work would be constant with respect to the optimization variables [41]. Therefore, the minimum cost can be expressed as

$$\min(J) = \min\left(\dot{W} - \dot{W}_{rev}\right) = \min(\dot{W}) \tag{4.3}$$

Exergy destruction is defined as a non-negative quantity. Therefore, the theoretical best system performance would result in zero exergy destruction. In order to minimize the exergy destruction from the system, one needs to minimize the work required to operate the system.

4.1.2 Exergy in the total system

When exergy destruction is minimized at the system level, it is possible to define the system boundaries around the closed system [21][22]. The only form of exergy transfer is through the work and heat. Equation 4.4 and 4.5 (originally introduced as Equations 3.13 and 3.14) gives a complete analysis of the exergy destruction for an open system.

$$\frac{dX_{cv}}{dt} = \sum_j \left(1 - \frac{T_0}{T_j}\right)\dot{Q}_j - \left(\dot{W}_{cv} - P_0\frac{dV_{cv}}{dt}\right) + \left(\sum_{in}\dot{m}_{in}\psi_{in} - \sum_{out}\dot{m}_{out}\psi_{out}\right) - \dot{X}_{dest} \tag{4.4}$$

$$\psi = (h - h_0) - T_0(s - s_0) + \frac{v^2}{2} + gz + \psi_{chem} \tag{4.5}$$

At steady state operation and with the closed system boundaries defined above

$$\frac{dX_{cv}}{dt} = \sum_j \left(1 - \frac{T_H}{T_j}\right)\dot{Q}_j - \left(-\dot{W}_{VCS}\right) \tag{4.6}$$

$$\frac{dX_{cv}}{dt} = \left(1 - \frac{T_H}{T_L}\right)\dot{Q}_L + \left(1 - \frac{T_H}{T_H}\right)\dot{Q}_H - \left(-\dot{W}_{comp} - \dot{W}_{evap,fan} - \dot{W}_{cond,fan}\right) \tag{4.7}$$

where the dead state temperature is the ambient temperature. The heat transfer from the condenser does not contribute to the total exergy destruction, as it exchanges heat with the environment at the dead state or reference temperature. The cost function for optimization is

$$J = \left(1 - \frac{T_H}{T_L}\right)\dot{Q}_L + \dot{W}_{comp} + \dot{W}_{evap,fan} + \dot{W}_{cond,fan} \tag{4.8}$$

where

$$\dot{Q}_L = \dot{m}_{ref}(h_1 - h_4) \tag{4.9}$$

$$\dot{W}_{comp} = \dot{m}_{ref}(h_2 - h_1) \tag{4.10}$$

$$\dot{W}_{evap,fan} = C_1\dot{m}_{evap}^2 + C_2\dot{m}_{evap} + C_3 \tag{4.11}$$

$$\dot{W}_{cond,fan} = C_4\dot{m}_{cond}^2 + C_5\dot{m}_{cond} + C_6 \tag{4.12}$$

and C_i for $i = \{1, \ldots, 6\}$ represents a constant coefficient, obtained by fitting data generated from the evaporator and condenser fan power versus mass flow rate of air with a second order polynomial, as shown in Section 3.3.2.

4.1.3 Optimization constraints

As introduced in Section 2.1.1, the thermodynamics of a VCS can be fully defined using four points on a pressure-enthalpy (P-h) diagram [21], see Figure 4.1. Each point consists of a pressure and enthalpy value, resulting in eight degrees of freedom. A VCS also has fluid dynamic properties: refrigerant mass flow rate, evaporator air mass flow rate, and condenser air mass flow rate. This yields eleven possible variables for optimization.

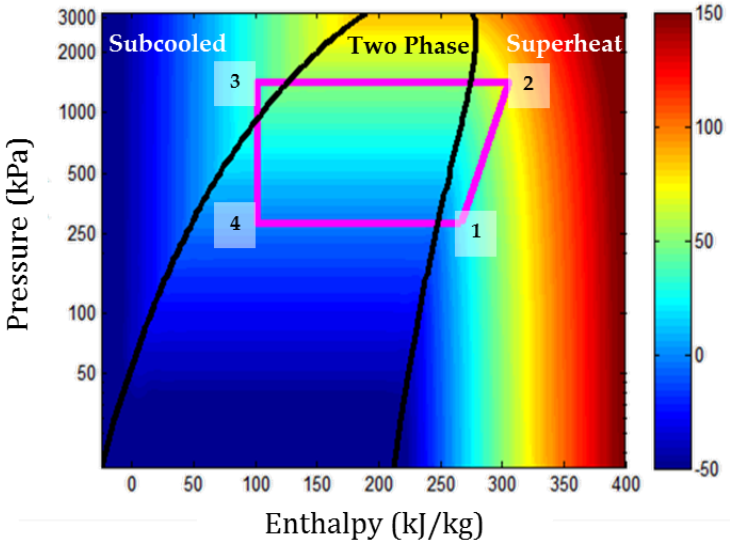

Figure 4.1: VCS represented on a pressure-enthalpy diagram

Physical constraints restrict the degrees of freedom available in the multivariable optimization problem. Three assumptions are made from the physical nature of the system: isobaric condensation, isobaric evaporation, and isenthalpic expansion. Furthermore, four constraints are generated by the performance requirements of the system, Equations 4.13 through 4.16, characterizing the cooling capacity, evaporator heat transfer, condenser heat transfer, and compressor isentropic efficiency, respectively.

$$C_{des} = \dot{m}_{ref}(h_1 - h_4) \tag{4.13}$$

$$\dot{Q}_L = \dot{m}_{ref}(h_1 - h_4) \tag{4.14}$$

$$\dot{Q}_H = \dot{m}_{ref}(h_2 - h_4) \tag{4.15}$$

$$\eta_{iso} = \frac{h_{2,static} - h_1}{h_2 - h_1} \tag{4.16}$$

From the original eleven optimization variables, the constraints serve to restrict seven with the choice of any values for the other four.

Inequality constraints are also used, to ensure the optimization procedure gives a result which can be implemented on a physical system. Equations 4.17 and 4.18 restrict the amount of superheat exiting the evaporator and the amount of subcooling exiting the condenser to be greater than zero. A non-zero superheat is needed because it is possible to damage a compressor if there is sufficient liquid entering the compression chamber. A non-zero subcooling is a simple metric to determine if enough heat transfer has taken place across the condenser. Equations 4.19 and 4.20 guarantee heat flow from the cooled space (T_L) into the evaporator and heat flow from the condenser into the ambient environment (T_H).

$$T_1 - T_4 \geq T_{sh} \tag{4.17}$$

$$T_{3,sat} - T_3 \geq T_{sc} \tag{4.18}$$

$$T_L - T_1 \geq 0 \tag{4.19}$$

$$T_3 - T_H \geq 0 \tag{4.20}$$

The nonlinear, constrained, multivariable optimization algorithm optimizes a vector of eight variables to describe the VCS, $[h_1 \quad h_2 \quad h_4 \quad P_1 \quad P_2 \quad \dot{m}_{ref} \quad \dot{m}_{evap} \quad \dot{m}_{cond}]$. The

vector represents the independent variables for the VCS, after the physical constraints have been applied. The eight variables represent the degrees of freedom available to the system after applying the isobaric condensation, isobaric evaporation, and isenthalpic expansion constraints. The performance and inequality constraints are applied internally to the optimization solver.

In order to ensure that the optimization method produces a solution that can be physically realized on the hardware, upper and lower boundaries were imposed. The numerical values represent the physical system discussed in [30][35][36][37] and would need to be refined for different hardware and refrigerants [42]. Note: due to a constant correction factor between the fan maps and the actual air flow rates, the air flow rate boundaries in the table do not exactly match the limits of the data given for the maps in Appendix A.

Table 4.1: Upper and lower boundaries for the exergy destruction minimization problem

Parameter	h_1	h_2	h_4	P_1	P_2	$\dot{m}_{ref}$	$\dot{m}_{evap}$	$\dot{m}_{cond}$
Upper Bound	350	350	220	550	960	0.009	0.21466	0.59993
Lower Bound	220	220	20	150	780	0.003	0.05547	0.04956

4.1.4 Predicting heat transfer in the heat exchangers

Due to the modeling complexity and dynamic behavior of the heat exchangers, the offline exergy destruction minimization framework employs an equivalent thermal circuit [43], which allows for a static, simplified representation of the heat exchangers, see Figure 4.2. This type of circuit analogy is common in heat transfer, relying upon the ratio of the driving potential of the system to the heat transfer rate to determine resistance. This analysis is valid for one dimensional heat transfer with constant properties and no internal energy generation. Using the resistive network, the heat transfer coefficient can be calculated as shown in Equation 4.21. F_a represents the fraction of the heat exchanger surface area which is covered in fins. The heat transfer correlations used to derive the convection coefficients α_{ref} and α_{air} are discussed in reference [44].

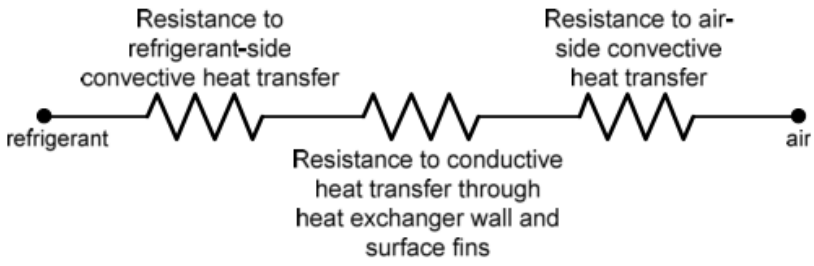

Figure 4.2: Resistive network representation of a heat exchanger

$$\frac{1}{UA} = \frac{1}{\alpha_{ref} A_i} + \frac{tkns}{k A_o F_a} + \frac{1}{\alpha_{air} A_o} \tag{4.21}$$

4.1.5 Actuator set point predictions

The nonlinear multivariable minimization solver *fmincon,* from the MATLAB Optimization Toolbox [45], is used in conjunction with the modeling framework described above to obtain a solution to the optimization problem using a sequential quadratic programming algorithm. *Fmincon* is able to handle optimization vectors which are defined as a system of equations or a system of inequalities. The optimization variables are bounded by user defined values unique to each parameter and subjected to equality and inequality constraints in evaluation of a solution. Appendix D provides the exergy destruction minimization code which determines the optimal values for a vector of eight different variables, $[h_1 \quad h_2 \quad h_4 \quad P_1 \quad P_2 \quad \dot{m}_{ref} \quad \dot{m}_{evap} \quad \dot{m}_{cond}]$.

From these variables, it is possible to determine a prediction for the values of the system actuators, $[a_{valve} \quad \omega_{comp} \quad \omega_{evap} \quad \omega_{cond}]$. The evaporator and condenser fan speeds are determined by a lookup table as a function of the mass flow rate, see Appendix A. The valve aperture and compressor speed are functions of the system pressures, as well as the mass flow rate. In order to determine the valve aperture and compressor speed, a single variable optimization solver *fminbnd* [45] is used, which minimizes the relative error between the optimization refrigerant mass flow rate and the mass flow rate at a given aperture or speed.

4.1.6 Modeling discrepancies in offline optimization solver

By nature, a model is unable to entirely capture the true nature of a physical system. Various techniques can be employed to reduce the inaccuracies between the model and the true

system. The static exergy destruction minimization technique is not able to completely capture the complexity of the VCS model. Knowledge of these shortcomings can help motivate specific advancements, especially when updating an existing model.

As outlined in Section 4.1.4, the heat exchangers are modeled using an equivalent thermal circuit. This analysis assumes that the heat exchanger is entirely two phase refrigerant, which has a very efficient heat transfer. In operation, the two phase refrigerant section takes up a significantly smaller portion of the heat exchangers, as low as half the length in the condenser. A constant correlation is used to reconcile the difference. This correlation is tuned once for a given cooling capacity and then held constant for all subsequent uses of the exergy destruction minimization procedure, see Section 5.2. A quantitative analysis of the general accuracy between the exergy destruction minimization technique and the VCS model is discussed in Section 5.4.3.1, specifically in regards to Figure 5.7.

As with most techniques to determine a minimum or maximum, this optimization technique requires an initial guess of the solution. The solver *fmincon* is only capable of finding local minima. Depending on the initial guess for the optimization variables, solutions can tend to converge to the same location (large local minimum) or fail to converge within the specified tolerance (shallow local minimum). The solver is most often able to converge to a solution when the initial guess for the optimization variables is approximately the same as what is seen in operation at a given cooling capacity.

Even with a good initial guess for the values of the optimization variables, the exergy destruction minimization solver may produce a solution which is at the boundaries of the allowable range. The solution at the boundary occurs most often in the superheat temperature, but has also been seen in the subcooled temperature [46]. Additionally, the condenser exit temperature is sometimes optimized to be the same as the ambient environment [11]. By producing an optimization vector which lies on the boundaries of the allowable region, the exergy destruction minimization technique suggests that lowest amount of exergy destruction may not by physically implementable on the VCS, i.e. the lowest exergy destruction is at an optimization point outside of the solution space. Despite the boundary suggestions for the temperature optimization values, the pressure set points consistently optimized to values away from the imposed boundaries and remained close to the pressures seen in the VCS model.

4.2 Set point control during operation

Due to modeling error and external disturbances, it is highly unlikely that the optimization predicted actuator values will exactly yield the optimized thermodynamic variables. Therefore, it is necessary to have a controller which will regulate the values of the thermodynamic variables. Due to the coupled nature of a VCS, it is necessary to use a multi input, multi output (MIMO) controller.

4.2.1 Controller format

The offline optimization is a useful tool to approximate the correct actuator input values for the VCS in order to achieve a desired operating condition while minimizing exergy destruction. However, uncertainty in the model motivates the use of a MIMO controller on the VCS. The eight outputs from the offline exergy destruction minimization metric are related trough the thermodynamic constraints, which only allow for the selection of four variables.

The order of information flow is shown in Figure 4.3. The optimization technique produces an eight dimensional vector of the optimized variables, v^*. The user is able to define a Λ matrix, which transforms the eight entry v^* vector into a linear combination of four control variables, y^*, as shown in Equation 4.22. The Λ matrix allows more flexibility in control design from the user by allowing selection of a subset of the exergy destruction minimization variables to become the control variables. Additionally, the v^* output is supplied to the set of nonlinear equations discussed in Section 4.1.5 to generate an estimate of the feed forward values, $\hat{u}^*$, to operate the system at the optimal thermodynamic values generated by the optimization method.

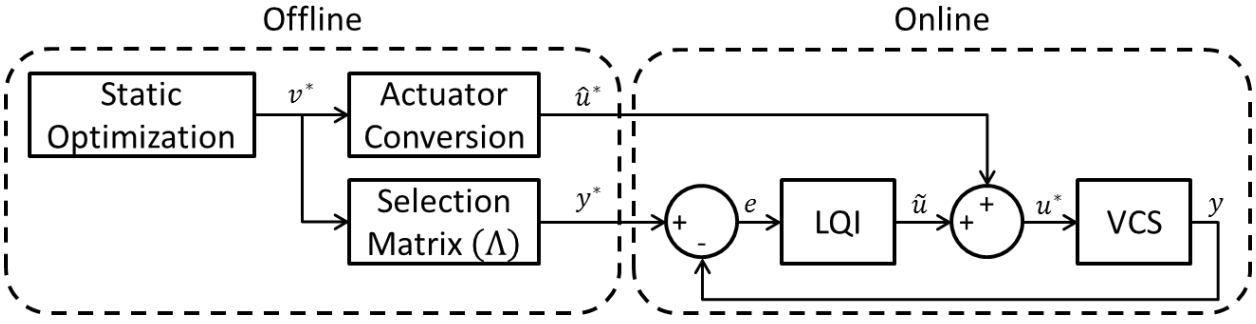

Figure 4.3: Information flow diagram for optimization and execution

$$y^* = \Lambda v^* \tag{4.22}$$

The influence of the controller to regulate to the input values is executed online. Using the y^* from the offline optimization and comparing it to the system output, y, the error between the two values can be found, such that

$$e = y^* - y \tag{4.23}$$

A feedback controller acts on the error and produces a deviation, $\tilde{u}$, from the predicted actuator input value obtained from the offline optimization. The two are combined in Equation 4.24 to give the true actuator value, u^*, to achieve the thermodynamic set points specified by the offline optimization.

$$u^* = \hat{u}^* + \tilde{u} \tag{4.24}$$

4.2.2 Motivation for LQI control

The coupled nature of the system dynamics restricts the choice of feedback controller to a MIMO design, rather than a combination of multiple single input, single output (SISO) controllers. Regulation to the optimal set points with minimum root mean square error motivates the use of a linear quadratic regulator (LQR). Since complete state information is known, see Appendix B, it is not necessary to use a linear quadratic Gaussian (LQG), which includes a Kalman filter prediction of the state information. By augmenting the LQR to include integral states, a zero steady state tracking error for a step change can be achieved [47], resulting in a linear quadratic integrator (LQI) controller.

4.2.3 Creation of LQI using state space transformation

Before designing the LQR, it is necessary to represent the system as a linear state space which maps u to y, see Appendix B for more details on generating the state space. The output of this analysis is shown below. Note that the bars represent a scaled quantity.

$$\dot{\bar{x}} = \bar{A}\bar{x} + \bar{B}\bar{u} \tag{4.25}$$

$$\bar{y} = \bar{C}\bar{x} \tag{4.26}$$

It is possible to transform the state space such that the output vector, y, is equal to the states of the system, x.

$$\dot{\bar{y}} = \tilde{A}\bar{y} + \tilde{B}\bar{u} \tag{4.27}$$

$$\bar{y} = \tilde{C}\bar{y} \tag{4.28}$$

where

$$\tilde{A} = \bar{C}\bar{A}\bar{C}^{-1} \tag{4.29}$$

$$\tilde{B} = \bar{C}\bar{B} \tag{4.30}$$

$$\tilde{C} = I_4 \tag{4.31}$$

This system is type zero, meaning it will only track step reference inputs with a non-zero error constant [47]. Augmenting the system with an integrator will allow it to have a zero error constant for a step change in the reference signal. The error between the actual output and desired output is used as the system states, such that

$$\bar{e} = \bar{y} - \bar{r} \tag{4.32}$$

$$\dot{\bar{z}} = \bar{e} \tag{4.33}$$

$$\begin{bmatrix} \dot{\bar{e}} \\ \dot{\bar{z}} \end{bmatrix} = \begin{bmatrix} \tilde{A} & 0 \\ I & 0 \end{bmatrix} \begin{bmatrix} \bar{e} \\ \bar{z} \end{bmatrix} + \begin{bmatrix} \tilde{B} \\ 0 \end{bmatrix} \bar{u} + \begin{bmatrix} \tilde{A} \\ 0 \end{bmatrix} \bar{r} \tag{4.34}$$

The cost function associated with the LQI is given by Equation 4.35.

$$J_{LQI} = \int_0^\infty \bar{e}^T Q_P \bar{e} + \bar{z}^T Q_I \bar{z} + \bar{u}^T R \bar{u} \tag{4.35}$$

The Q terms were tuned to ensure good transient performance of the controller. R was tuned to restrict excessive wear on the actuators caused by large spikes in actuator input commands. All numerical information regarding the LQI controllers is given in Appendix C.

The exergy destruction minimization technique and the LQI controller design will be applied to a VCS in the next chapter. Without the optimization method, there would be no clear recommendation as to the thermodynamic set points of the system to achieve a given cooling capacity. Without the LQI controller, the coupled system may not be able to reach the proposed values. The offline portion of the overall exergy destruction minimization of a VCS is critical to determining the overall exergy destruction of the system.

Chapter 5
Evaluation of Actuator Combinations

In this chapter, the actuators on a vapor-compression cycle system (VCS) are analyzed to determine a nominal combination which results in less exergy destruction during system operation. Beginning from a fully fixed system running at a given cooling capacity, the four actuators are made variable in turn as well as in combination with each other. Each combination is subjected to the offline optimization code, state space analysis, and linear quadratic integrator (LQI) design. Recommendations for actuator combinations resulting in less exergy destruction are given over three cooling capacities.

5.1 Advancements in VCS actuation

A VCS needs to have four basic components to operate, a compressor, condenser, expansion device, and evaporator. It is possible to construct a system such that none of these components are variable. The expansion device can be an orifice tube, the compressor can run at a constant mass displacement, and the heat exchangers can have a constant flow rate of the secondary side medium. However, this results in a system with no flexibility in operation.

Throughout its lifetime, the heating, ventilation, and air conditioning (HVAC) industry has made strides to introduce increased flexibility in operation to VCS systems. In the 1970s, the variable speed drive for a compressor was invented, allowing for user selection of the system mass flow rate through changes in the compression speed [16][17]. Orifice tubes were replaced by thermostatic expansion valves, which sought to maintain a constant superheat at the evaporator exit through the use of mechanical coupling and a preload spring [14]. Studies have shown an increased efficiency in the use of the variable valve over an orifice tube [48]. The need

for manual coupling and offline tuning of the preload spring was removed through the use of the electronic expansion valve, which uses external control signals to adjust the opening area [15]. Finally, the addition of variable motor control for the heat exchanger fans, or variable speed pumps for a liquid secondary side, showed significant improvement over fixed speed [18].

Current VCSs can have up to four actuators which can be adjusted to alter the system performance: compressor speed, valve opening, and mass flow rate of the secondary side medium in both heat exchangers. However, increased ability to manipulate a VCS does not necessarily mean an increased efficiency [19]. Monetary costs associated with the purchase of flexible components over fixed components may outweigh the benefit given by the variable components. This is especially true in commercial systems, which are manufactured and sold on a large scale and in direct competition with similar priced systems. The rest of this chapter performs an in depth search of the actuation of VCSs and gives a recommendation regarding the best variable actuator combination to achieve energy savings over the system operation, while still keeping initial investment for flexible components low.

5.2 Variable actuator evaluation and analysis

With four actuators available, a VCS can have anywhere from none to all four variable actuators in a variety of combinations. This results in the combinations given in Table 5.1 below. For the valve, the percent opening of the reducing area is varied. For the compressor, the speed is varied. For the evaporator, the percent fan speed is varied. For the condenser, the percent fan speed is varied. In this analysis, the exergy destruction of the combinations of variable actuators will be compared against a baseline with no variable actuators for three cooling capacities. For simplicity, all combinations will be referred to as an acronym of the variable actuators, given in parenthesis.

As outlined in Section 4.1.3, four variables are needed to fully constrain the operation of a VCS. Accurate representations of a subset of system dynamics can be obtained using less than four parameters. For all of the actuator combinations, the number of parameters being controlled was chosen to be the same as the number of actuators available. For the four variable actuator combination, the average pressure (P_{ave}), delta pressure (ΔP), superheat temperature (T_{sh}), and subcool temperature (T_{sc}) were regulated: Equations 5.1 through 5.4. For all of the three variable

Table 5.1: Combinations of variable actuators

One Variable Actuator	Two Variable Actuators	Three Variable Actuators	Four Variable Actuators
Valve (V)	Valve, Compressor (VK)	Valve, Compressor, Evaporator (VKE)	Valve, Compressor, Evaporator, Condenser (VKEC)
Compressor (K)	Valve, Evaporator (VE)	Valve, Compressor, Condenser (VKC)	
Evaporator (E)	Valve, Condenser (VC)	Valve, Evaporator, Condenser (VEC)	
Condenser (C)	Compressor, Evaporator (KE)	Compressor, Evaporator, Condenser (KEC)	
	Compressor, Condenser (KC)		
	Evaporator, Condenser (EC)		

actuator combinations, the average pressure, delta pressure, and superheat temperature were regulated. For the two variable actuator combinations, the average pressure and the delta pressure were regulated. For the one variable actuator combinations, only the superheat temperature was regulated.

$$P_{ave} = \frac{1}{2}(P_2 - P_1) \tag{5.1}$$

$$\Delta P = P_2 - P_1 \tag{5.2}$$

$$T_{sh} = T_1 - T_4 \tag{5.3}$$

$$T_{sc} = T_{3,sat} - T_3 \tag{5.4}$$

The selection of which parameters to control was based off of convention and the recommendations in [6]. The superheat temperature was chosen due to its history of regulation. Thermostatic expansion valves were designed to manually regulate this variable. The delta and average pressures were chosen over the evaporator and condenser pressures due to the findings in [6]. It was shown that this combination results in less coupling than the evaporator and condenser pressures alone. The subcool temperature was chosen to preserve the combination of pressure and thermal dynamics. Additionally, if the valve aperture and compressor speed are considered to be the driving forces behind the pressure values, then the evaporator fan speed can be seen as the driver behind the superheat temperature and the condenser fan speed is the driver of the subcool temperature.

5.3 Quantifying errors

Due to imperfections in modeling and natural variation in data, there are a few errors that need to be addressed. The two main locations for these errors occur when comparing the optimization routine to the complete ATTMO (AFRL Transient Thermal Modeling and Optimization) model and when comparing the results from different combinations of actuators to one another.

5.3.1 Comparison between models

Recall from Sections 4.1.5 that the exergy destruction minimization technique gives predictions for the thermodynamic operating points of the VCS from static models. Through a series of non-linear equations, it is possible to calculate actuator input commands to be used as feed forward values, $\hat{u}^*$ based off the solution to the optimization problem. Figure 5.1 highlights this concept and shows the alteration to the feed forward values predicted by the offline optimization to produce the final actuator values, u^*, through Equation 5.5.

When the recommended set points are achieved by the ATTMO model, there is a mismatch between the predicted and the final actuator values. Through this discrepancy, it is possible to calculate a relative fit between the optimization code and the ATTMO model. Equation 5.6 takes the difference between the predicted actuator value and the final actuator value, normalizes the difference across the allowable actuator range, and sums in quadrature.

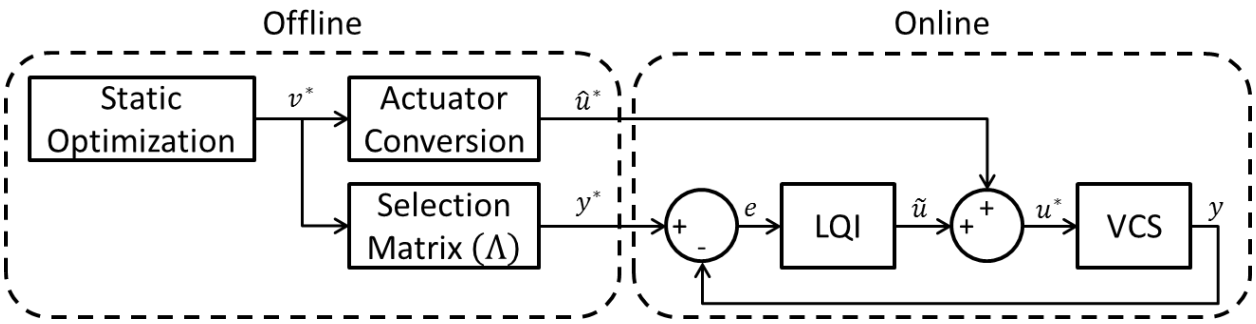

Figure 5.1: Information flow diagram for optimization and execution

$$u^* = \hat{u}^* + \tilde{u} \tag{5.5}$$

$$\delta = \sqrt{\left(\frac{\hat{u}^*_{valve} - u^*_{valve}}{88}\right)^2 + \left(\frac{\hat{u}^*_{comp} - u^*_{comp}}{1700}\right)^2 + \left(\frac{\hat{u}^*_{evap} - u^*_{evap}}{85}\right)^2 + \left(\frac{\hat{u}^*_{cond} - u^*_{cond}}{90}\right)^2} \tag{5.6}$$

Through this parameter, it is possible to see if there is a trend to the deviations between the static exergy destruction minimization code and the ATTMO model of the VCS. If such trends exist, they can be used to refine the static model and produce better recommendations for the individual component behavior.

5.3.2 Comparison between actuator combinations

As previously mentioned, the exergy destruction caused by the fifteen actuator combinations outlined in Section 5.2 was analyzed at three different cooling capacities: 0.82 kW, 0.90 kW, and 1.00 kW, modeled on the VCS located at the University of Illinois at Urbana-Champaign (UIUC) [30][35][36][37]. The state space linearization was performed and the LQI controllers were designed at 0.90 kW, due to its central nature in the three cooling capacities.

While the exergy destruction minimization code was able to perfectly converge on the specified cooling capacity, the ATTMO model was not. The differences in cooling capacities across the various actuator configurations gave a meaningful way to determine the relative trustworthiness of the exergy destruction values. In Equation 5.7, the deviation between the achieved cooling capacity and the desired cooling capacity is normalized by the desired capacity to produce a percent error. The same percent error is then applied to the rate of exergy destruction, to produce the error in the exergy destruction measurement.

$$\dot{X}_{dest,error} = \frac{|C - C_{des}|}{C_{des}} \dot{X}_{dest} \tag{5.7}$$

Through this error metric, it is possible to see which actuators are able to accurately hold a desired cooling capacity and which are not. If an actuator combination is able to achieve lower exergy destruction than the baseline, but it is unable to reasonably meet the cooling requirements for a given operation, then that actuator combination would be insufficient for the operation.

5.4 Results from reduced actuator combinations

In order to extract meaningful information regarding the exergy destruction caused by operation of the VCS, three cooling capacities were chosen to serve as reference points. They are 1.00 kW, 0.90 kW, and 0.82 kW. The theoretical maximum cooling capacity for the system is 1.35 kW. However, this cooling capacity requires all actuators to be operating at their maximum value. Increasing nonlinearity in the VCS model is introduced as the cooling capacity is increased.

The controllers for every combination were designed at a cooling capacity of 0.90 kW. They were then applied to cooling capacities of 0.82 kW and 1.00 kW to demonstrate the robustness of the controller. For every combination of actuators, a linear state space was generated which mapped the active actuators to the thermodynamic variables of interest, as discussed in Section 5.2. The state space representation of the system was used to design an LQI controller. Additionally, recommended set points for the parameters of interest were obtained from the static exergy destruction minimization technique. For all combinations, information regarding the state space representation can be found in Appendix B and controller information can be found in Appendix C.

5.4.1 Baseline set points

For each cooling capacity, a nominal value was determined for each actuator, as outlined in Table 5.2. When constructing the state space model, perturbations about these nominal values were applied to the system and the resulting outputs were recorded. Specific information regarding the magnitude of the perturbations, as well as the validity of the linear model, is given in Appendix B.

Table 5.2: Nominal actuator input commands

Cooling Capacity (kW)	Valve Aperture (%)	Compressor Speed (RPM)	Evaporator Fan (%)	Condenser Fan (%)
1.00	40	1500	50	50
0.90	35	1300	40	40
0.82	30	1100	35	35

The nominal actuator input commands outlined above became the default settings when an actuator was said to be in the fixed configuration, see Table 5.1. For example, if the combination VE was being tested at 0.82 kW of cooling, the compressor would be operated at 1100 rpm, the condenser fan at 35%, and the valve aperture and evaporator fan allowed to vary with an LQI controller.

Figure 5.2 captures the system performance to meet a 0.90 kW cooling capacity using the actuator input value and thermodynamic operating condition recommendations supplied by the exergy destruction minimization technique. For the first 1500 seconds, the system operates in a feed forward only condition, using the actuator input values recommened by the algorithm. At 1500 seconds, the LQI controller designed for the VEC confirguration is activated, which attempts to drive the thermodynamic variables to the values provided by the offline optimization method.

As expected, there is not a perfect agreement between the offline optimization technique and the ATTMO model. The superheat temperature is about 2 degrees too high using only the feed forward values, which motivates the 8% drop in evaporator fan speed. The three simultaneous step changes in the control variables cause the delta pressure to move further from the desired value, but convergence in all three variables is seen in about 500 seconds. While there is some spiking behavior from the actuators, the magnitude of the spikes is relatively small compared to the actuator range.

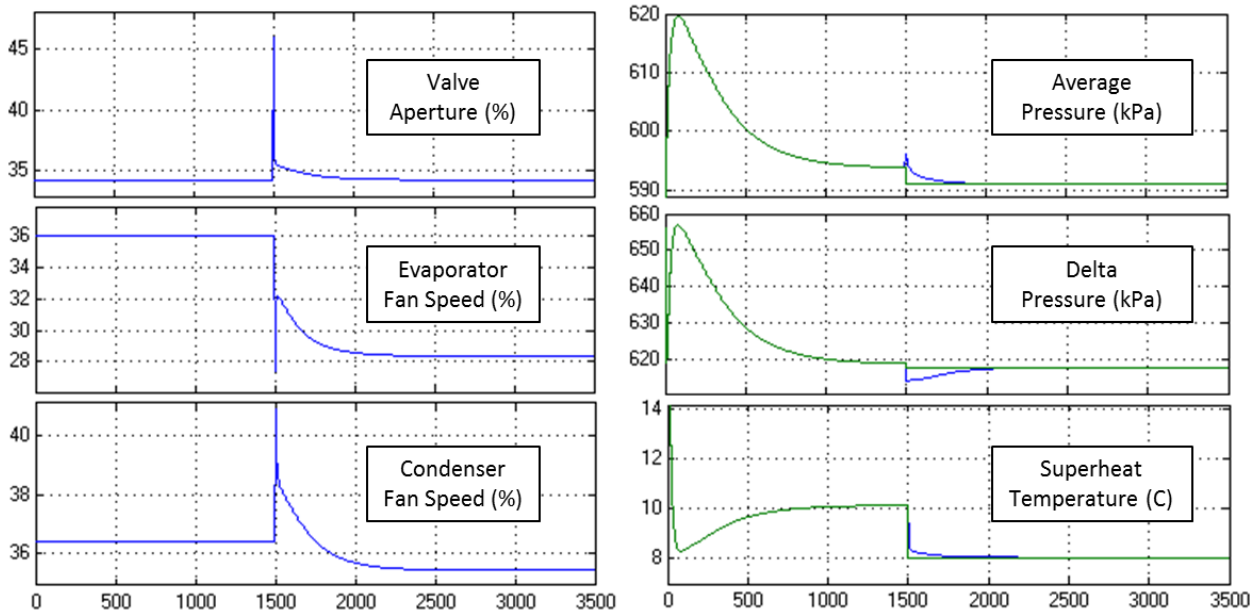

Figure 5.2: VEC set point regulation at 0.90 kW

5.4.2 Missing configurations

Unfortunately, some of the actuator configurations were unable to yield results. For the VKEC combination (all actuators variable), the system responded poorly to control efforts. There was saturation in the actuators without convergence between the desired set point supplied to the ATTMO model and the given thermodynamic variable measured in operation. This is likely caused by modeling mismatch between the exergy destruction minimization method and the ATTMO model of the VCS. Recall from Section 4.1.3 that the optimization technique produces a vector of eight thermodynamic parameters, which yield four independent parameters. The result defines a very specific point of operation. If modeling error exists between the optimization method and the ATTMO model, the specific point of operation may be different between the two models. Since all parameters are being controlled, there is no opportunity for an uncontrolled parameter to converge to different values between the two models, thus allowing the controlled parameters to converge to the same value.

The VE combination was also unable to supply information about the exergy destruction, as no controller was able to be stably implemented for this configuration. In order to design an LQI controller, a linearized model of the system being controlled must be created through a state

space transformation. To ensure accuracy of the fit between the linear and nonlinear models, data is compared and a percent fit is determined. All of the other combinations have percent fits greater than 58% with most above 75%, except for the VE combination. This combination produces a 37% match to the differential pressure based on variations in the valve and evaporator. The poor fit shows that these actuators do not have sufficient control over the delta pressure. While a controller was able to be created from the state space model, the difference between the linearized model and the non-linear model caused the controller to go unstable after the system experienced a step change in the ATTMO model.

The final combination which was not able to give results was the VKC combination at a cooling capacity of 1.00 kW (the other cooling capacities did not display this same problem). This combination resulted in actuator saturation without parameter convergence, shown in Figure 5.3. By comparing Figure 5.2 with Figure 5.3, the relative size of the step change between the feed forward and regulated conditions is much larger in Figure 5.3, which could indicate a divergence between the offline optimization technique and the ATTMO model as the origin of the poor controller performance. As previously mentioned, the model of the VCS becomes increasingly nonlinear with increased cooling, making it difficult for a linear controller to regulate parameters within the system. Further increasing cooling beyond 1.00 kW should show similar behavior for other combinations as well. While it is possible to design a new controller at a higher cooling capacity, the controller relies on a linearized model of the system. To attempt to linearize the VCS at UIUC at higher cooling capacities results in poor model fits, as seen in the VE case outlined above.

5.4.3 Exergy destruction results

For each of the three cooling capacities, the rate of exergy destruction is given below. The dashed line represents the exergy destruction destroyed at the nominal actuator conditions given in Section 5.4.1. It serves as a baseline comparison for the other configurations. The error bars are calculated as outlined in Section 5.3.2. Additionally, all of the results are outlined in Table 5.3.

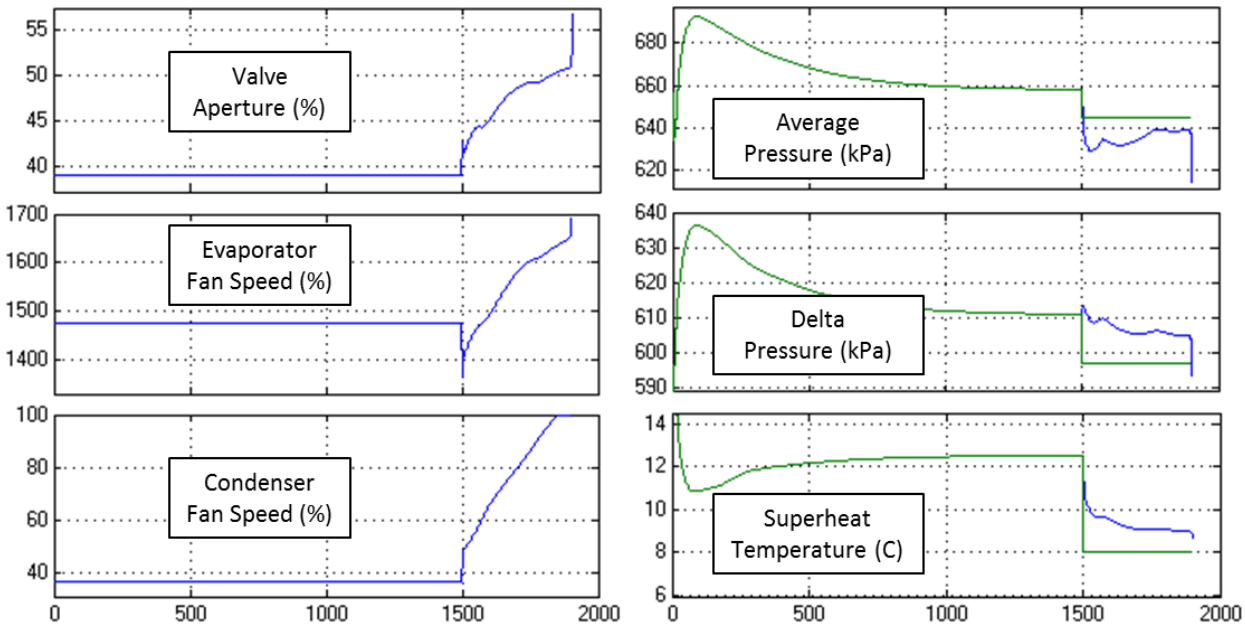

Figure 5.3: VKC set point regulation at 1.00 kW

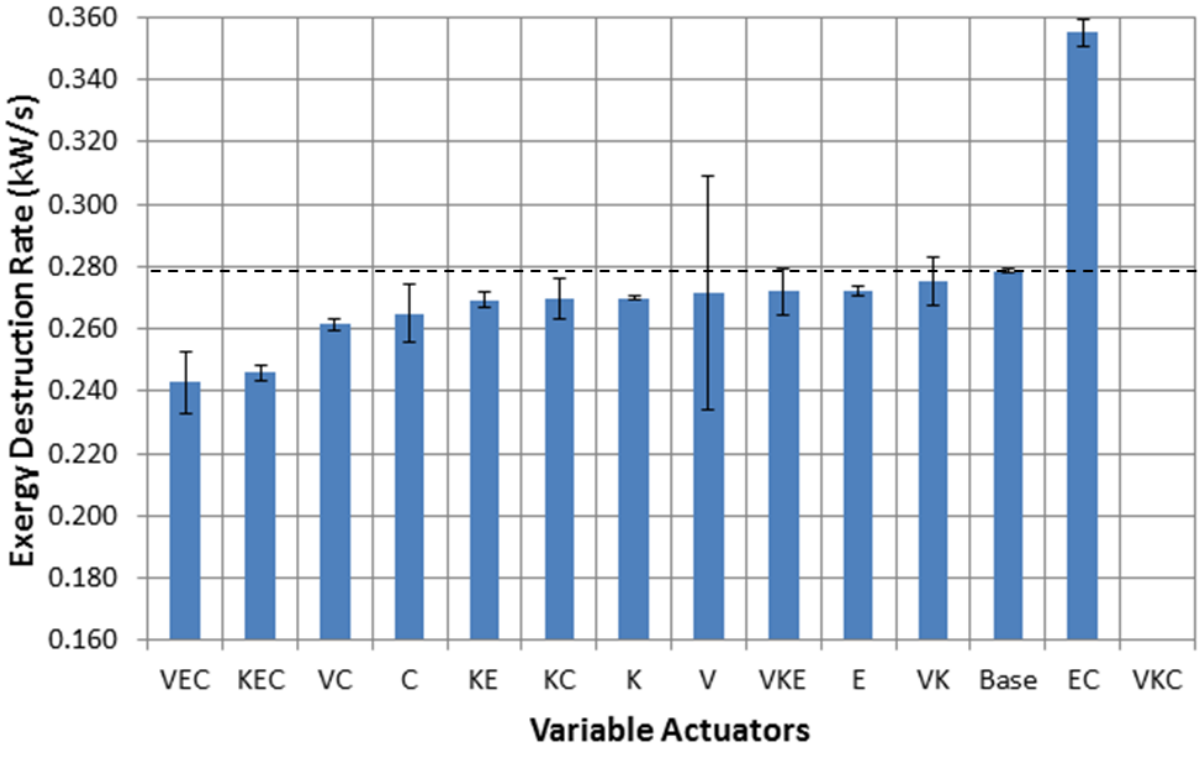

Figure 5.4: Exergy destruction with 1.00 kW cooling capacity

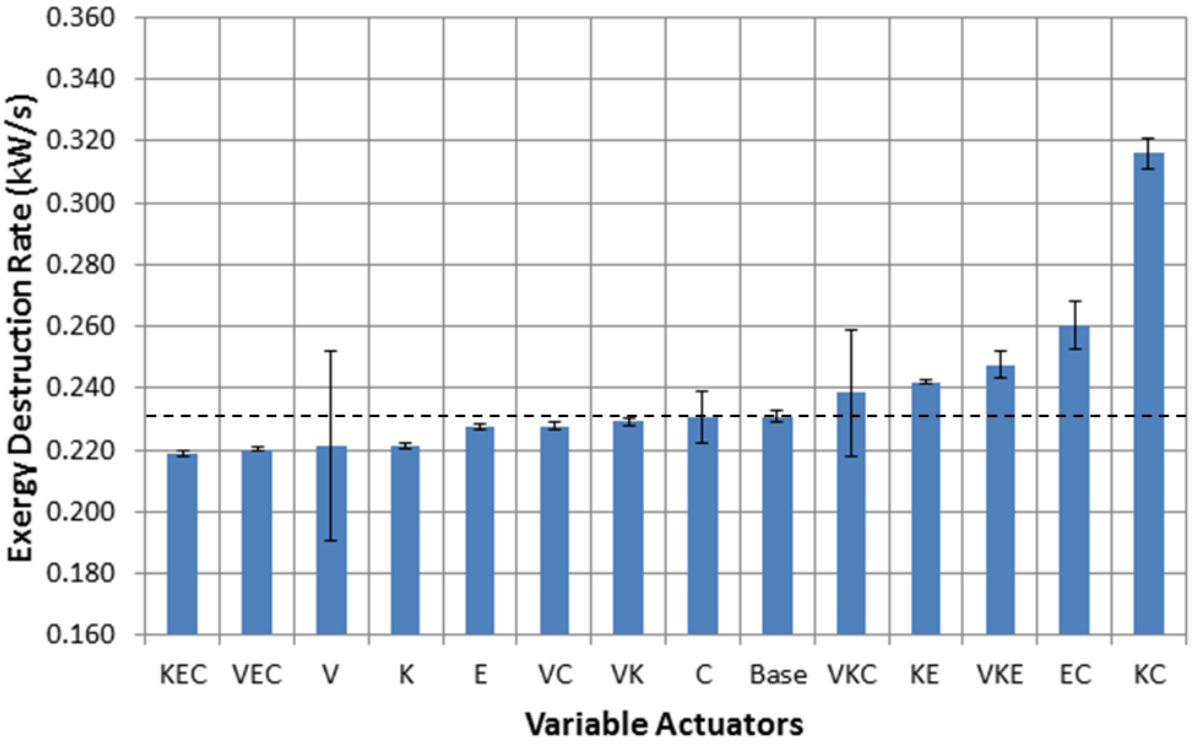

Figure 5.5: Exergy destruction with 0.90 kW cooling capacity

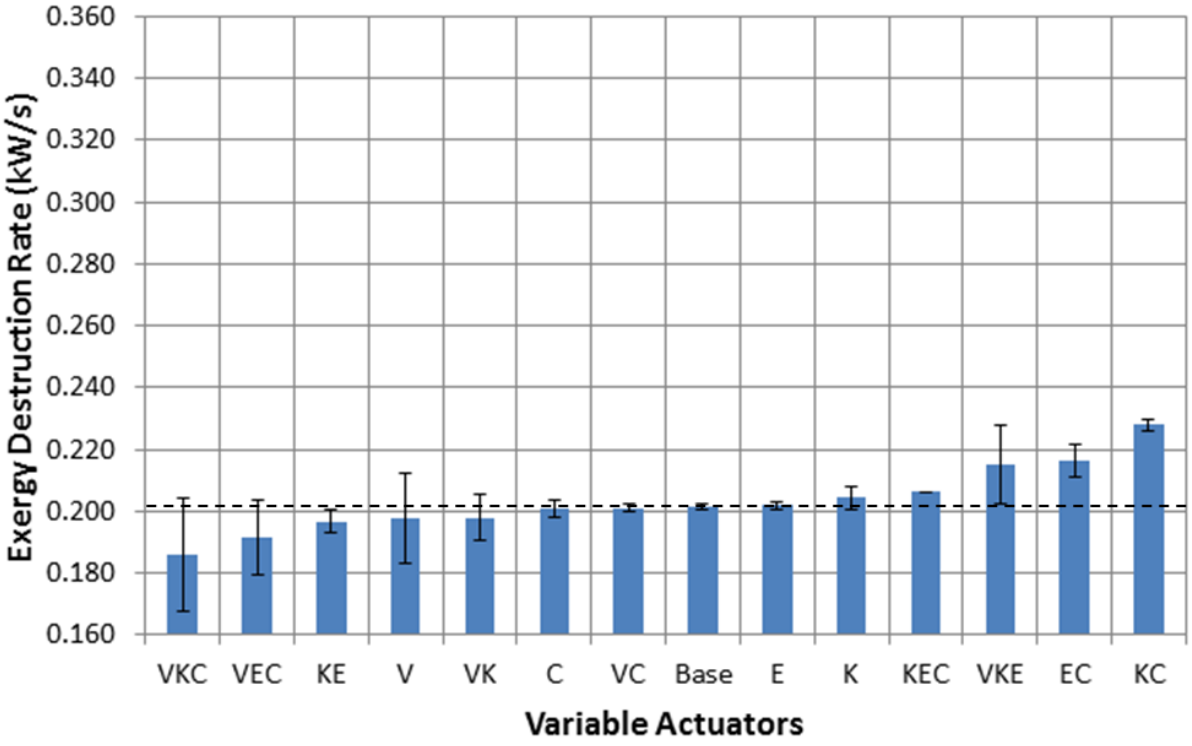

Figure 5.6: Exergy destruction with 0.82 kW cooling capacity

Table 5.3: Exergy destruction results summary

C = 1.00 kW		C = 0.90 kW		C = 0.82 kW	
Case (variable)	Results over baseline	Case (variable)	Results over baseline	Case (variable)	Results over baseline
VKEC	N/A	VKEC	N/A	VKEC	N/A
KEC	Better	KEC	Better	KEC	Worse
VEC	Better	VEC	Better	VEC	Within Error
VKC	N/A	VKC	Within Error	VKC	Within Error
VKE	Within Error	VKE	Worse	VKE	Worse
VK	Within Error	VK	Within Error	VK	Within Error
VE	N/A	VE	N/A	VE	N/A
VC	Better	VC	Within Error	VC	Within Error
KE	Better	KE	Worse	KE	Within Error
KC	Better	KC	Worse	KC	Worse
EC	Worse	EC	Worse	EC	Worse
V	Within Error	V	Within Error	V	Within Error
K	Better	K	Better	K	Within Error
E	Better	E	Better	E	Within Error
C	Better	C	Within Error	C	Within Error

In order to facilitate the discussion of these results, they will be broken up by relative category, namely a discussion on the effect of cooling capacity, trends in actuation to be avoided, and trends in actuation to be encouraged.

5.4.3.1 Cooling capacity

It is important to note the relationship between cooling capacity and exergy destruction. As the required cooling capacity decreased, the spread of the exergy destruction caused by the various combinations of actuators also decreased, giving the largest benefit in variable actuation at the highest cooling capacity. Unfortunately, this results in a tradeoff between the desire to control the system and the ability to do so. As the cooling capacity increases, the modeled VCS becomes more nonlinear, resulting in a system which is harder to control. It is in this same region

that there is the most benefit from control. Arriving at a balance between these two parameters would fall to the judgment of the engineer.

In addition to the difficulties controlling the system at higher cooling capacities, the exergy destruction minimization technique has a higher failure rate for converging to a solution. As explained in 4.1.6, the correlation between the calculated heat transfer and the actual heat transfer is only computed at the nominal conditions for each cooling capacity. All subsequent results from the optimization technique are run with the same correlation. Therefore, as the nonlinearity in the system increases with a higher cooling capacity, it becomes more challenging to fix the value of the correlation. When the minimization method converges to parameter values which are different than the conditions at which the heat transfer was synced, errors will be introduced into the results.

One method of quantifying the errors seen between the exergy destruction minimization routine and the ATTMO model is outlined in Section 5.3.1. By restricting the two models to operate at the same thermodynamic set points, the relative difference in actuator values can be used to determine accuracy across the two models. The results of this analysis are presented in Figure 5.7 for all three cooling capacities.

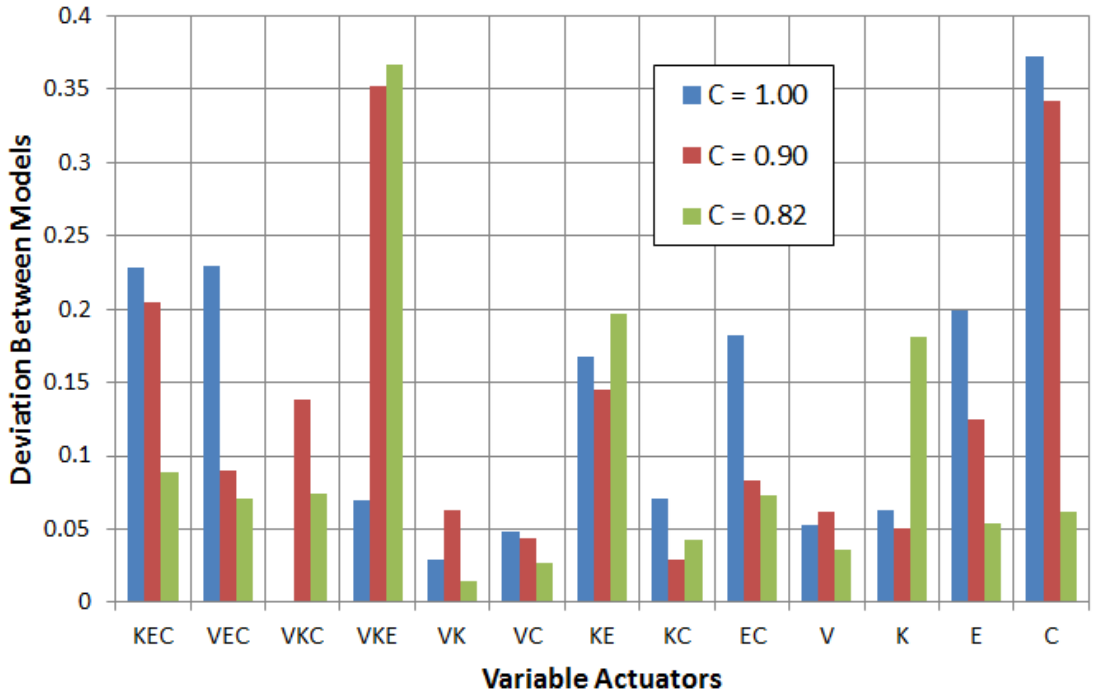

Figure 5.7: Exergy destruction with 0.82 kW cooling capacity

There does not appear to be much correlation between the exergy efficiency results and the relative match between the two models. However, the relative error in the condenser at higher cooling capacities is a cause for concern. It is possible that this component is not accurately modeled in the optimization technique. Error from the condenser alone may be bleeding over into the KEC and VEC cases, resulting in a poor actuator fit despite encouraging exergy destruction results. However, this is not the only source of error, as other combinations with a condenser do not seem to suffer from the same problem, e.g. VC. The error in KC and EC is very low, suggesting that the poor exergy destruction seen in the ATTMO model is not a result of modeling inaccuracies.

The maximum achievable value for the deviation is 2, which corresponds to all of the actuators moving across the entire range of actuation. However, individual combinations will have a maximum deviation value corresponding to the square root of the number of active actuators (i.e. $\sqrt{4}$, $\sqrt{3}$, $\sqrt{2}$, $\sqrt{1}$). This analysis breaks down slightly as the actuator number decreases. For example, the EC combination at 0.90 kW of cooling requires a fixed value of the value and compressor at 35% and 1300 rpm, respectively. Imposing these values as equality constraints in the exergy destruction minimization technique resulted in a failure to converge to a solution. If they were imposed as inequality constraints, the optimization routine was able to find a minimum value for the exergy destruction, but suggested 34.7% and 1264 rpm for the two actuators. Therefore, the maximum deviation for this case would not be $\sqrt{2}$, but some slightly larger value corresponding to the initial difference in predicted actuator value.

5.4.3.2 Poorly performing actuator combinations

When converting from a fully fixed system to a partially variable system, it can be tempting to want to only make one actuator variable in order to save money. If the compressor is chosen as the variable actuator, there is some potential for exergy savings (maximum of 4% for 0.90 kW) but larger decreases in exergy destruction can be achieved if more than one actuator is allowed to vary. Also, given the large cost associated with a variable compressor, it is possible to use a higher combination of actuators to achieve a better exergy destruction rate with the same amount of initial investment.

In terms of low cost components, electronic expansion valves are one of the first components to become variable on a VCS. As with the compressor, care should be taken to not only use a valve to control system parameters. Across all three cooling capacities, the valve alone has displayed an inability to accurately reach a desired cooling capacity, as evidenced by the large error bars.

Both the KC and EC configurations have displayed significantly more exergy destruction over the baseline case, despite optimization efforts. The compressor and condenser are fairly close to each other in terms of exergy destruction and fairly far from the other actuators. The poor behavior seen in this configuration is likely due to direct competition between the two components. For both 0.90 kW and 0.82 kW of cooling, the optimization technique cites the compressor as the highest source of exergy destruction. For 1.00 kW of cooling, the optimization routine switches to the condenser as the largest source of exergy destruction. By actively trying to lower the condenser destruction at higher cooling capacities, significant improvement is seen in the overall exergy destruction over the lower cooling capacities.

For the EC configuration the poor exergy destruction is caused by an ineffective actuation. Recall that the two actuator combinations attempt to regulate the average and delta pressures in the system. Both of these control variables are more closely tied to the valve aperture and compressor speed than the heat exchanger fan speeds. By forcing the heat exchangers to regulate the two parameters, larger deviations from the nominal conditions are required. With exergy destruction growing as a square of mass flow rate of air across the heat exchangers, even marginally larger fan speeds can produce significantly higher exergy destruction.

The relative difference in power consumption by the two heat exchangers is also obvious in these results. The KE case hovers near the baseline for all three cooling capacities. This is partially due to the condenser's ability to move more air than the evaporator (about three times more at the same percent fan speed) and partially by the coefficients of power consumption in the two fans, which cause the condenser to consume six times as much power as the evaporator at full speed.

5.4.3.3 Well performing actuator combinations

The strongest candidates for variable actuation are the KEC and VEC combinations. Both combinations are close to the baseline for 0.82 kW of cooling, but rapidly drop off as the lowest destroyers of exergy beyond that point. The success of these two combinations is likely due to the integration of both thermal and fluid dynamic control. The valve and compressor are large drivers of the mass flow rates in the VCS and the evaporator and condenser control the heat transfer interfaces at the low and high sides, respectively. By pulling all three domains together, the VCS is able to operate with a 12.8% savings in exergy destruction over the baseline at 1.00 kW of cooling. The other three actuator combinations, VKE and VKC, tended to hover near the baseline and even performed worse at lower cooling capacities.

Between the KEC and VEC combinations, the VEC is the optimal solution. Both combinations destroy approximately the same amount of exergy in operation. However, the cost of a variable valve compared to a variable compressor highlights potential savings due to initial investment. By using the VEC combination, there is possibility for exergy destruction savings even beyond what is given here. A static compressor will be optimized at the speed which it runs, unlike the variable compressor used in this example. Additionally, the VCS in this model uses a reciprocating compressor, which has been shown to be less efficient over scroll compressors [16].

5.4.4 Motivation behind including fan work

Previous work has been conducted within the context of exergy destruction which focused exclusively on the refrigerant side of the VCS without inclusion of the work required by the heat exchanger fans [22]. Applying the same controllers and set points as shown above, the exergy destruction for 0.90 kW of cooling is presented in Figure 5.8. This analysis produces near trivial results. Since the compressor has the only power draw in the VCS, all cases where the compressor is allowed to be variable (save for combination VKC) resulted in a lower exergy destruction.

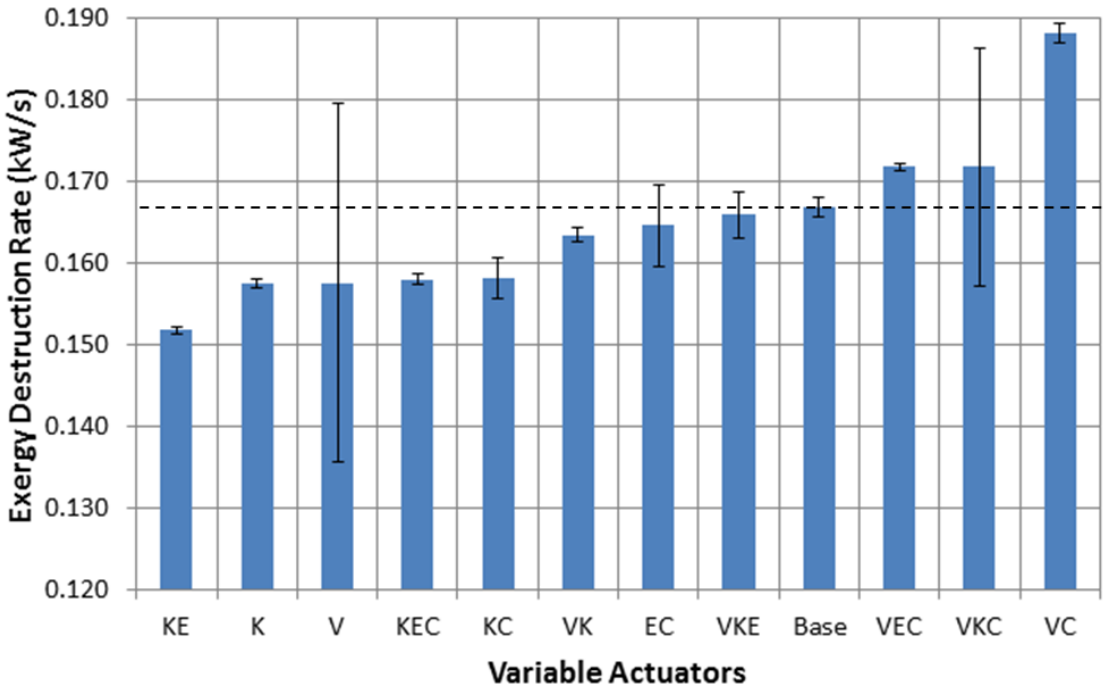

Figure 5.8: Exergy destruction at 0.90 kW cooling without fan work

When looking at the raw data, the error becomes even more obvious. The compressor is responsible for about 0.13 kJ of exergy destruction, with the valve as the second highest at 0.017 kJ of exergy destruction. Previous research has confirmed that the compressor is the largest source of exergy destruction [11][12], but the condenser is cited as the second highest, with some researchers showing it is the highest source [49].

If the condenser fan work is included in the analysis, the exergy destroyed by the condenser becomes the second highest in the system, around 0.065 kJ. While this gain is not enough for the condenser to overtake the compressor as the largest source of exergy destruction, it does put the condenser firmly ahead of the valve and evaporator, both with about 0.017 kJ of exergy destruction.

5.5 Generalizability to different systems

The results given in Section 5.4.3 are highly dependent on the power consumed in the compressor, condenser, and evaporator, specifically relative to each other. For the results presented, the compressor uses about twice the power of the condenser and about ten times the power of the evaporator. Sizing guides from Standard Refrigeration Company offer insight in the

applicability of these ratios. If no other data exists, it is acceptable to choose the condenser horsepower to be the same as the compressor horsepower [50]. The evaporator, however, must be designed to fit the system parameters, e.g. cooling required, flow rate, etc. [51].

The thermal potential of the VCS is another location where exergy may be destroyed. By taking the general exergy destruction equation and solving for only the heat transfer at steady state, the exergy destruction becomes

$$\dot{X}_{dest} = \left(1 - \frac{T_0}{T_w}\right)\dot{Q} \tag{5.8}$$

Applying this to the evaporator and condenser yields

$$\dot{X}_{dest,e} = \left(1 - \frac{T_0}{T_{w,e}}\right)\dot{Q}_e \tag{5.9}$$

$$\dot{X}_{dest,c} = \left(1 - \frac{T_0}{T_{w,c}}\right)\dot{Q}_c \tag{5.10}$$

in which the bulk wall temperature and bulk heat transfer are used, rather than the wall temperature and heat transfer for each zone. T_0 corresponds to the dead state of the system and is the same for both components. Due to the nature of a VCS, the condenser must reject more heat than the evaporator absorbs in order to compensate for the heat generated by the compressor. Assuming the heat rejection can be related by a constant $K > 1$ such that

$$\dot{Q}_c = K\,\dot{Q}_e \tag{5.11}$$

the exergy destruction in the two components is related by

$$\frac{\dot{X}_{dest,e}}{\left(1-\frac{T_0}{T_{w,e}}\right)} = \dot{Q}_e = \frac{\dot{X}_{dest,c}}{K\left(1-\frac{T_0}{T_{w,c}}\right)} \tag{5.12}$$

By the physical nature of a VCS, the condensation stage occurs at a higher temperature than the evaporation stage. Following this inequality

$$T_{r,c} > T_{r,e} \tag{5.13}$$

$$T_{w,c} > T_{w,e} \tag{5.14}$$

$$1 - \frac{T_0}{T_{w,c}} > 1 - \frac{T_0}{T_{w,e}} \tag{5.15}$$

$$1 > \frac{1-\frac{T_0}{T_{w,e}}}{1-\frac{T_0}{T_{w,c}}} \tag{5.16}$$

where the above ratio will be defined as r. Equation 5.12 becomes

$$\dot{X}_{dest,e} = \frac{r}{K}\dot{X}_{dest,c} \tag{5.17}$$

Since $\frac{r}{K}$ is always less than one, the exergy destroyed by the heat transfer across the condenser will always be larger than the exergy destroyed in the evaporator. The actuator suggestions outlined above are insensitive to the thermal potential of the heat exchangers.

The use of a secondary side fluid other than air has not been explicitly explored. In Section 5.4.4, it was shown that the addition of the fan power consumption by the two heat exchangers played a significant part in the exergy destruction. For a liquid secondary side, it is expected that this analysis still hold true, so long as the power required to pump the liquid is accurately addressed. Even with the thermodynamic differences in the secondary side medium, the amount of heat rejected by the VCS should remain constant for a given operating condition. Therefore, a change in secondary side fluid would mostly affect the exergy destruction created by the work required to pump the fluid. If the required power follows a similar trend as the fan power consumption, the results outlined above should be qualitatively predictive for other types of systems with a liquid secondary side fluid.

The working refrigerant within the VCS also plays a large role in the exergy destruction analysis. Generally, researchers have found that the exergy losses are highest in the compressor across many different types of refrigerant (R744, R134a, R600a, R290) [11]. However, some researchers have shown that the exergy losses are greatest in the condenser using R404a, R502, and R507 [49]. Shilliday et. al. found that the largest exergy losses occur in the compressor for R290 and R404a, but the valve is the highest source of exergy destruction when R744 is used as the working refrigerant [52]. Due to the conflicting nature of the results surrounding different refrigerant types, caution should be exercised before applying the recommendations of this thesis outside of R134a and it is advised that a new study be performed before applying these results to systems using other types of refrigerant.

Chapter 6
Conclusions and Future Work

6.1 Summary of findings

Increased actuation of VCS has made it possible to maneuver the thermodynamic characteristics of the system to independently chosen set points. However, greater actuation does not guarantee better performance. Furthermore, variable actuators require an additional monetary investment over fixed actuators. A nominal combination of variable actuators can reduce energy consumption associated with system operation while requiring a small upfront expense, which will have far reaching effect in a consumer market.

Through a joint effort between the University of Illinois at Urbana-Champaign (UIUC), PC Krause and Associates (PCKA), and the Air Force Research Laboratory (AFRL), the ATTMO model was created, which accurately captures the performance of the VCS at UIUC [30][35][36][37]. The model uses both physical equations and empirically derived maps to produce a Simulink based framework with faster than real time execution.

Exergy destruction minimization was proposed as an efficiency metric for the VCS in operation. Exergy incorporates the first and second laws of thermodynamics, allowing insight into the efficiency of the system relative to the supplied energy. An offline optimization framework was created which provided recommendations for exergy efficiency of the VCS. The exergy destruction minimization technique focused on the work required by the system to produce the cooling desired. Using the offline optimization routing, suggested thermodynamic set point values were supplied to the VCS and convergence to these values was achieved through the use of a LQI controller.

Numerous combinations of variable and fixed actuators were supplied to the static, offline exergy destruction method and tested on the ATTMO model. For each combination, a unique LQI controller was designed with 0.90 kW of cooling. All combinations of actuators were able to achieve the recommended control parameters given by the optimization technique at three unique cooling capacities, 0.82 kW, 0.90 kW, and 1.00 kW, thus highlighting the robustness of the controller. Deviation in actuator command input between the two models was captured through the use of the δ parameter. There does not appear to be a repeatable correlation between the deviation between the two models and the active actuators.

The largest benefit in the overall exergy destruction comes from the use of variable actuators at higher cooling capacities. At lower cooling capacities, variable actuators give a smaller relative benefit to the overall exergy destruction making the contributions challenging to observe. Higher cooling capacities are more susceptible to greater nonlinearity in the model, which increases the difficulty of applying an LQI controller. Due to a constant coefficient which correlates the heat transfer between the optimization method and the ATTMO model, higher cooling capacities can move quickly outside of an acceptable region for a given coefficient. This results in a higher failure rate for convergence of the exergy destruction minimization technique.

The best actuator combination is a variable valve aperture, evaporator fan, and condenser fan (VEC). This combination was shown to give nearly 13% savings in exergy destruction over the basic operation of the VCS at 1.00 kW of cooling. It also benefits from using components that are relatively inexpensive compared to the second best combination of a variable compressor speed, evaporator fan, and condenser fan (KEC), which also gave approximately 13% savings in exergy destruction. The VEC combination benefits from having a component which controls the internal dynamics of the refrigeration system (valve) by being able to alter the mass flow rate of refrigerant, while also having two components which control the interfaces between the system and the high and low thermal sinks (condenser and evaporator, respectively).

In addition to determining which actuator combination produces results in the lowest exergy destruction, there are a few combinations to avoid. It is not recommended that any single component be the only variable actuator on the system. While the compressor speed and condenser fan show some promise, the maximum savings for exergy destruction was found to be

only 4%. Additionally, it is not recommend that a variable valve be used over a fixed valve, as the variable valve was unable to hold a consistent cooling capacity.

Actuation combinations of a variable evaporator fan and condenser fan (EC) and variable compressor speed and condenser fan (KC) both result in consistently higher than baseline exergy destruction. The EC combination gives inefficient actuation for the VCS, since the heat exchanger fans are better suited to controlling thermal characteristics and not pressure characteristics. The KC combination uses the two largest exergy destroying components in the system. When the optimization technique is used to find an exergy destruction minimum, fighting between the two components can occur, specifically at lower cooling capacities. When the offline model of the condenser destroys more exergy than the compressor (cooling of 1.00 kW), the optimization routine actively favors the condenser and gives an exergy destruction close to the system baseline.

Previous attempts to characterize the exergy destruction of VCSs have focused on the refrigerant as a control volume, while ignoring the secondary side. For the valve and compressor, the two approaches yield the same results. The two heat exchangers are severely impacted if the work associated with the fans is neglected. To ignore the fan work results in the trivial suggestion that the compressor be made variable over all other actuator combinations. However, it has been shown in this thesis that this is not the case.

6.2 Future work

This work has assumed that the VCS is operated in isolation but this is rarely true in practice. A logical avenue for improvement on the results given here is to couple the VCS with heat generating components. As shown in this thesis, the most efficient exergy destruction is achieved when multiple actuators are used in combination with each other. It is logical that further energy savings can be provided, if the VCS and the heat generating system are optimized simultaneously. Some work has already been undertaken, which looks at exergy as a minimization technique across coupled energy domains [22].

Control schemes beyond the LQI presented herein can be designed. It was found that the exergy destruction savings are most pronounced at higher cooling capacities. It is theoretically possible to have the VCS run at a higher cooling capacity for a shorter period of time in order to

save exergy during operation and take advantage of longer non-operational times. However, this type of control would be dependent on the nature of the heat load and whether it requires a constant, low intensity cooling or short bursts of high intensity cooling.

Risk assessment can be performed using the results obtained through this analysis. If an actuator cannot be controlled and becomes stuck at a fixed value, exergy can be used as a metric to determine the relative performance loss in the system. Depending on the cooling capacity and the combination of originally active actuators, it may be possible to operate with a higher efficiency if an informed choice of actuators is used, rather than the remaining available. I.e. if the VEC (theoretical best) combination is used, and the valve malfunctions, it is better to use only the condenser fan for actuation, instead of trying to use both the evaporator and condenser fans.

The VCS presented here can be coupled to a model predictive network in order to respond to potential loading demands before they occur. There has already been work in Japan to use weather condition predictions to drive the operation of the HVAC system of a school house [53]. By using predictive data, it is possible to determine the optimal actuator combination ahead of changes in the system load.

Hardware verification must be conducted for the results presented here. The generalizability of this approach was previously discussed, which motivates wider verification and integration of these results to other VCSs with different cooling capacities, types of refrigerant, and configurations of hardware components. The analysis can be adapted to include multiple evaporators as is common for a building system. Additional actuators may also be possible, such as using the receiver to control the charge in the system [54].

List of References

[1] American Housing Survey, US Census Bureau, 2009. [Online] Available: http://www.census.gov/prod/2011pubs/h150-09.pdf

[2] Highway Statistics Summary to 2000, U.S. Department of Transportation, Federal Highway Administration, 2000. [Online] Available: http://www.rita.dot.gov/bts/sites/rita.dot.gov.bts/files/publications/transportation_statistics_annual_report/2001/html/chapter_06_figure_01_147_table.html

[3] Current Applications of Refrigeration Systems, Wikipedia. [Online] Available: http://en.wikipedia.org/wiki/Refrigeration#Current_applications_of_refrigeration

[4] Bendapudi, S., Braun, J., "A Review of Literature on Dynamic Models of Vapor Compression Equipment," *ASHRAE Report* #4036-5, May 2002.

[5] He, X., Liu, S., Asada, H., "Modeling of Vapor Compression Cycles for Advanced Controls in HVAC Systems." *Proceedings of the ACC*. Seattle, WA, 3664-3668, 1995.

[6] Jain, N., Li, B., Keir, M., et. al. "Decentralized Feedback Structures of a Vapor Compression Cycle System," *IEEE Transactions on Control Systems Technology*, January 2010.

[7] He, X., Liu, S., Asada, H., "Multivariable Control of Vapor Compression Systems," *HVAC&R Research,* vol. 4, no. 3, July 1998.

[8] Schurt, L., Hermes, C., Neto, A., "Assessment of the Controlling Envelope of a Model-Based Multivariable Controller for Vapor Compression Refrigeration Systems," *Applied Thermal Engineering*, 2010.

[9] Jiang, J., Zhu, R., Lui, X., "A Study on Control of Refrigeration Systems with LQG Method," *Cryogenics and Refrigeration-Proceedings of ICCR*, 2003.

[10] Moran, M., *Availability Analysis: A Guide to Efficient Energy Use*, Englewood Cliffs, New Jersey, Prentice-Hall, 1982.

[11] Ahamed, J., Saidur, R., Masjuki, H., "A Review on Exergy Analysis of Vapor Compression Refrigeration System," *Renewable and Sustainable Energy Reviews*, vol. 15, no. 3, p. 1593-1600, 2011.

[12] Kotas, T., *The Exergy Method of Thermal Plant Analysis*, London: Butterworths, 1985.

[13] Wagner, T., DeBlois, R., Young, D., "Energy and Exergy Analysis of the Scroll Compressor," *International Compressor Engineering Conference*, paper 1053, 1994.

[14] Sporlan Thermostatic Expansion Valves: RACE Catalog 10-10 UK, Sporlan Valve Company, Washington, MO, April 2010.

[15] SEI Electronic Expansion Valves: Bulletin 100-20, Sporlan Valve Company, Washington, MO, Jul. 2000.

[16] Qureshi, T., Tassou, S., "Variable-speed capacity control in refrigeration systems," *Applied Thermal Engineering*, vol. 16, no. 2, pp. 103-113, 1996.

[17] Rishel, J., "History of HVAC Variable-Speed Pumping," *ASHRAE Transactions*, vol. 100:1, 1995.

[18] Braven, K., Penoncello, S., Herold, K., et. al., "Improving heat pumps and air conditioning," *Mechanical Engineering*, vol. 115, no. 9, 1993.

[19] Sellers, D., "21 Century HVAC Controls: Progress and Paradox," *Heating, Piping, and Air Conditioning Engineering: HPAC*, Jul 2003.

[20] "The 'World's Largest Fridge' to Open in SW Philly," Philadelphia Inquirer, 07 April 2011. [Online] Available: http://articles.philly.com/2011-04-07/news/29392777_1_refrigeration-john-vena-farmers-markets

[21] Cengel, Y., Boles, M., *Thermodynamics: An Engineering Approach*, 6th edition, Boston: The McGraw-Hill Companies, Inc. 2008.

[22] Jain, N., *Thermodynamics Based Optimization and Control of Integrated Energy Systems*. Urbana, Illinois: University of Illinois, PhD Thesis, 2013.

[23] Stoecker, W., Jones, J., *Refrigeration and Air-Conditioning*, New York: McGraw-Jill Book Company, 1983.

[24] Eldredge, B., *Improving the Accuracy and Scope of Control – Oriented Vapor Compression Cycle System Models*. Urbana, Illinois: University of Illinois, MS Thesis, 2006.

[25] McKinley, T., Alleyne, A., "An Advanced Nonlinear Switched Heat Exchanger Model for Vapor Compression Cycles using the Moving-Boundary Method." *International Journal of Refrigeration*, 1253-1264, 2008.

[26] Jensen, J., Tummescheit, H., "Moving Boundary Models for Dynamic Simulations of Two-Phase Flows." *Proceedings of the Second International Modelica Conference*. Oberpfaffenhofen, Germany, 235-244, 2002.

[27] Cheng, T., Asada, H., "Nonlinear Observer Design for a Varying-Order Switched System with Application to Heat Exchangers." *Proceedings of the ACC.* Minneapolis, MN, p 2898-2903, 2006.

[28] Leducq, D., Guilpart, J., Trystram, G., "Low Order Dynamic Model of a Vapor Compression Cycles for Process Control Design." *Journal of Food Process*, 193-199, 2003.

[29] Willatzen, M., Pettit, N., Ploug-Sorenson, L., "A General Dynamic Simulation Model for Evaporators and Condensers in Refrigeration." *International Journal of Refrigeration*, 398-403, 1998.

[30] Li, B., *Dynamic Modeling and Control of Vapor Compression Cycle Systems with Shut-down and Start-up Operations.* Urbana, Illinois: University of Illinois, MS Thesis, 2010.

[31] Wedekind, G., Bhatt, B., Beck, B., "A System Mean Void Fraction Model for Predicting Various Transient Phenomena Associated with Two-Phase Evaporating and Condensing Flows." *International Journal of Multiphase Flow*, vol. 4, p 97-114, 1978.

[32] Harpster, J., Putman, R., "The Economic Effects of Condenser Backpressure on Heat Rate, Condensate Sub-Cooling, and Feedwater Dissolved Oxygen," *International Joint Power Conference*, Miami Beach, FL, 2000.

[33] Jain, N. *Dynamic Modeling and Validation of a Commercial Transport Refrigeration System.* Urbana, Illinois: University of Illinois, MS Thesis, 2009.

[34] Rasmussen, B., Alleyne, A., "Control – Oriented Modeling of Transcritical Vapor Compression Systems." *Journal of Dynamic Systems, Measurement, and Control*, p 54 – 64, 2004.

[35] Keir, M., *Dynamic Modeling, Control, and Fault Detection in Vapor Compression Systems.* Urbana, Illinois: University of Illinois, MS Thesis, 2005.

[36] Otten, R., *Superheat Control for Air Conditioning and Refrigeration Systems: Simulation and Experiments.* Urbana, Illinois: University of Illinois, MS Thesis, 2010.

[37] Kania, M., et al., "A Dynamic Modeling Toolbox for Air Vehicle Vapor Cycle Systems." SAE Technical Paper, doi: 10.4271/2012-01-2172, 2012.

[38] Karnopp, D., Margolis, D., Rosenberg, R., *System Dynamics: Modeling and Simulation of Mechatronic Systems* 4th edition, Hoboken, New Jersey: John Wiley and Sons Inc., 2006.

[39] Bejan, A., *Entropy Generation Minimization*, Boca Raton: CRC Press LLC, 1996.

[40] Doty, J., Camberos, J., Yerkes, K., "Approximate Approach for Direct Calculation of Unsteady Entropy Generation Rate for Engineering Applications," *Proceedings of the 50th AIAA Aerospace Sciences Meeting*, Nashville, 2012.

[41] Bejan, A., "Fundamentals of exergy analysis, entropy generation minimization, and the generation of flow architecture," *International Journal of Energy Research*, vol. 26, p 545-565, 2002.

[42] ASHRAE Handbook: Fundamentals, American Society of Heating, Refrigeration, and Air-Conditioning Engineers, Inc., 2009.

[43] Incropera, F., DeWitt, D., *Fundamentals of Heat and Mass Transfer* 5th edition, New York: John Wiley and Sons Inc., 2007.

[44] Rasmussen, B., *Control-Oriented Modeling of Transcritical Vapor Compression Systems*, Urbana, Illinois: University of Illinois, MS Thesis, 2000.

[45] MATLAB Optimization Toolbox, *The Mathworks Inc.*, Natick, MA, 2002.

[46] Adegoke, C., Akintunde, M., Fapetu, O., "Comparative exergetic analysis of vapor compression refrigeration systems in the superheated and subcooled regions," *AU Journal of Technology*, 10:254–63, 2007.

[47] Ogata, K., *Modern Control Engineering* 4th edition, Prentice Hall, 2002.

[48] Whitman, C., Johnson, W., Tomczyk, J., *Refrigeration and Air Conditioning Technology*, 5th edition, Thomson Delmar Learning, 2005.

[49] Arora, A., Kaushik, S., "Theoretical analysis of vapor compression refrigeration system with R502, R404A and R507A," *International Journal of Refrigeration*, 31:998–1005, 2008.

[50] Water Cooled Condensers: Selection Guide, Standard Refrigeration Company, 2004.

[51] Evaporators: Selection Guide, Standard Refrigeration Company, 2004.

[52] Shilliday, J., Tassou, S., Shilliday, N., "Comparative energy and exergy analysis of R744, R404a, and R290 refrigeration cycles," *International Journal of Low-Carbon Technologies Advance*, 2009.

[53] Utsumi, Y., et. al. "Feed-forward air-conditioning control using a weather forecasting data in school building in heating season," Proceedings of Building Simulation 2011: 12th Conference of International Building Performance Simulation Association, Sydney, 14-16 November, 2011.

[54] Jenson, J., Skogestad, S., "Optimal operation of simple refrigeration cycles, Part I: Degrees of freedom and optimality of sub-cooling," *Computers and Chemical Engineering*, p 712-721, 2007.

[55] Ljung, L., MATLAB System Identification Toolbox, *The Mathworks Inc*., Natick, MA, 2007.

[56] Jain, N., Alleyne, A., "A framework for the optimization of integrated energy systems," *Applied Thermal Engineering*, vol. 48, p 495-505, 2012.

Appendix A
Component Maps

After all the physical equations which can be used to describe the behavior of a system or component have been applied, it is still possible to have a mismatch between the predictive model and the physical system. Capturing this behavior through increasingly precise and detailed equations may not be worth the time invested and proprietary information may limit the available knowledge of the system. Mapping serves as a way to obtain a good static agreement between a system model and the hardware, while having the benefit of being relatively easy to implement [24]. In this appendix, the procedure for map generation is discussed. The maps used in the ATTMO model are provided for each component.

A.1 Procedure for map creation

Maps are created from a set of data generated by running the system at expected operating conditions. It is important to exercise the system to the bounds of the operating range, as the maps generally contain powers of variables which can have very dynamic behavior outside of the range which they were created.

Engineering judgment is critical in selecting the parameters which influence the map and iteration through a couple of different options is to be expected. In addition to a linear combination of the influential parameters, other powers and cross terms may be required to produce a more accurate map. Determining which parameters are most important, as well as the order and coupling of the parameters, is what accounts for the necessary iteration.

From the data set, the actual value of the mapped parameter, C, is recorded or calculated at each time step. The input matrix, X, is created by applying the input parameters with all

powers and cross terms. The matrix dimension will be n by m, where n is the number of time steps and m is the number of terms in the mapping polynomial. The mapping equation can be solved by

$$a = X^{+}C \tag{A.1}$$

where a represents the polynomial coefficient vector, and $^{+}$ represents the pseudo-inverse, an approximate matrix inverse specifically for non-square matrices, given in Equation A.2. The exactness of the mapped solution can be determined by comparing the error between Xa and C, consequentially iterating with different input variables, powers, and cross terms to reduce this error to an acceptable value.

$$A^{+} = (A^{T}A)^{-1}A^{T} \tag{A.2}$$

If desired, a map can be converted to a lookup table, rather than left in the equation format. When discretizing the equations, care must be taken to balance a fine resolution with a reasonable amount of storage space. While the equation will be more accurate, the lookup table is advantageous for speed and, as presented in Sections A.2.3 and A.2.4, is simple when there is a 1:1 mapping between the input and output.

A.2 Individual maps

All of the maps given below were generated using the procedure above. Data was taken from the physical test stand at the University of Illinois at Urbana-Champaign and compared to the ATTMO model of the system [37]. Engineering judgment was used to determine the order and cross coupling of the terms. Applying this procedure to different hardware will result in different coefficients and variables for the polynomials.

A.2.1 Valve

The value only uses one map in its operation, to describe the discharge coefficient. The input u represents the percent opening of the valve.

$$C_d = a_1 + a_2u + a_3P_{in} + a_4P_{out} + a_5P_{in}P_{out} \tag{A.3}$$

$$a = \begin{bmatrix} 6.83E^{-7} & 1.09E^{-7} & 2.01E^{-9} & 8.48 * 10^{-9} & -7.87E^{-12} \end{bmatrix}^{T} \tag{A.4}$$

A.2.2 Compressor

The compressor uses three separate maps. The adiabatic efficiency is a measure of the heat lost to the metal compressor shell. The volumetric efficiency captures the efficient usage of the compressor stroke displacement. The isentropic efficiency relates back to the assumption that the compressor is isentropic. For Equations A.5 to A.10, u refers to the compressor speed.

$$\eta_{adb} = a_1 + a_2 u + a_3 P_{in} + a_4 P_{out} + a_5 u P_{in} + a_6 u P_{out} + a_7 P_{in} P_{out} \quad \text{(A.5)}$$

$$a = [1.79E^{1} \quad -1.65E^{-3} \quad -1.90E^{-2} \quad -1.95E^{-2} \quad 7.88E^{-6} \quad 1.95E^{-6} \quad 1.57E^{-5}]^T \quad \text{(A.6)}$$

$$\eta_{vol} = b_1 + b_2 u + b_3 P_{in} + b_4 P_{out} + b_5 u P_{in} + b_6 u P_{out} + b_7 P_{in} P_{out} \quad \text{(A.7)}$$

$$b = [-6.32E^{-1} \quad -6.01E^{-5} \quad 4.75E^{-3} \quad 1.29E^{-3} \quad 3.35E^{-7} \quad -1.24E^{-8} \quad -4.97E^{-6}]^T \quad \text{(A.8)}$$

$$\eta_{iso} = c_1 + c_2 u + c_3 P_{in} + c_4 P_{out} + c_5 u P_{in} + c_6 u P_{out} + c_7 P_{in} P_{out} \quad \text{(A.9)}$$

$$c = [-3.16E^{-1} \quad 2.94E^{-4} \quad 5.78E^{-4} \quad 1.09E^{-3} \quad 1.38E^{-6} \quad -6.19E^{-7} \quad -2.02E^{-6}]^T \quad \text{(A.10)}$$

A.2.3 Evaporator

The evaporator uses the fan speed to directly map to the mass flow rate of air. Due to the physical limitations of the fan blades, an input signal of less than 15% will result in no mass flow rate.

Table A.1: Mapping between evaporator fan speed and air mass flow rate

Input	100	95	90	85	80	75	70	65	60	55
Mass Flow	0.241	0.230	0.220	0.209	0.199	0.188	0.178	0.167	0.157	0.146
Input	50	45	40	35	30	25	20	15	10	5
Mass Flow	0.136	0.125	0.115	0.102	0.094	0.083	0.073	0.062	0	0

A.2.4 Condenser

As with the evaporator, the condenser also uses the fan speed to directly map to the mass flow rate of air. The condenser is able to achieve air movement with an input signal as low as 10%.

Table A.2: Mapping between condenser fan speed and air mass flow rate

Input	100	95	90	85	80	75	70	65	60	55
Mass Flow	0.471	0.447	0.423	0.399	0.375	0.351	0.327	0.303	0.279	0.255
Input	50	45	40	35	30	25	20	15	10	5
Mass Flow	0.231	0.207	0.183	0.159	0.135	0.111	0.087	0.063	0.039	0

Appendix B

State Space Modeling

A state space transformation is used to reduce a complicated system into a linearized model of only a few states. The original system is perturbed by a random series of step changes about a nominal condition shown in Table B.1. The performance of the system is recorded and a linear model is created to mimic the observed system performance. The MATLAB System Identification toolbox was used in this analysis [55].

Table B.1: Nominal actuator input commands

	Valve Aperture (%)	Compressor Speed (RPM)	Evaporator Fan (%)	Condenser Fan (%)
Nominal	35	1300	40	40

Each of the data sets is 8,000 seconds long. In the first 2,000 seconds, the system is allowed to achieve a steady state operating condition with the nominal values for the actuator inputs. The next 6,000 seconds capture the system's response to changes in the actuators. From these 6,000 seconds, the first 3,000 are used to generate a model of the system in the form

$$\dot{\bar{x}} = \bar{A}\bar{x} + \bar{B}\bar{u} \tag{B.1}$$

$$\bar{y} = \bar{C}\bar{x} \tag{B.2}$$

And the last 3,000 seconds are used as a comparison. The newly generated state space is compared to fresh data which was not used in the creation of the state space. The range of perturbation in the actuators, visual comparison of the state space fit to the data, eigenvalues, and

matrix values are given for all actuator combinations below.

B.1 One actuator models

One actuator is used to regulate the superheat temperature at the exit of the evaporator. For more information regarding the choice of control variables, see Section 5.2. The section titles refer to the active variable actuators.

B.1.1 Valve (V)

Table B.2: Actuator range for state space V

	Valve Aperture (%)	Compressor Speed (RPM)	Evaporator Fan (%)	Condenser Fan (%)
Minimum	31.5	1300	40	40
Maximum	38.5	1300	40	40

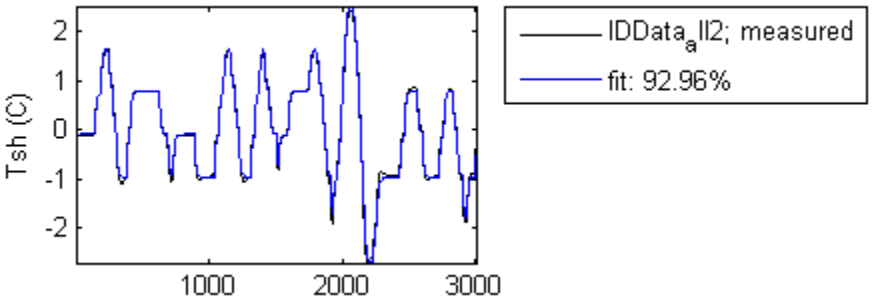

Figure B.1: State space representation V

Eigenvalues: -0.0909

$$A = [0.913] \quad B = [0.006] \quad C = [-14.7] \tag{B.3}$$

B.1.2 Compressor (K)

Table B.3: Actuator range for state space K

	Valve Aperture (%)	Compressor Speed (RPM)	Evaporator Fan (%)	Condenser Fan (%)
Minimum	35	1202.5	40	40
Maximum	35	1397.5	40	40

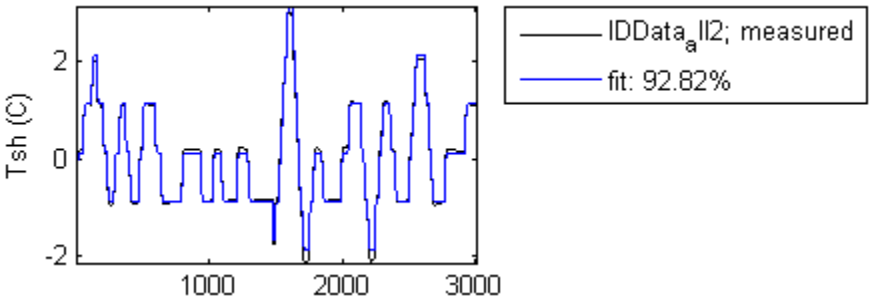

Figure B.2: State space representation K

Eigenvalues: -0.1623

$$A = [0.850] \quad B = [-0.013] \quad C = [-12.3] \tag{B.4}$$

B.1.3 Evaporator (E)

Table B.4: Actuator range for state space E

	Valve Aperture (%)	Compressor Speed (RPM)	Evaporator Fan (%)	Condenser Fan (%)
Minimum	35	1300	36	40
Maximum	35	1300	44	40

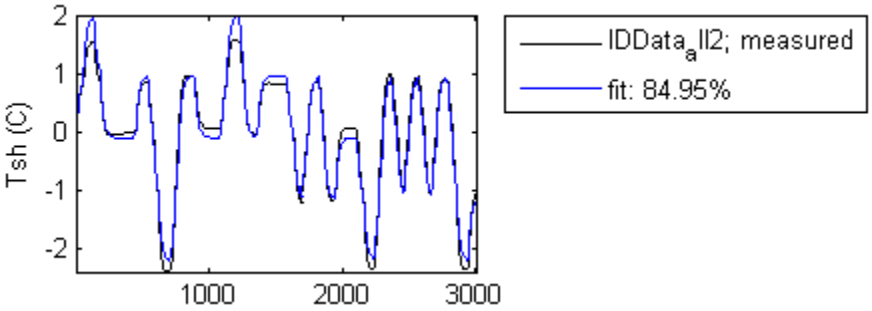

Figure B.3: State space representation E

Eigenvalues: -0.0458

$$A = [0.955] \quad B = [-0.002] \quad C = [-24.3] \tag{B.5}$$

B.1.4 Condenser (C)

Table B.5: Actuator range for state space C

	Valve Aperture (%)	Compressor Speed (RPM)	Evaporator Fan (%)	Condenser Fan (%)
Minimum	35	1300	40	34
Maximum	35	1300	40	46

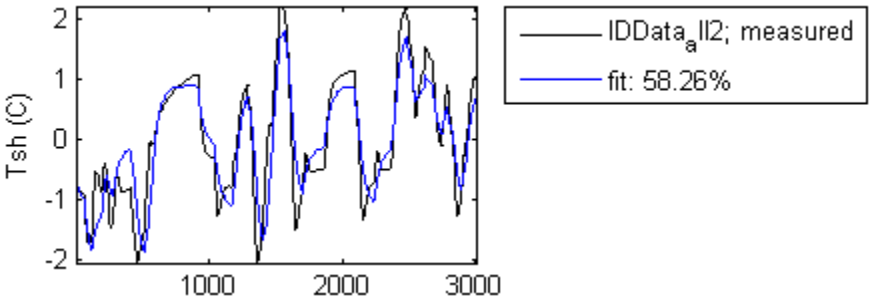

Figure B.4: State space representation C

Eigenvalues: -0.0227

$$A = [0.978] \quad B = [0.001] \quad C = [28.8] \tag{B.6}$$

B.2 Two actuator models

Two actuators are used to regulate the system average pressure and delta pressure. For more information regarding the choice of control variables, see Section 5.2. The section titles refer to the active variable actuators.

B.2.1 Valve, Compressor (VK)

Table B.6: Actuator range for state space VK

	Valve Aperture (%)	Compressor Speed (RPM)	Evaporator Fan (%)	Condenser Fan (%)
Minimum	31.5	1235	40	40
Maximum	38.5	1365	40	40

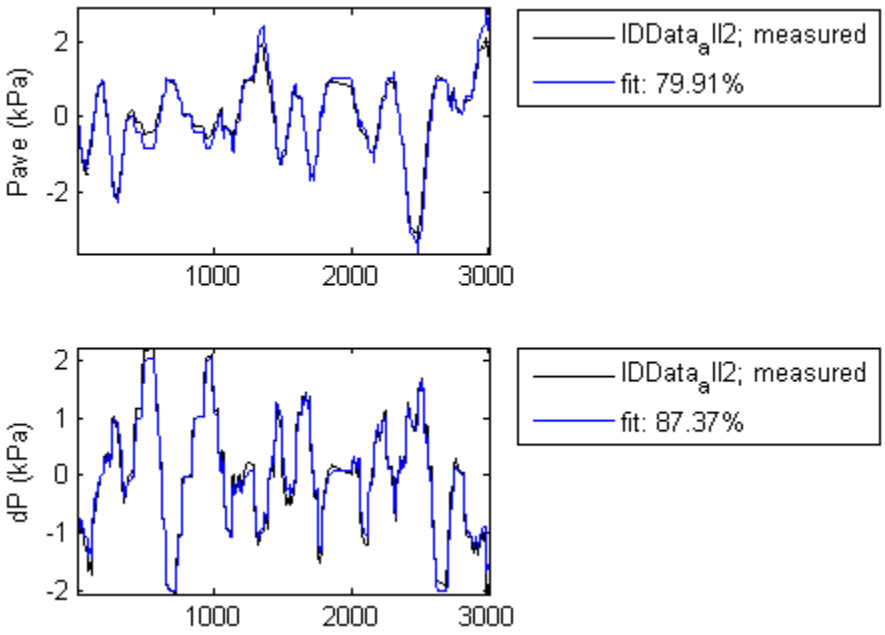

Figure B.5: State space representation VK

Eigenvalues: -0.0419, -0.1869

$$A = \begin{bmatrix} 0.958 & 0.001 \\ 0.071 & 0.830 \end{bmatrix} \quad B = \begin{bmatrix} 0.002 & 0.000 \\ -0.009 & 0.017 \end{bmatrix} \tag{B.7}$$

$$C = \begin{bmatrix} 18.9 & -5.09 \\ 9.55 & 9.07 \end{bmatrix}$$

B.2.2 Valve, Evaporator (VE)

Table B.7: Actuator range for state space VE

	Valve Aperture (%)	Compressor Speed (RPM)	Evaporator Fan (%)	Condenser Fan (%)
Minimum	31.5	1300	34	40
Maximum	38.5	1300	46	40

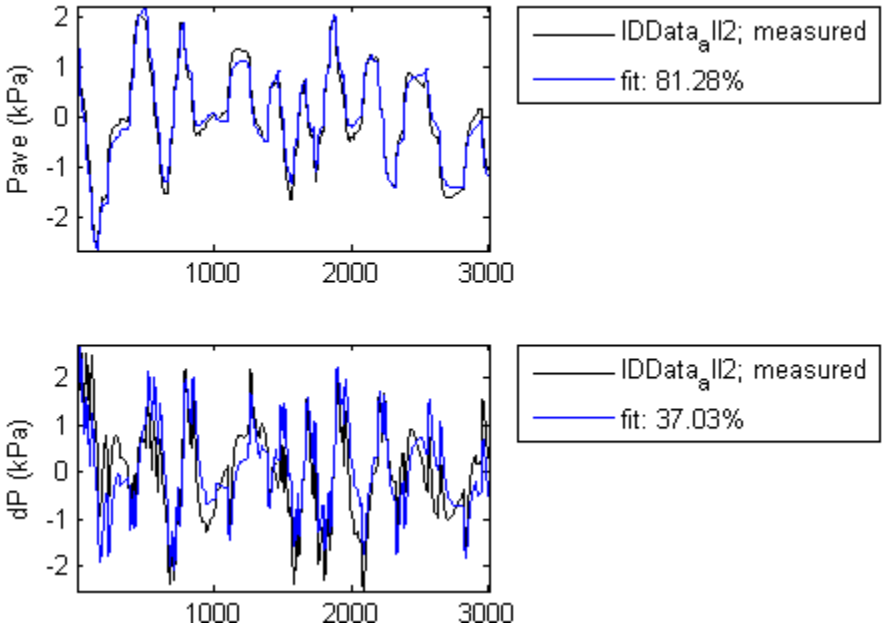

Figure B.6: State space representation VE

Eigenvalues: -0.0405, -0.1419

$$A = \begin{bmatrix} 0.966 & 0.003 \\ -0.147 & 0.863 \end{bmatrix} \quad B = \begin{bmatrix} -0.001 & -0.000 \\ -0.020 & -0.004 \end{bmatrix} \tag{B.8}$$

$$C = \begin{bmatrix} -18.1 & -2.99 \\ -46.9 & 13.6 \end{bmatrix}$$

B.2.3 Valve, Condenser (VC)

Table B.8: Actuator range for state space VC

	Valve Aperture (%)	Compressor Speed (RPM)	Evaporator Fan (%)	Condenser Fan (%)
Minimum	31.5	1300	40	34
Maximum	38.5	1300	40	46

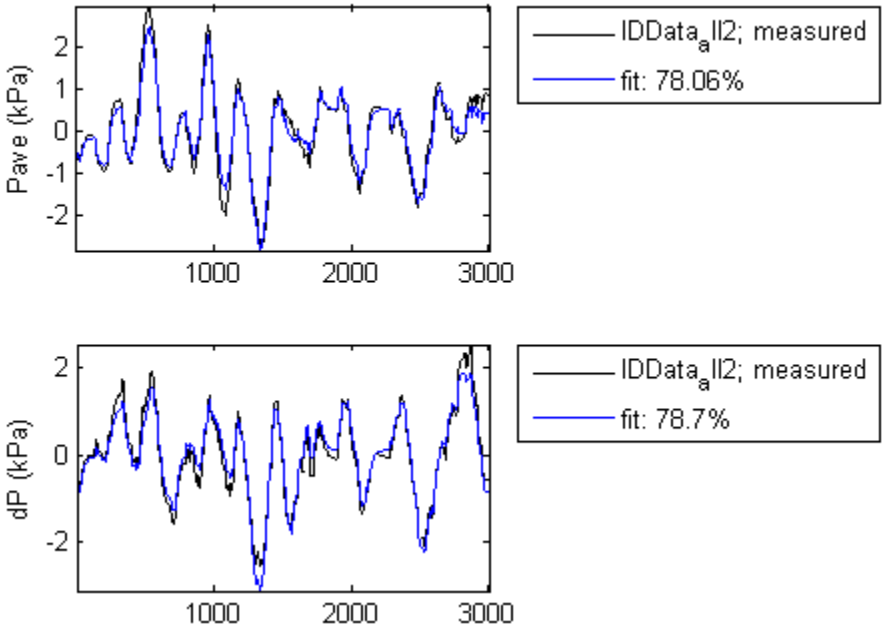

Figure B.7: State space representation VC

Eigenvalues: -0.0368, -0.1374

$$A = \begin{bmatrix} 0.961 & 0.004 \\ 0.062 & 0.875 \end{bmatrix} \quad B = \begin{bmatrix} 0.001 & -0.001 \\ -0.0126 & -0.000 \end{bmatrix} \tag{B.9}$$

$$C = \begin{bmatrix} 23.8 & -1.39 \\ 30.1 & 7.43 \end{bmatrix}$$

B.2.4 Compressor, Evaporator (KE)

Table B.9: Actuator range for state space KE

	Valve Aperture (%)	Compressor Speed (RPM)	Evaporator Fan (%)	Condenser Fan (%)
Minimum	35	1202.5	34	40
Maximum	35	1397.5	46	40

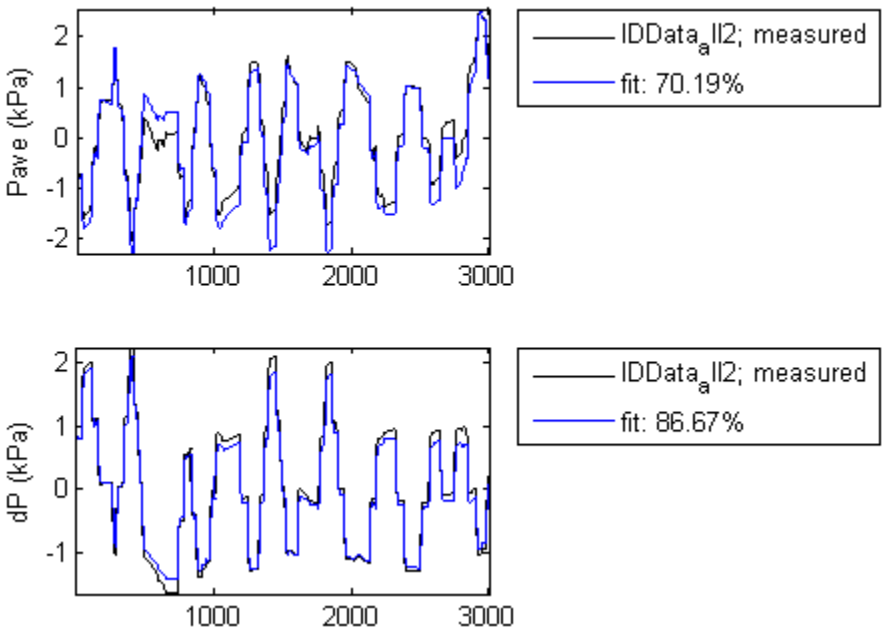

Figure B.8: State space representation KE

Eigenvalues: -0.0021, -0.1814

$$A = \begin{bmatrix} 0.992 & 0.039 \\ 0.026 & 0.0840 \end{bmatrix} \quad B = \begin{bmatrix} 0.004 & -0.001 \\ -0.017 & 0.002 \end{bmatrix} \tag{B.10}$$

$$C = \begin{bmatrix} -15.3 & 7.33 \\ -4.07 & -9.80 \end{bmatrix}$$

B.2.5 Compressor, Condenser (KC)

Table B.10: Actuator range for state space KC

	Valve Aperture (%)	Compressor Speed (RPM)	Evaporator Fan (%)	Condenser Fan (%)
Minimum	35	1235	40	34
Maximum	35	1365	40	46

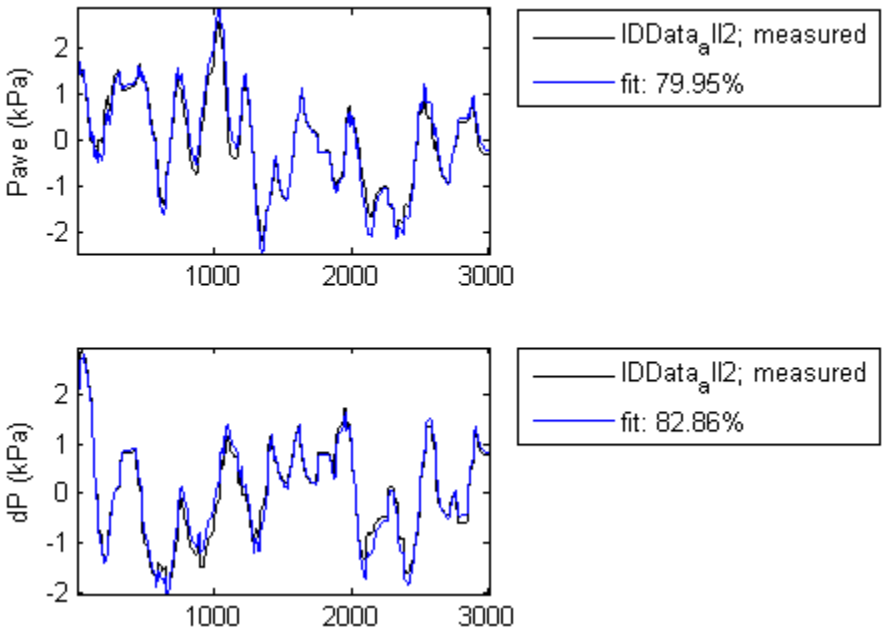

Figure B.9: State space representation KC

Eigenvalues: -0.0343, -0.1869

$$A = \begin{bmatrix} 0.966 & 0.009 \\ 0.001 & 0.830 \end{bmatrix} \quad B = \begin{bmatrix} 0.001 & 0.001 \\ -0.017 & -0.001 \end{bmatrix} \tag{B.11}$$

$$C = \begin{bmatrix} -27.4 & 3.32 \\ -18.3 & -7.86 \end{bmatrix}$$

B.2.6 Evaporator, Condenser (EC)

Table B.11: Actuator range for state space EC

	Valve Aperture (%)	Compressor Speed (RPM)	Evaporator Fan (%)	Condenser Fan (%)
Minimum	35	1300	34	34
Maximum	35	1300	46	46

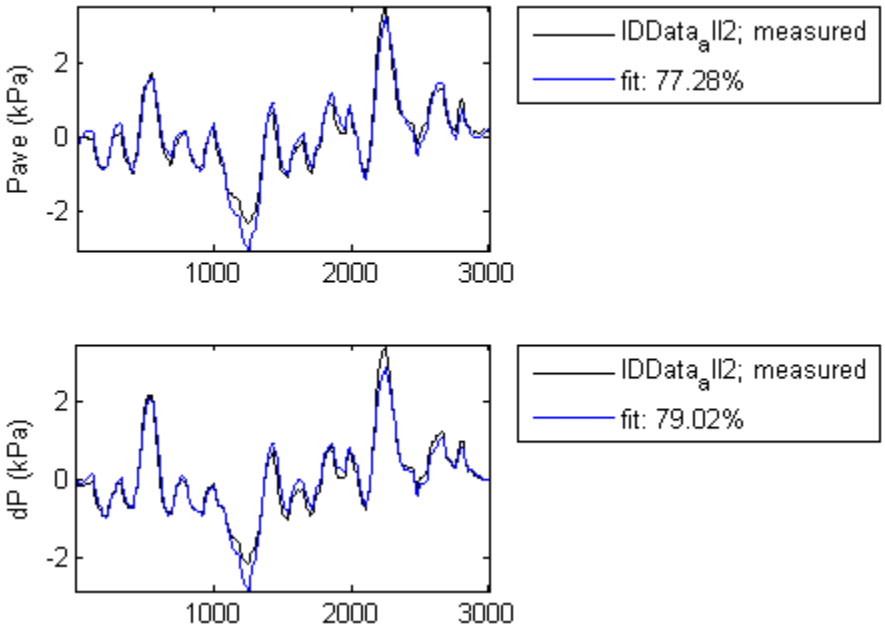

Figure B.10: State space representation EC

Eigenvalues: -0.0313+0.0049i, 0.0313-0.0049i

$$A = \begin{bmatrix} 0.970 & 0.004 \\ -0.006 & 0.968 \end{bmatrix} \quad B = \begin{bmatrix} -0.000 & -0.001 \\ 0.002 & -0.000 \end{bmatrix} \tag{B.12}$$

$$C = \begin{bmatrix} 26.9 & 1.36 \\ 26.3 & -3.56 \end{bmatrix}$$

B.3 Three actuator models

Three actuators are used to regulate the system average pressure, delta pressure, and superheat temperature. For more information regarding the choice of control variables, see Section 5.2. The section titles refer to the variable actuators.

B.3.1 Valve, Compressor, Evaporator (VKE)

Table B.12: Actuator range for state space VKE

	Valve Aperture (%)	Compressor Speed (RPM)	Evaporator Fan (%)	Condenser Fan (%)
Minimum	31.5	1202.5	34	40
Maximum	38.5	1397.5	46	40

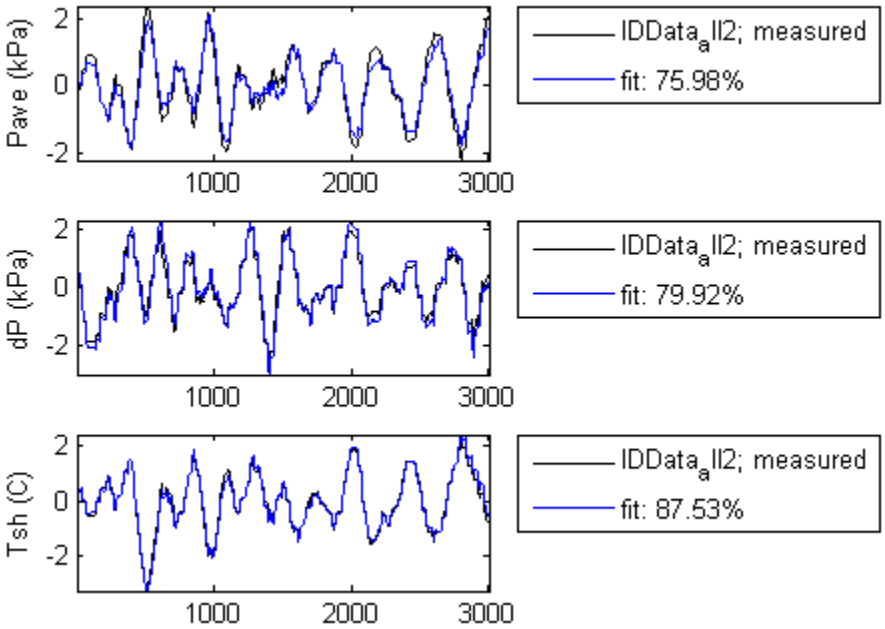

Figure B.11: State space representation VKE

Eigenvalues: -0.0244, -0.0499, -0.1872

$$A = \begin{bmatrix} 0.965 & -0.015 & -0.012 \\ -0.0544 & 0.838 & 0.015 \\ 0.005 & 0.030 & 0.954 \end{bmatrix}$$

$$B = \begin{bmatrix} 0.002 & -0.001 & -0.000 \\ 0.010 & -0.016 & 0.002 \\ -0.001 & 0.004 & -0.002 \end{bmatrix} \quad \text{(B.13)}$$

$$C = \begin{bmatrix} 17.6 & 3.26 & -0.790 \\ 12.2 & -10.1 & 2.06 \\ -6.36 & -9.18 & -12.2 \end{bmatrix}$$

B.3.2 Valve, Compressor, Condenser (VKC)

Table B.13: Actuator range for state space VKC

	Valve Aperture (%)	Compressor Speed (RPM)	Evaporator Fan (%)	Condenser Fan (%)
Minimum	31.5	1235	40	34
Maximum	38.5	1365	40	46

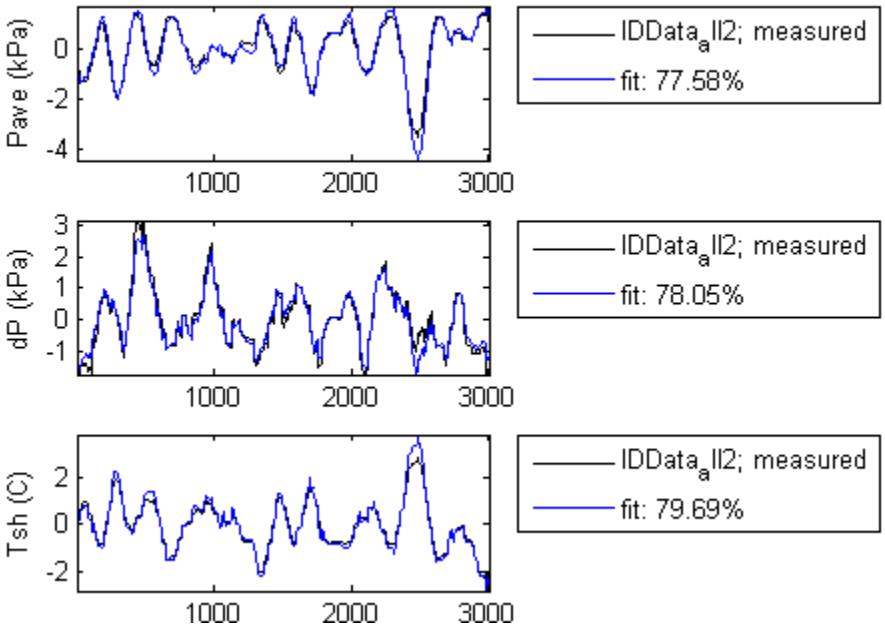

Figure B.12: State space representation VKC

Eigenvalues: -0.0295, -0.0527, -0.1801

$$A = \begin{bmatrix} 0.958 & -0.010 & -0.005 \\ -0.051 & 0.843 & 0.010 \\ 0.001 & 0.051 & 0.954 \end{bmatrix}$$

$$B = \begin{bmatrix} 0.002 & -0.001 & -0.002 \\ 0.009 & -0.015 & -0.000 \\ -0.002 & 0.008 & 0.000 \end{bmatrix} \quad \text{(B.14)}$$

$$C = \begin{bmatrix} 20.9 & 2.14 & -0.312 \\ 19.0 & -8.11 & 0.511 \\ -9.91 & -10.1 & -5.34 \end{bmatrix}$$

B.3.3 Valve, Evaporator, Condenser (VEC)

Table B.14: Actuator range for state space VEC

	Valve Aperture (%)	Compressor Speed (RPM)	Evaporator Fan (%)	Condenser Fan (%)
Minimum	31.5	1300	34	36
Maximum	38.5	1300	46	44

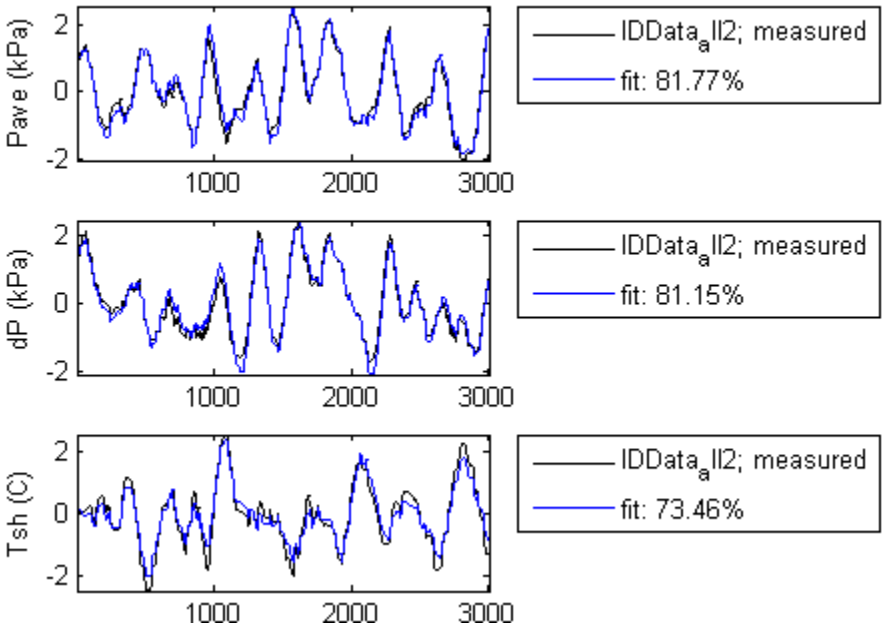

Figure B.13: State space representation VEC

Eigenvalues: -0.0329, -0.0487, -0.1402

$$A = \begin{bmatrix} 0.962 & -0.009 & -0.004 \\ -0.053 & 0.873 & -0.002 \\ 0.004 & 0.013 & 0.954 \end{bmatrix}$$

$$B = \begin{bmatrix} 0.002 & 0.000 & -0.001 \\ 0.012 & 0.002 & 0.000 \\ -0.001 & -0.003 & 0.000 \end{bmatrix} \quad \text{(B.15)}$$

$$C = \begin{bmatrix} 21.7 & 1.55 & -0.793 \\ 23.9 & -8.04 & 0.497 \\ -10.6 & -7.48 & -14.7 \end{bmatrix}$$

B.3.4 Compressor, Evaporator, Condenser (KEC)

Table B.15: Actuator range for state space KEC

	Valve Aperture (%)	Compressor Speed (RPM)	Evaporator Fan (%)	Condenser Fan (%)
Minimum	35	1202.5	34	36
Maximum	35	1397.5	46	44

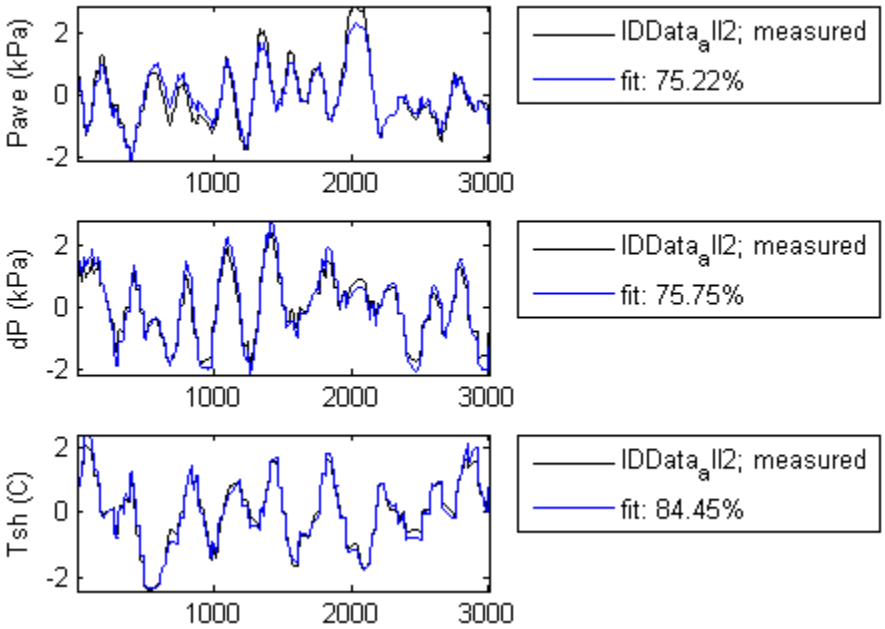

Figure B.14: State space representation KEC

Eigenvalues: -0.0341, -0.0484, -0.1830

$$A = \begin{bmatrix} 0.964 & 0.0127 & -0.003 \\ 0.026 & 0.839 & 0.029 \\ -0.002 & 0.015 & 0.949 \end{bmatrix}$$

$$B = \begin{bmatrix} 0.002 & -0.000 & 0.002 \\ -0.018 & 0.002 & 0.000 \\ 0.003 & -0.002 & -0.000 \end{bmatrix} \quad \text{(B.16)}$$

$$C = \begin{bmatrix} -21.0 & 2.78 & -0.670 \\ -16.7 & -8.62 & 1.92 \\ 1.73 & -10.5 & -14.3 \end{bmatrix}$$

B.4 Four actuator model (VKEC)

Four actuators are used to regulate the system average pressure, delta pressure, superheat temperature, and subcooling temperature. Since there are only four actuators on the system, there is only one available state space for this configuration. For more information regarding the choice of control variables, see Section 5.2.

Table B.16: Actuator range for state space VKEC

	Valve Aperture (%)	Compressor Speed (RPM)	Evaporator Fan (%)	Condenser Fan (%)
Minimum	31.5	1202.5	34	34
Maximum	38.5	1397.5	46	46

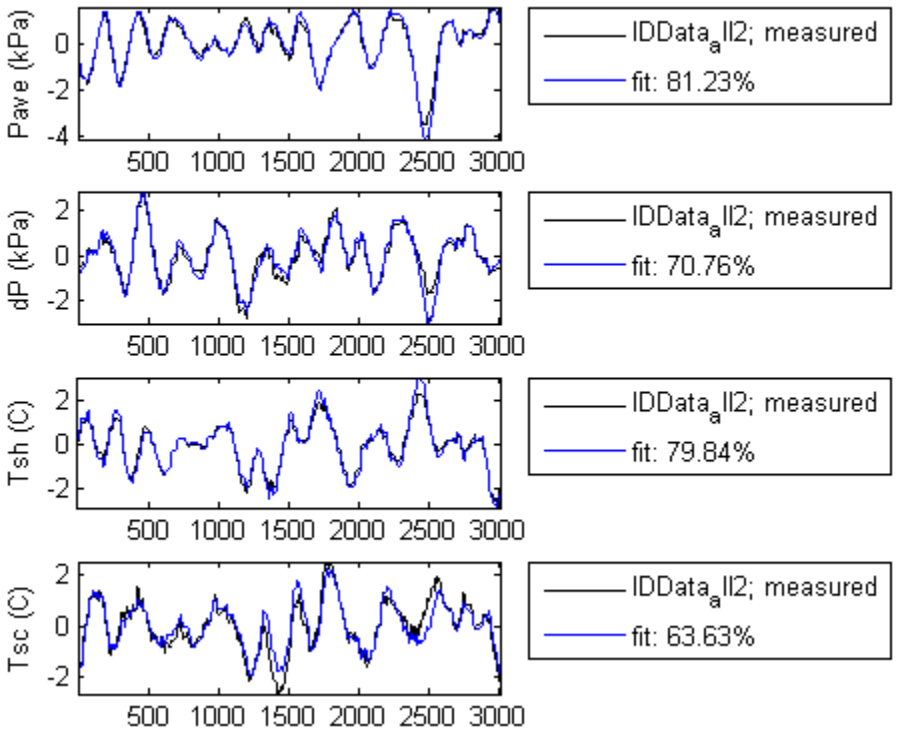

Figure B.15: State space representation VKEC

Eigenvalues: -0.0349+0.0224i, -0.0349-0.0224i, -0.0368, 0.1498

$$A = \begin{bmatrix} 0.965 & -0.004 & -0.006 & 0.003 \\ 0.055 & 0.856 & 0.012 & -0.006 \\ 0.051 & -0.021 & 0.984 & 0.013 \\ -0.045 & 0.007 & -0.021 & 0.951 \end{bmatrix}$$

$$B = \begin{bmatrix} -0.001 & -0.000 & -0.000 & 0.001 \\ 0.010 & -0.012 & 0.001 & -0.000 \\ 0.002 & -0.001 & 0.000 & 0.002 \\ -0.002 & 0.001 & 0.002 & 0.002 \end{bmatrix} \quad \text{(B.17)}$$

$$C = \begin{bmatrix} -21.7 & 2.93 & 1.41 & 0.290 \\ -22.4 & -7.75 & 1.39 & -1.09 \\ 8.78 & -8.19 & 8.17 & 10.9 \\ 20.2 & 0.042 & 27.5 & -3.05 \end{bmatrix}$$

Appendix C
Linear Quadratic Integrator (LQI) Controllers

The LQI controller is a particular class of controllers which uses integral action to give zero steady state error when a type zero system is tracking a step change [47]. The derivation regarding the states of the controller is given in Section 4.2.3. The cost function associated with the LQI is given as

$$J_{LQI} = \int_0^\infty \bar{e}^T Q_P \bar{e} + \bar{z}^T Q_I \bar{z} + \bar{u}^T R \bar{u} \tag{C.18}$$

The gains used to design the controllers are given below, grouped by the number of active actuators. All controllers were created at a cooling capacity of 0.90 kW from the linearized system models given in Appendix B. The controllers were used at 0.82 kW and 1.00 kW of cooling to demonstrate robustness.

In some actuator configurations, the controller designed at 0.90 kW of cooling did not cause the system to converge in a reasonable amount of time for the other cooling capacities. Changes in the relative weighting of the Q_I matrix were used to address this problem. Because of these changes, there is a difference in the cost function of the controller at the two different cooling capacities. However, all data used to compare actuator configurations to each other were taken from the total exergy destruction of the vapor-compression cycle system (VCS). Since all controllers were able to drive the control variables to the reference values, there was no need to normalize the output caused by the differences in the LQI cost function.

C.1 One actuator controllers

One actuator is used to regulate the superheat temperature at the exit of the evaporator. For more information regarding the choice of control variables, see Section 5.2. The section titles refer to the active variable actuators.

C.1.1 Valve (V)

$$Q_P = [10] \quad Q_I = [1E^{-3}] \quad R = [1] \tag{C.19}$$

C.1.2 Compressor (K)

$$Q_P = [10] \quad Q_I = [1E^{-3}] \quad R = [2] \tag{C.20}$$

C.1.3 Evaporator (E)

$$Q_P = [10] \quad Q_I = [1E^{-3}] \quad R = [5] \tag{C.21}$$

C.1.4 Condenser (C)

$$Q_P = [10] \quad Q_I = [1E^{-3}] \quad R = [5] \tag{C.22}$$

C.2 Two actuator controllers

Two actuators are used to regulate the system average pressure and delta pressure. For more information regarding the choice of control variables, see Section 5.2. The section titles refer to the active variable actuators.

C.2.1 Valve, Compressor (VK)

$$Q_P = \begin{bmatrix} 500 & 0 \\ 0 & 500 \end{bmatrix} \quad Q_I = \begin{bmatrix} 5E^{-1} & 0 \\ 0 & 1E^{-1} \end{bmatrix} \quad R = \begin{bmatrix} 20 & 0 \\ 0 & 75 \end{bmatrix} \tag{C.23}$$

C.2.2 Valve, Evaporator (VE)

No controller was able to be designed from this condition. A detailed description regarding the failure to produce a controller is given in Section 5.4.2.

C.2.3 Valve, Condenser (VC)

$$Q_P = \begin{bmatrix} 10 & 0 \\ 0 & 10 \end{bmatrix} \quad Q_I = \begin{bmatrix} 1E^{-2} & 0 \\ 0 & 1E^{-2} \end{bmatrix} \quad R = \begin{bmatrix} 1 & 0 \\ 0 & 5 \end{bmatrix} \tag{C.24}$$

C.2.4 Compressor, Evaporator (KE)

$$Q_P = \begin{bmatrix} 50 & 0 \\ 0 & 100 \end{bmatrix} \quad Q_I = \begin{bmatrix} 1E^{-1} & 0 \\ 0 & 1E^{-1} \end{bmatrix} \quad R = \begin{bmatrix} 1 & 0 \\ 0 & 100 \end{bmatrix} \tag{C.25}$$

For a cooling capacity of 1.00 kW, the controller above gave insufficient performance characteristics. The controller given below was used instead.

$$Q_P = \begin{bmatrix} 50 & 0 \\ 0 & 100 \end{bmatrix} \quad Q_I = \begin{bmatrix} 1E^{-2} & 0 \\ 0 & 1E^{-1} \end{bmatrix} \quad R = \begin{bmatrix} 1 & 0 \\ 0 & 100 \end{bmatrix} \tag{C.26}$$

C.2.5 Compressor, Condenser (KC)

$$Q_P = \begin{bmatrix} 10 & 0 \\ 0 & 10 \end{bmatrix} \quad Q_I = \begin{bmatrix} 1E^{-2} & 0 \\ 0 & 1E^{-2} \end{bmatrix} \quad R = \begin{bmatrix} 1 & 0 \\ 0 & 10 \end{bmatrix} \tag{C.27}$$

C.2.6 Evaporator, Condenser (EC)

$$Q_P = \begin{bmatrix} 10 & 0 \\ 0 & 10 \end{bmatrix} \quad Q_I = \begin{bmatrix} 1E^{-2} & 0 \\ 0 & 1E^{-2} \end{bmatrix} \quad R = \begin{bmatrix} 1 & 0 \\ 0 & 10 \end{bmatrix} \tag{C.28}$$

C.3 Three actuator controllers

Three actuators are used to regulate the system average pressure, delta pressure, and superheat temperature. For more information regarding the choice of control variables, see Section 5.2. The section titles refer to the variable actuators.

C.3.1 Valve, Compressor, Evaporator (VKE)

$$Q_P = \begin{bmatrix} 100 & 0 & 0 \\ 0 & 10 & 0 \\ 0 & 0 & 1000 \end{bmatrix} \quad Q_I = \begin{bmatrix} 1E^{-1} & 0 & 0 \\ 0 & 1E^{-2} & 0 \\ 0 & 0 & 1E^{-1} \end{bmatrix} \quad R = \begin{bmatrix} 10 & 0 & 0 \\ 0 & 30 & 0 \\ 0 & 0 & 50 \end{bmatrix} \tag{C.29}$$

C.3.2 Valve, Compressor, Condenser (VKC)

$$Q_P = \begin{bmatrix} 100 & 0 & 0 \\ 0 & 10 & 0 \\ 0 & 0 & 100 \end{bmatrix} \quad Q_I = \begin{bmatrix} 1E^{-1} & 0 & 0 \\ 0 & 1E^{-2} & 0 \\ 0 & 0 & 1E^{-1} \end{bmatrix} \quad R = \begin{bmatrix} 10 & 0 & 0 \\ 0 & 30 & 0 \\ 0 & 0 & 50 \end{bmatrix} \qquad \text{(C.30)}$$

For a cooling capacity of 1.00 kW, no controller was able to be designed from this condition. A detailed description regarding the failure to produce a controller is given in Section 5.4.2.

C.3.3 Valve, Evaporator, Condenser (VEC)

$$Q_P = \begin{bmatrix} 400 & 0 & 0 \\ 0 & 10 & 0 \\ 0 & 0 & 1000 \end{bmatrix} \quad Q_I = \begin{bmatrix} 5E^{-2} & 0 & 0 \\ 0 & 1E^{-2} & 0 \\ 0 & 0 & 1E^{-1} \end{bmatrix} \quad R = \begin{bmatrix} 30 & 0 & 0 \\ 0 & 50 & 0 \\ 0 & 0 & 50 \end{bmatrix} \qquad \text{(C.31)}$$

C.3.4 Compressor, Evaporator, Condenser (KEC)

$$Q_P = \begin{bmatrix} 100 & 0 & 0 \\ 0 & 10 & 0 \\ 0 & 0 & 100 \end{bmatrix} \quad Q_I = \begin{bmatrix} 5E^{-2} & 0 & 0 \\ 0 & 5E^{-3} & 0 \\ 0 & 0 & 5E^{-2} \end{bmatrix} \quad R = \begin{bmatrix} 10 & 0 & 0 \\ 0 & 50 & 0 \\ 0 & 0 & 50 \end{bmatrix} \qquad \text{(C.32)}$$

For a cooling capacity of 1.00 kW, the controller above gave insufficient performance characteristics. The controller given below was used instead.

$$Q_P = \begin{bmatrix} 100 & 0 & 0 \\ 0 & 10 & 0 \\ 0 & 0 & 100 \end{bmatrix} \quad Q_I = \begin{bmatrix} 5E^{-2} & 0 & 0 \\ 0 & 5E^{-2} & 0 \\ 0 & 0 & 5E^{-2} \end{bmatrix} \quad R = \begin{bmatrix} 10 & 0 & 0 \\ 0 & 50 & 0 \\ 0 & 0 & 50 \end{bmatrix} \qquad \text{(C.33)}$$

C.4 Four actuator controllers (VKEC)

Four actuators are used to regulate the system average pressure, delta pressure, superheat temperature, and subcooling temperature. Since there are only four actuators on the system, there is only one available controller for this configuration. For more information regarding the choice of control variables, see Section 5.2.

No controller was able to be designed from this condition. A detailed description regarding the failure to produce a controller is given in Section 5.4.2.

Appendix D
Optimization Code

In order to determine a minimum exergy destruction for the VCS, an optimization technique was created. The technique is discussed in depth in Chapter 4. Three main programs were used to properly interface the user inputs, the thermodynamic calculations, and the exergy destruction cost analysis, as shown in Figure D.1.

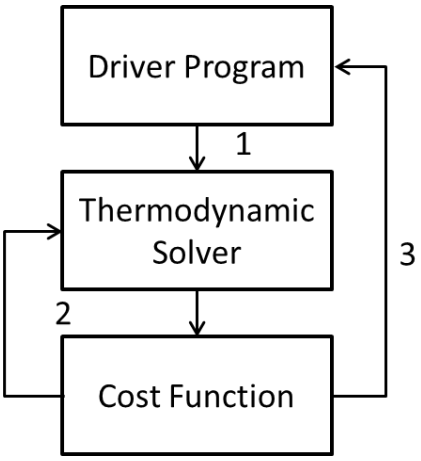

Figure D.1: Logical flow for optimization routine

The driver program accepts user inputs such as the cooling capacity required, high and low side temperatures, and initial guesses at the thermodynamic properties. The requisite information is passed to a thermodynamic solver at step one. The thermodynamic solver and the cost function analysis work in tandem at step two, to drive the exergy destruction to a minimum value by altering the thermodynamic variables. Constraints are applied to ensure the variables do not move outside of the allowable operating range. Once convergence to a minimum exergy

destruction has been established, the driver program is alerted at step three and all thermodynamic and exergetic information is passed to the driver.

In addition to the three main programs, three auxiliary programs are used in the exergy minimization technique. A converter program takes the raw thermodynamic information given by the optimization method and converts it into usable set point values for the VCS, see Section 4.1.5. Two functions are used to determine the valve aperture and compressor speed by minimizing the error in mass flow rate between the function and the thermodynamic information given by the optimization routine.

The code for the optimization technique is given below. The names of the files are provided, as some files reference another in operation. The files also reference the FluidProp structure, which contains thermodynamic information stored in arrays. FluidProp is used to determine thermodynamic conditions given known information, e.g. returning the saturation temperature when passed the saturation pressure.

The driver program, thermodynamic solver, and cost function analyzer were originally developed by Neera Jain to support the work in [22] and [56]. Minor adjustments were made to arrive at the versions presented below.

D.1 Driver program

This program is named “Optim_Exergy_R134a”

```
clear all;clc;

%%%%%%%%%%%%%%%%%%%%%%%%%%%%%%%%%%%%%%%%%%%%%%%%%%%%%%%%%%%%%%%%%%%%%%%%%%%%%%%
% Stage 1: Set Up
%%%%%%%%%%%%%%%%%%%%%%%%%%%%%%%%%%%%%%%%%%%%%%%%%%%%%%%%%%%%%%%%%%%%%%%%%%%%%%%

tic;  % Starts timer
u = [0.90 0.02 23 17 0.0048 0.10 0.3];

C_des               = u(1);  % desired cooling capacity (kW)
gamma               = u(2);  % size of band on cooling capacity constraint
Tamb                = u(3);  % ambient temperature (deg C)
Teai                = u(4);  % evaporator air inlet temperature (deg C)
mdot_ref_guess      = u(5);  % mass flow rate of refrigerant
me_air_guess        = u(6);  % mass flow rate evaporator secondary side
mc_air_guess        = u(7);  % mass flow rate condenser secondary side

Tamb_K      = Tamb + 273.15;
Teai_K      = Teai + 273.15;

%Sets unique options for the fmincon solver
OPTIONS =
optimset('FunValCheck','on','UseParallel','always','Display','iter',...
    'MaxFunEvals',100000,'MaxIter',100000,'Algorithm','sqp','Diagnostics',...
    'on','TolX',1e-10,'TolCon',1e-4,'TolFun',1e-10);

%%
%%%%%%%%%%%%%%%%%%%%%%%%%%%%%%%%%%%%%%%%%%%%%%%%%%%%%%%%%%%%%%%%%%%%%%%%%%%%%%%
% Stage 2: Optimization
%%%%%%%%%%%%%%%%%%%%%%%%%%%%%%%%%%%%%%%%%%%%%%%%%%%%%%%%%%%%%%%%%%%%%%%%%%%%%%%

load FluidProp_R134a

%Guess at initial thermodynamic variables
h1_guess        = 250.2;
h2_guess        = 286.6;
h4_guess        = 86.95;
P2_guess        = 835;
P1_guess        = 180;

% Run fmincon for Stage 1 objective function
x_guess      = [h1_guess h2_guess h4_guess P1_guess P2_guess
mdot_ref_guess...
    me_air_guess mc_air_guess];

%Set boundaries for thermodynamic variables
lb          = [220  220  20   150  780  0.00300  0.05547  0.049559];
```

```
ub           = [350  350  220  550  960  0.00900  0.21466  0.599927];

%Specify h1 < h2, h4 < h1
A = [1 -1 0 0 0 0 0 0; -1 0 1 0 0 0 0 0];
b = [0; 0];

%Start the fmincon minimization technique
[x_soln,J_fval,Exitflag] = fmincon(@Solver_Exergy_R134a,x_guess,A,b,[],[],...
    lb,ub,@Nonlcon_Exergy_R134a,OPTIONS,C_des,gamma,Tamb,Teai);
%Extra terms after OPTIONS are passed between m files

%Read solution
h1          = x_soln(1);
h2          = x_soln(2);
h4          = x_soln(3);
P1          = x_soln(4);
P2          = x_soln(5);
mdot_ref    = x_soln(6);
me_air      = x_soln(7);
mc_air      = x_soln(8);

output = [x_soln J_fval];

%%
%%%%%%%%%%%%%%%%%%%%%%%%%%%%%%%%%%%%%%%%%%%%%%%%%%%%%%%%%%%%%%%%%%%%%%%%%%%%%%%
% Stage 3: Actuation
%%%%%%%%%%%%%%%%%%%%%%%%%%%%%%%%%%%%%%%%%%%%%%%%%%%%%%%%%%%%%%%%%%%%%%%%%%%%%%%

%Determine the valve aperture
rho_v_sat   = interp1(FluidProp.Psat,FluidProp.Rhof,P2);
a_v = fminbnd(@(x) valveOpen(x,rho_v_sat,P1,P2,mdot_ref), 0, 100);
Controls(1) = a_v;

%Determine the compressor speed
rho1    =
interp2(FluidProp.H_mg_ph,FluidProp.P_mg_ph,FluidProp.Rho_ph,h1,P1);
omega = fminbnd(@(x) compSpeed(x,rho1,P1,P2,mdot_ref), 0, 2200);
Controls(2) = omega;

%Determine the evaporator fan speed
EvapFan_2_Map = [
    100 0.2407
    95  0.2302
    90  0.2197
    85  0.2092
    80  0.1987
    75  0.1882
    70  0.1777
    65  0.1672
    60  0.1567
    55  0.1462
    50  0.1357
    45  0.1252
```

```
    40  0.1147
    35  0.1024
    30  0.0937
    25  0.0832
    20  0.0727
    15  0.0622
    10  0
    5   0
    0   0];

Evap_Corr_Factor    = 0.7;
EvapFan_2_Map(:,2)  = EvapFan_2_Map(:,2)*Evap_Corr_Factor;

EvapFan_Map.input  = EvapFan_2_Map(1:end-3,1);
EvapFan_Map.Ve_air = EvapFan_2_Map(1:end-3,2);

fan_e = interp1(EvapFan_Map.Ve_air,EvapFan_Map.input,me_air/1.274);
Controls(3) = fan_e;

%Determine the condenser fan speed
CondFan_Map = [
    100 0.4709
    95  0.4469
    90  0.4229
    85  0.3989
    80  0.3749
    75  0.3509
    70  0.3269
    65  0.3029
    60  0.2789
    55  0.2549
    50  0.2309
    45  0.2069
    40  0.1829
    35  0.1589
    30  0.1349
    25  0.1109
    20  0.0869
    15  0.0629
    10  0.0389
    5   0
    0   0];

CondFanMap.power  = CondFan_Map(1:end-1,1);
CondFanMap.Vc_air = CondFan_Map(1:end-1,2);

fan_c = interp1(CondFanMap.Vc_air,CondFanMap.power,mc_air/1.274);
Controls(4) = fan_c;

T = toc; %End timer
```

D.2 Thermodynamic solver

This program is named “Nonlcon_Exergy_R134a”

```
function [c,ceq] = Nonlcon_Exergy_R134a(x,C_des,gamma,Tamb,Teai)

load FluidProp_R134a

h1          = x(1);
h2          = x(2); %Corresponds to actual power consumed by the compressor
h4          = x(3);
P1          = x(4);
P2          = x(5);
mdot_ref    = x(6);
me_air      = x(7);
mc_air      = x(8);

Tamb_K      = Tamb + 273.15;
Teai_K      = Teai + 273.15;

%%%%%%%%%%%%%%%%%%%%%%%%%%%%%%%%%%%%%%%%%%%%%%%%%%%%%%%%%%%%%%%%%%%%%%%%%%%%%%%
% VCS Calculations

%Starting entropy
s1      = interp2(FluidProp.H_mg_ph,FluidProp.P_mg_ph,FluidProp.S_ph,h1,P1);
s2_IS   = s1;

% Coefficients for eta_is map
a = [
    -0.316241613386002
    0.000293577373228
    0.000577648388009
    0.001088200155236
    0.000001383247342
    -0.000000618819011
    -0.000002018706930];

% Coefficients for eta_vol map
b = [
    -0.632140973972956
    -0.000060114191319
    0.004747130863476
    0.001288217866798
    0.000000335369026
    -0.000000012403162
    -0.000004968489928];

% Coefficients for valve map
d = [
    0.000000682529858
    0.000000108528381
```

```
    0.000000002005617
    0.000000008480014
    -0.000000000007865];

% Coefficients for eta_adb map
e = [
    17.906699611397900
    -0.001652164783143
    -0.018978914115588
    -0.019542172208376
    0.000007876382813
    0.000001946287236
    0.000015688408301];

%Determine the compressor speed
rho1    =
interp2(FluidProp.H_mg_ph,FluidProp.P_mg_ph,FluidProp.Rho_ph,h1,P1);
omega = fminbnd(@(x) compSpeed(x,rho1,P1,P2,mdot_ref), 0, 2200);

%Compressor efficiency
eta_is       = a(1) + a(2)*omega + a(3)*P1 + a(4)*P2 + a(5)*P1*omega + ...
               a(6)*P2*omega + a(7)*P1*P2;
eta_adb      = e(1) + e(2)*omega + e(3)*P1 + e(4)*P2 + e(5)*P1*omega + ...
               e(6)*P2*omega + e(7)*P1*P2;

%Compressor enthalpy
h2s     =
interp2(FluidProp.S_mg_ps,FluidProp.P_mg_ps,FluidProp.H_ps,s2_IS,P2);
h2_adb  = ( h2s - h1 )/eta_adb + h1;

%Other properties
T1      = interp2(FluidProp.H_mg_ph,FluidProp.P_mg_ph,FluidProp.T_ph,h1,P1);
T2      =
interp2(FluidProp.H_mg_ph,FluidProp.P_mg_ph,FluidProp.T_ph,h2_adb,P2);
T3      = interp2(FluidProp.H_mg_ph,FluidProp.P_mg_ph,FluidProp.T_ph,h4,P2);
T4      = interp1(FluidProp.Psat,FluidProp.Tsat,P1);
T3sat   = interp1(FluidProp.Psat,FluidProp.Tsat,P2);
h4_g    = interp1(FluidProp.Psat,FluidProp.Hg,P1);

%%%%%%%%%%%%%%%%%%%%%%%%%%%%%%%%%%%%%%%%%%%%%%%%%%%%%%%%%%%%%%%%%%%%%%%%%%%%
% Compute maximum allowable heat transfer across evaporator and condenser
% given current choice of mdot_ref and Pe

% Condenser (Table 6.4 - Brian Eldredge MS Thesis)
Ae_i        = 0.29166;      %m^2
Ae_o        = 3.068;        %m^2
Ae_fr       = 0.0584;       %m^2
ke_wall     = 0.354;        %added to match ATTMO
te_wall     = 7.112e-4;     %m
Ae_total    = Ae_i + Ae_o;  %m^2
Ae_cs       = 5.156e-5;     %m^2
L_e         = 11.4579;      %m
D_e         = 0.0081026;    %m
```

```
% Condenser (Table 6.4 - Brian Eldredge MS Thesis)
Ac_i        = 0.275;        %m^2
Ac_o        = 2.793;        %m^2
Ac_fr       = 0.0898;       %m^2
kc_wall     = 0.177;        %added to match ATTMO
tc_wall     = 7.112e-4;     %added to match ATTMO
Ac_total    = Ac_i + Ac_o;  %m^2
Ac_cs       = 5.156e-005;   %m^2
L_c         = 10.6895;      %m
D_c         = 8.103e-3;     %m

%  Assumptions:
%      1. constant 2-phase quality of 0.5 in each HX
%      2. constant 2-phase length fraction of 0.95 in evaporator
%      3. constant 2-phase length fraction of 0.85 in condenser
%     me_air_max = 0.21466;   %kg/s determined from EvapFan_2_Map
%     mc_air_max = 0.599927;  %kg/s determined from CondFan_Map

% Compute UA across the evaporator
Qe_1        = mdot_ref*(h4_g-h4);
Xe_ri       = 0.5;
Ae_i1       = 1*Ae_i;
G_ri        = mdot_ref/Ae_cs;

alpha_e_i   = H_EVAP_WATTLET(D_e, G_ri, P1, Xe_ri, Qe_1/Ae_i1);
alpha_e_o   = H_COLBURN_FACTOR(25, me_air, Ae_fr, Teai);

R1          = 1/(alpha_e_i*Ae_i);
R2          = te_wall/(ke_wall*(1-0.8882)*Ae_total);
R3          = 1/(alpha_e_o*Ae_o);
UA_e        = 1/(R1 + R2 + R3);

clear R1 R2 R3

% Compute UA across the condenser
G_r         = mdot_ref/Ac_cs;
Xc_ro       = 0.5;

alpha_c_i   = H_COND_DOBSON(D_c, G_r, P2, Xc_ro);
alpha_c_o   = H_COLBURN_FACTOR(23, mc_air, Ac_fr, Tamb);

R1          = 1/(alpha_c_i*Ac_i);
R2          = tc_wall/(kc_wall*(1-0.8855)*Ac_total);
R3          = 1/(alpha_c_o*Ac_o);
UA_c        = 1/(R1 + R2 + R3);

clear R1 R2 R3

% Compute maximum heat transfer across evaporator and condenser
UA_e_corr_factor = 1/2.00; %Determined through fit between ATTMO and code
UA_c_corr_factor = 1/1.67; %Determined through fit between ATTMO and code
Qdot_L_max  = UA_e_corr_factor*UA_e*(Teai - T4);
```

```
Qdot_H_max  = UA_c_corr_factor*UA_c*(T3sat - Tamb);

%%%%%%%%%%%%%%%%%%%%%%%%%%%%%%%%%%%%%%%%%%%%%%%%%%%%%%%%%%%%%%%%%%%%%%%%%%%%
% Constraints

c(1) = 8 - (T1-T4);      %At least 8 degrees superheat
c(2) = 4 - (T3sat - T3); %At least 4 degrees subcooling
c(3) = 0 - (Teai - T1);  %Heat transfer into evaporator
c(4) = 0 - (T3 - Tamb);  %Heat transfer out of condenser

ceq(1) = C_des - mdot_ref*(h1-h4);          %Cooling capacity
ceq(2) = (h2 - h1) - (h2s - h1)/eta_adb;    %Isentropic efficiency
ceq(3) = mdot_ref*(h1-h4) - Qdot_L_max;     %to ensure evaporator heat
transfer
ceq(4) = mdot_ref*(h2_adb-h4) - Qdot_H_max; %to ensure condenser heat
transfer

return
```

D.3 Cost function analyzer

This program is named “Solver_Exergy_R134a”

```
function J = Solver_Exergy_R134a(x,C_des,gamma,Tamb,Teai)

load FluidProp_R134a

h1          = x(1);
h2          = x(2); %Corresponds to actual power consumed by the compressor
h4          = x(3);
P1          = x(4);
P2          = x(5);
mdot_ref    = x(6);
me_air      = x(7);
mc_air      = x(8);

Tamb_K      = Tamb + 273.15;
Teai_K      = Teai + 273.15;

%%%%%%%%%%%%%%%%%%%%%%%%%%%%%%%%%%%%%%%%%%%%%%%%%%%%%%%%%%%%%%%%%%%%%%%%%%%%%%%
% Evaluating J

Wdot_k      = mdot_ref*(h2-h1);                                 %Units of kW
Wdot_fe     = (1760.9*me_air^2 - 165.83*me_air + 7.092)/1000;  %Units of kW
Wdot_fc     = (697.12*mc_air^2 + 86.419*mc_air - 2.7083)/1000; %Units of kW
Wdot_total  = Wdot_k + Wdot_fe + Wdot_fc; %Units of kW

A           = (1 - Tamb_K/Teai_K); %Unitless
Q_L         = mdot_ref*(h1-h4); %Units of kW

%Computing J (Exergy destruction)
J = (Q_L*A + Wdot_total); %Units of kW

return
```

D.4 Thermodynamic converter

This program is called “Controller_Converter”

```
P = FluidProp;

%Reads in solution
h1          = x_soln(1);
h2          = x_soln(2);
h4          = x_soln(3);
P1          = x_soln(4);
P2          = x_soln(5);
mdot_ref    = x_soln(6);
me_air      = x_soln(7);
mc_air      = x_soln(8);

%Determines thermodynamic points
Pave = (P1 + P2) / 2;
dP = P2 - P1;
T1    = interp2(P.H,P.P,P.T_ph,h1,P1);
T1sat = interp1(P.Psat,P.Tsat,P1);
T2    = interp2(P.H,P.P,P.T_ph,h2,P2);
T3    = interp2(P.H,P.P,P.T_ph,h4,P2);
T3sat = interp1(P.Psat,P.Tsat,P2);
T4    = interp1(P.Psat,P.Tsat,P1);

Setpoints(1) = Pave;        %Average pressure
Setpoints(2) = dP;          %Delta pressure
Setpoints(3) = T1 - T1sat;  %Superheat temperature
Setpoints(4) = T3sat - T3;  %Subcool temperature
```

D.5 Valve aperture

This program is called “valveOpen”

```
function error = valveOpen(a_v, rho_v_sat, P1, P2, mdot_ref)

%Valve map
d = [
        0.000000682529858
        0.000000108528381
        0.000000002005617
        0.000000008480014
        -0.000000000007865];

%Mass flow rate calculation
Pdelta      = P2-P1;
Cf          = d(1) + d(2)*a_v + d(3)*P2 + d(4)*P1 + d(5)*P2*P1;
mdot_v      = Cf*sqrt(rho_v_sat*Pdelta);

%Returns error between actual and calculated mass flow
error    = (mdot_v - mdot_ref)^2;
```

D.6 Compressor speed

This program is called “compSpeed”

```
function error = compSpeed(omega, rho1, P1, P2, mdot_ref)

%Compressor map
b = [
        -0.632140973972956
        -0.000060114191319
        0.004747130863476
        0.001288217866798
        0.000000335369026
        -0.000000012403162
        -0.000004968489928];

%Mass flow rate calculation
rps     = omega/60;
eta_vol = b(1) + b(2).*omega + b(3).*P1 + b(4).*P2 + b(5).*P1.*omega + ...
    b(6).*P2.*omega + b(7).*P1.*P2;
volume  = 3.042e-5;
mdot_k  = rps.*volume.*rho1.*eta_vol;

%Returns error between actual and calculated mass flow
error = (mdot_ref - mdot_k).^2;
```